

Review

New Developments of Ti-Based Alloys for Biomedical Applications

Yuhua Li, Chao Yang *, Haidong Zhao, Shengguan Qu, Xiaoqiang Li and Yuanyuan Li

National Engineering Research Center of Near-net-shape Forming for Metallic Materials, South China University of Technology, Guangzhou 510640, Guangdong, China; E-Mails: liyuhuascut@126.com (Y.L.); hdzhao@scut.edu.cn (H.Z.); qusg@scut.edu.cn (S.Q.); lixq@scut.edu.cn (X.L.); mehjli@scut.edu.cn (Y.L.)

* Author to whom correspondence should be addressed; E-Mail: cyang@scut.edu.cn; Tel.: +86-20-8711-0099; Fax: +86-20-8711-2111.

Received: 20 November 2013; in revised form: 24 December 2013 / Accepted: 24 January 2014 /

Published: 4 March 2014

Abstract: Ti-based alloys are finding ever-increasing applications in biomaterials due to their excellent mechanical, physical and biological performance. Nowadays, low modulus β -type Ti-based alloys are still being developed. Meanwhile, porous Ti-based alloys are being developed as an alternative orthopedic implant material, as they can provide good biological fixation through bone tissue ingrowth into the porous network. This paper focuses on recent developments of biomedical Ti-based alloys. It can be divided into four main sections. The first section focuses on the fundamental requirements titanium biomaterial should fulfill and its market and application prospects. This section is followed by discussing basic phases, alloying elements and mechanical properties of low modulus β -type Ti-based alloys. Thermal treatment, grain size, texture and properties in Ti-based alloys and their limitations are discussed in the third section. Finally, the fourth section reviews the influence of microstructural configurations on mechanical properties of porous Ti-based alloys and all known methods for fabricating porous Ti-based alloys. This section also reviews prospects and challenges of porous Ti-based alloys, emphasizing their current status, future opportunities and obstacles for expanded applications. Overall, efforts have been made to reveal the latest scenario of bulk and porous Ti-based materials for biomedical applications.

Keywords: β -type Ti-based alloys; porous Ti-based alloys; microstructure; mechanical properties

1. Introduction

With the development of economy and technology, the number of aged people demanding failed tissue replacement is rapidly increasing. Elderly people have a higher risk of hard tissue failure. It is estimated that 70%–80% of biomedical implants are made of metallic materials. Metallic implants are remarkably important for the reconstruction of failed hard tissue and the market growth rate remains at around 20% and 25%. The population ratio of the aged people of representative countries is rapidly growing [1]. As human life span grows, the need of biomaterials will definitely continue to increase. This can stimulate the market and research process in a large scale. However, from the application viewpoint, there is still a huge gap between the supply and demand, especially in economically underdeveloped areas where medical technology is very limited. From the research viewpoint, biomaterial is an increasingly important topic, calling for a good mastery of knowledge in materials, biology, physics, chemistry, *etc.* One feature of biomaterial research is that it has a clear goal and possible applications. In terms of implantation materials, comprehensive properties of low elastic modulus, high strength, excellent wear and corrosion resistance, and good biocompatibility are those characteristics researchers have always been pursuing [2].

Metals and their alloys are widely used as biomedical materials. On one hand, metallic biomaterials cannot be replaced by ceramics or polymers at present. Because mechanical strength and toughness are the most important safety requirements for a biomaterial under load-bearing conditions, metallic biomaterials like stainless steels, Co-Cr alloys, commercially pure titanium (CP Ti) and its alloys are extensively employed for their excellent mechanical properties. On the other hand, metallic materials sometimes show toxicity and are fractured because of their corrosion and mechanical damages [3] (Figure 1). Therefore, development of new alloys is continuously trialed. Purposes of the development are as follows:

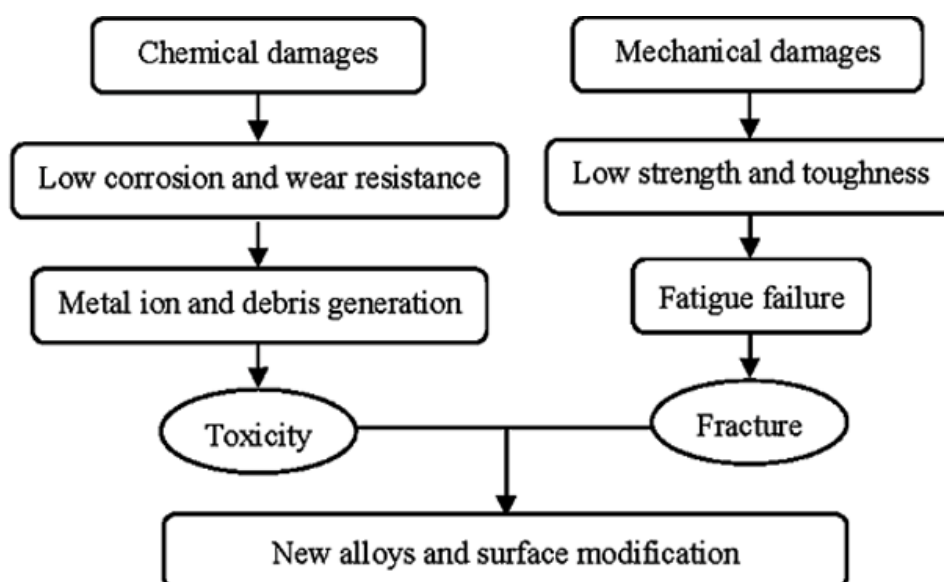
- To remove toxic elements;
- To decrease the elastic modulus to avoid stress shield effect in bone fixation;
- To improve tissue and blood compatibility;
- To miniaturize medical devices.

The development must be performed on the basis of metallurgy and the resultant alloys must have a good balance between mechanical properties and corrosion resistance. Among metallic materials, titanium and its alloys are considered as the most suitable materials for biomedical applications for their superior comprehensive properties, and they satisfy the requirements of implantation materials better than other competing materials, such as stainless steels, Cr-Co alloys, CP niobium and tantalum [4,5].

The development of titanium and its alloys used as implant material perfectly reflect the research goal of biomaterials. Firstly, CP Ti was proposed as an alternative for the 316L stainless steel and Co-Cr alloys owing to better biocompatibility and corrosion resistance [6–8], since stainless steels and Co-Cr alloys usually contain some harmful elements, such as Ni, Co and Cr. Despite this fact, the mechanical properties of CP Ti cannot satisfy the requirements of biomaterials in some cases when high strength is necessary, such as hard tissue replacement or under intensive wear use [9]. To overcome such restrictions, CP Ti was substituted by $\alpha + \beta$ -type Ti-based alloys, particularly Ti-6Al-4V alloy [10]. However, Ti-6Al-4V alloy is composed of cytotoxic elements like Al and V, which may cause severe problems once released inside human body. To overcome the potential V toxicity, V was replaced

by Nb and Fe, leading to two new V-free $\alpha + \beta$ -type Ti-based alloys, *i.e.*, Ti-6Al-7Nb and Ti-5Al-2.5Fe [5,11]. Both alloys show good mechanical and metallurgical behavior comparable to those of Ti-6Al-4V. Nevertheless, several studies have recently shown that the elastic modulus of α -type and some $\alpha + \beta$ -type Ti-based alloys is much higher than that of human bone [12–16], which can cause stress shielding effect [17]. Therefore, low modulus β -type Ti-based alloys have been extensively developed [18–20] to alleviate the stress shielding effect [17], among which the representatives are Ti-15Mo, Ti-13Nb-13Zr, Ti-12Mo-6Zr-2Fe, Ti-35Nb-5Ta-7Zr, and Ti-29Nb-13Ta-4.6Zr [21–23]. Especially, Ti-Nb-Ta-Zr alloys have much lower elastic modulus of about 48–55 GPa, about half of conventional Ti-6Al-4V alloy [24–26]. The lowest elastic modulus reported so far in bulk Ti-based alloys developed for biomedical applications is 40 GPa for Ti-35Nb-4Sn alloy [27]. However, it is still greater than that of cortical bone (10–30 GPa), especially higher than that of cancellous bone with a modulus of about 0.01–2 GPa [28]. At present, it is very difficult to lower the elastic modulus of bulk Ti-based alloys below 40 GPa.

Figure 1. Degradation of metallic materials.



The main reason why good fixation of implantation materials to the bone tissue remains a problem is the elastic modulus mismatch between biomaterials and the surrounding bones [29–31]. However, the implanted materials must be strong and durable enough to withstand the physiological loads exerted on it and expected to serve for much longer period or until lifetime without failure or revision surgery. A suitable balance between strength and stiffness to best match that of bone is highly essential.

In order to further reduce elastic modulus of Ti-based alloys, porous materials have been introduced. As we all know, elastic modulus is a property that does not vary easily. The reason why porous materials work is that the amount of materials supporting the same cross section area for porous materials is much less than bulk materials. Thus, if the stress is increased deformation is larger and stiffness is smaller. The main idea of porous alloys is to reduce the stiffness. In addition, porous materials can provide better biological fixation by promoting bone tissue ingrowth into the pores of the implants, which enables homogeneous stress transfer between bones and implants [32,33].

Presently, porous titanium and its alloys have become an important aspect of biomaterials. They are attracting broad interest from biomaterial researchers. Ti-based biomaterials with tailored porosity are important for cell adhesion, viability, differentiation and growth. There have been numerous research investigations about different porous coatings and fully porous matrixes [34–38]. Porous titanium and its alloys have already been developed as an alternative orthopedic implantation material to alleviate the inherent problems of bulk metallic biomaterials by reducing stiffness mismatch. Besides, they can obtain long-term biological fixation through complete bone ingrowth.

The fabrication of porous materials has been actively investigated since 1943 [39]. Sosnik first attempted to introduce pores into Al by adding mercury to the melt [39]. However, porous materials being used as biomaterials have been investigated much later. One of the earliest works that mention the concept of applying porous metals to osseointegration was the work of Weber and White in 1972 [40]. Subsequently, numerous researches on porous materials began in the 1970s, including porous ceramics [41], polymers [34,42] and metallic materials [43–45], which were demonstrated to be potential candidates for porous implants in animal experiment. Though porous ceramics and polymers have been studied as scaffold materials, they cannot satisfy requirements under load-bearing conditions [46,47]. Although ceramics portray excellent corrosion resistance, the porous ceramics might fracture due to intrinsic brittleness. Likewise, porous polymeric systems cannot endure mechanical force present in joint replacement surgery. This impels researchers to focus on porous metals due to their superior mechanical strength and good biocompatibility required for load-bearing applications.

Therefore, porous Ti-based alloys are fast emerging as the first choice for biomedical applications. Porous Ti-based alloys exhibit a good combination of mechanical strength with low elastic modulus. Besides, porous structure and rough surface provide better biological fixation and biocompatibility compared with other porous materials [48,49]. Various methods for fabricating porous Ti-based alloys have been studied recently, including investment casting [50], sintering loose titanium powder or fibre [51], slurry sintering [52], rapid prototyping [53], sintering a mixture of titanium powder and space holder method [48].

Mechanical properties and architecture of porous Ti-based alloys can be adjusted to be suitable for human bone through the approaches mentioned above. Therefore, porous Ti-based alloys can overcome the mechanical weakness of porous ceramics and polymeric materials as well as eliminating problems of biomechanical mismatch of elastic modulus. At the same time, they possess interconnected structure to provide space for maintenance of stable blood supply and ingrowth of new bone tissues. Interconnectivity is very important for porous biomaterials, as the connected pores will allow cells to grow inside biomaterials and body fluid to circulate [53]. Thus, high porosity is preferable for porous scaffold biomaterials. However, high porosity causes a decrease in mechanical strength of porous materials [54]. In order to achieve a porous biomaterial combined with high strength and high porosity, some new porous Ti-based alloys were developed [55]. New porous Ti-based alloys are expected to combine high mechanical strength with good biocompatibility to best meet the demands of biomedical implants.

This paper presents an overview of recent research and developments of Ti-based alloys. It can be divided into four main sections, beginning with basic aspects of Ti-based alloys, outlining fundamental properties titanium biomaterial should possess to fulfill the requirements of human bone and its market and application prospects as biomedical implants. This section is followed by discussing all phases and alloying elements in Ti-based alloys and summarizing mechanical properties of various low modulus

β -type Ti-based alloys. The third section considers effect of thermal treatment, grain size, texture and other factors on mechanical properties, describing the status of current β -type Ti-based alloys used as biomaterials and their limitations. This section is followed by discussing influence of microstructural configurations such as microstructure, pore characteristics on the mechanical properties of porous Ti-based alloys, including local and systemic factors that enhance bone ingrowth and biological fixation, which are initial problems associated with porous implant materials. Besides, various methods used for fabricating porous Ti-based alloys with high strength and much lower modulus superior to bulk metallic implants are summarized on the basis of suitability for use in orthopedic implants. This section also reviews the status of porous Ti-based alloys, emphasizing on their current status, future opportunities and obstacles for expanded applications. Overall, efforts have been made to reveal the latest scenario of biomedical Ti-based material.

2. Basic Aspects of Ti-Based Alloys for Biomedical Applications

2.1. Fundamental Requirements of Ti-Based Alloys Used as Biomedical Implants

Biomedical implants are desired to satisfy various requirements demanded by human body, because they could be applied to approximately any organ of human body. The basic properties that an implant should have are biomechanical properties (stiffness, strength, fracture toughness, wear resistance, fatigue strength, corrosion resistance) and biomedical properties (toxicity, surface state, osseointegration) [5,24]. Biomechanical properties should match those of autogenous human tissues without adverse effects.

Ti-based alloys are widely used for manufacturing orthopedic and dental devices under load-bearing applications [56]. One of their major applications is the replacement of worn or damaged joints to restore lost structure and functions of human bone. Higher elastic modulus of biomaterials over human bone can result in bone resorption in the connection part. Since β -type Ti-based alloys possess higher strength and lower modulus compared to α -type or $\alpha + \beta$ -type Ti-based alloys, there is an increasing research interest in developing new generation porous β type Ti-based alloys composed of non-toxic alloying elements. Synthesis of porous equiaxed nanostructured/ultrafine-grained β -type Ti-based alloys with high strength and low modulus may be a major project to be solved in biomedical material field. Entangled titanium wire materials exhibit distinct yielding strength that corresponds to startup of the wire sliding in large scale [57]. Both the yield strength and ultimate strength increase as the porosity decreases. The elastic modulus is very low for this material because of its structural flexibility. Typically, 44.7% porosity corresponds to 75 MPa yield strength, 108 MPa ultimate tensile strength, and 1.05 GPa elastic modulus. The larger porosity also leads to larger average pore size, but results in lower strength and smaller elastic modulus. Generally, the elastic modulus of the entangled titanium wire materials is comparable to that of the cancellous bone, but lower than the cortical bone. It is possible to enhance the stiffness of this material via the entangled wire structure design and the strengthening of the wire cross joints. All these need comprehensive research on the structural mechanics and the fabrication procedures of this kind of material. Presently, one of the principal destinations of biomaterial researchers is to design and select biomaterials based on the specific requirements of human tissue and predict long-term, *in vivo* properties of implants.

Development of new biomaterials is an interdisciplinary effort requiring collaboration between material scientists, biomedical researchers, mechanical engineers, pathologists, pharmacists, traumatologists and clinicians. In order to serve for a longer period without failure, the fundamental properties that biomaterials should possess are as follows.

2.1.1. Mechanical Properties

Mechanical Properties of Human Bones

Age-related bone fractures impose a significant social and economic problem on our increasingly aging population. The age-related mechanical properties of both cortical and cancellous human bone tissues will be reviewed in this section. Cortical bone is a solid, compact tissue constituting the diaphyses of long bones and outer shell of the metaphyses. The macroscopic structure of cancellous bone is composed of an interconnected series of rods and plates. Cortical bone is the dense exterior that confers the majority of strength to bone, and cancellous, or trabecular bone is the relatively porous interior that allows for flow of physiological fluids. The tensile mechanical properties for human cortical bone tissue in relation to age are provided in Table 1 and the ultimate strength and elastic modulus in relation to age, as determined in compression tests, are given in Table 2. Consistent decreases with age for all mechanical properties but not in the tibial specimens. No significant differences were found between the mechanical properties of male and female specimens [58]. The compressive properties of human cancellous bone related to age are listed in Table 3.

Table 1. Tensile properties of human cortical bone. (*N* being the number of bones tested and *n*, the number of machined specimens obtained from them; *—male; **—female; 41.5 and 71—average age value from 36 to 75 years of age, 41.5—a younger group, 71—an older group).

Ref. No.	Age	<i>N</i>	<i>n</i>	Yield strength (MPa)	Ultimate strength (MPa)	Elastic modulus (GPa)	Ultimate strain (%)	Density (g/cm ³)
Fibula								
[12]	41.5	17	20	—	100	19.2	2.10	1.91
[12]	71	17	16	—	80	15.2	1.19	1.73
Humerus								
[13] *	15–89	64	27	—	149	15.6	2.20	1.77
[13] **	15–89	64	16	—	151	16.1	1.90	1.72
Tibia								
[12]	41.5	17	67	—	106	18.9	1.76	1.96
[12]	71	17	34	—	84	16.2	1.56	1.83
[58]	20–89	28	123	129.00	156.71	23.83	3.09	—
Femur								
[12]	41.5	17	35	—	102	14.9	1.32	1.91
[12]	71	17	35	—	68	13.6	1.07	1.85
[13] *	15–89	64	29	—	141	15.2	2.00	1.90
[13] **	15–89	64	30	—	134	15.0	1.80	1.80
[58]	20–89	33	178	114.14	132	16.8	2.83	—

Table 2. Compressive properties of human cortical bone. (*N* being the number of bones tested and *n*, the number of machined specimens obtained from them).

Ref. No.	Tissuesource	Age	<i>N</i>	<i>n</i>	Ultimate strength (MPa)	Elastic modulus (GPa)	Hardness (MPa)
[14]	Tibia osteons (longitudinal)	57/61	2	2	–	22.5	614
[14]	Tibial interstitial lamellae (longitudinal)	57/61	2	2	–	25.8	736
[58]	Femur	20–89	19	95	194	17.6	–
[58]	Tibia	30–89	11	38	195	28.0	–

Table 3. Compressive properties of human cancellous bone (*N* being the number of bones tested and *n*, the number of machined samples obtained from them; 395 specimens for elastic modulus, 183 specimens for ultimate strength and ultimate strain).

Tissue source	Age	<i>N</i>	<i>n</i>	Ultimate strength (MPa)	Elastic modulus (GPa)	Ultimate strain (%)	Mean apparent density (g/cm ³)
Lumbar vertebra [15] (male)	14–89	60	32	4.60	0.06	6.70	0.20
Lumbar vertebra [15] (female)	14–89	60	32	2.70	0.04	6.10	0.20
Tibia head [15] (male)	14–89	60	32	3.90	0.03	8.30	0.22
Tibia head [15] (female)	14–89	60	32	2.20	0.02	6.90	0.22
Tibia [16]	16–83	31	395/183	8.80	0.64	2.20	0.45
Vertebra [16] (vertical)	15–87	42	84	2.5	0.07	7.40	–
Vertebra [16] (horizontal)	15–87	42	84	0.9	0.02	8.50	–
Proximal tibia [59]	59–82	9	121	5.33	0.45	–	0.29
Femur [59]	58–83	10	299	7.36	0.39	–	0.50
Lumbar spine [59]	15–87	42	40	2.45	0.07	–	0.24
Lumbar spine [59]	71–84	3	231	1.55	0.02	–	0.19
Average values				3.85	0.17	6.59	0.28

Researchers [60] have found that the mechanical properties and composition of human cortical bone tissue undergo significant changes in the process of aging. It was found that the mechanical properties do not correlate with the quantitative composition of the bone tissue components in dependence on age. The mechanical properties depend mainly on the ultrastructure of bone tissue, especially on the thickness of the collagen fibrils and dimensions of the mineral crystals. Both these indices increase with increasing age. In childhood, compact bone tissue has greater elasticity and plasticity and less strength and hardness than in the bones of adults. Bones of the aged have reduced elasticity, plasticity, and strength relative to bones of adults.

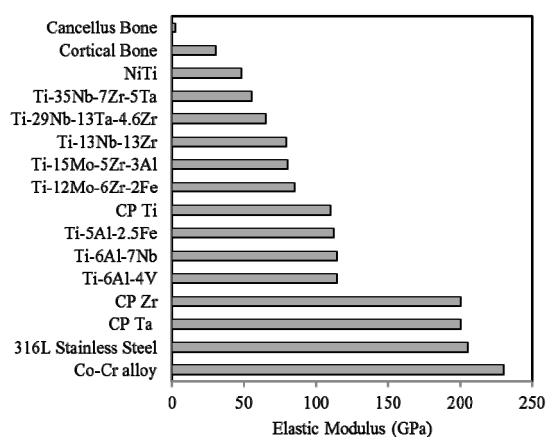
What kind of material will be chosen for a specific biomedical application is decided by the mechanical properties this material possesses. Therefore, the mechanical properties obtained in the designed Ti-based alloys should fulfill requirements of human hard tissues. The elastic modulus and compressive strength of human cortical bone and cancellus bone are approximately 4–30 GPa [61] and 20–193 MPa [62], 0.2–2 GPa and 2–80 MPa [63], respectively. The maximum bending strength for human cortical bone are about 110–184 MPa [51]; yield strength of femoral bone and tibial bone are in the scope of 104–121 MPa and 120–140 MPa [51], respectively. Therefore, titanium and its alloys designed for implantation have to be fulfilled by excellent combination of high strength and low modulus close to the mechanical properties of real human bones.

Stress Shielding

If an implant fractures due to inadequate mechanical strength or mismatch in elastic modulus between bone tissue and implant, this phenomenon is called biomechanical incompatibility. With regard to the biomechanical compatibility, elastic modulus mismatch between bones and implants has already been identified as a major reason for stress shielding of human bones [29–31].

The elastic modulus of the most commonly used biomedical alloys being compared with human bone is shown in Figure 2. The intended applications for most metallic biomaterial are load-bearing orthopaedic joint replacement (hip and knee) and dental implants. Ti-based alloys show much lower elastic modulus than other metallic alloys such as Co-Cr alloy and 316L stainless steel. However, current used implant materials such as stainless steels (190–210 GPa), Co-Cr alloys (210–253 GPa) and Ti-based alloys (55–110 GPa) [61] exhibit a much larger elastic modulus than the tissues they are replacing. Stress shielding [17] occurs due to this stiffness mismatch where the metal carries a majority of applied loads, leaving the more compliant tissue effectively unstressed. In this state, bone will resorb back into the body, a process termed disuse atrophy [63]. Moreover, the stiffness mismatch will lead to excessive relative movement between implant and bone. This prevents stress being transferred from implant material to the neighboring bone. Then, the contact region between implant material and bone will loosen [64] and inhibit new bone formation and ingrowth, thus isolating the implant from their surroundings and preventing the desired implant osseointegration. Generally, elastic modulus of most metallic materials is nearly 10–20 times higher than that of hard tissues.

Figure 2. Elastic modulus of currently used biomedical alloys.

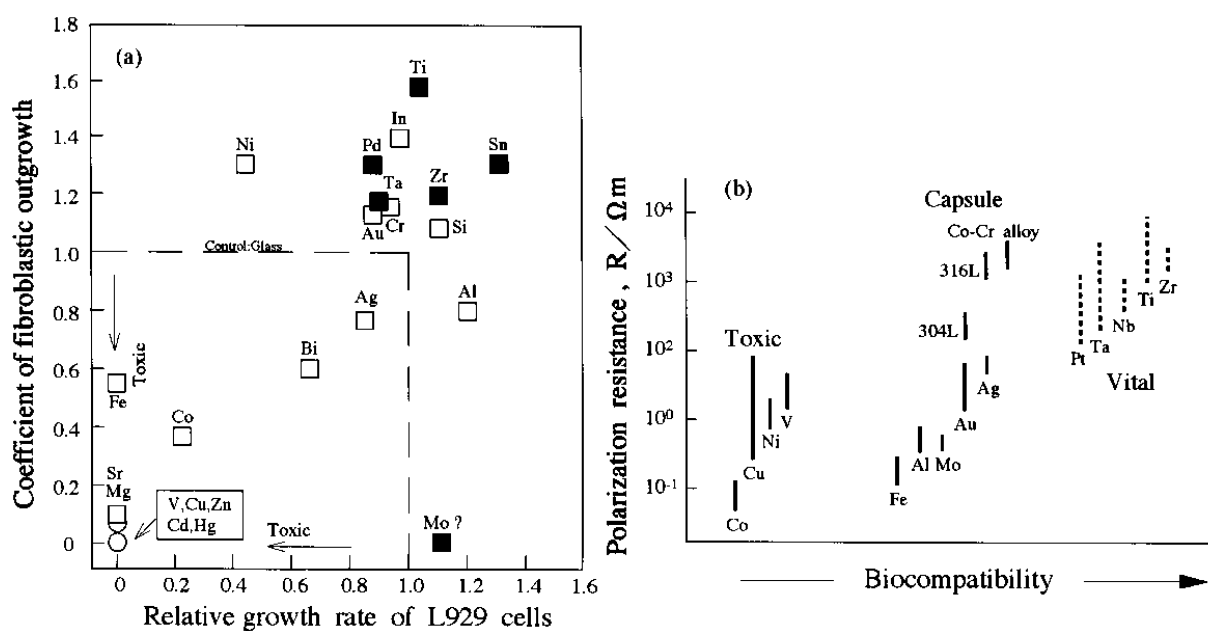


Low modulus alloys are effective in inhibiting bone resorption and enhancing the remodeling of bones, which may be due to the excellent stress transmission between the bone and the implant. Therefore, biomedical implant should have a modulus matching that of human bone to alleviate stress shielding effect.

2.1.2. Biocompatibility

Ideally, biomedical implants are required to be highly innocuous without any inflammatory or allergic reactions in human body. Whether implant surgery is successful mainly depends on the reaction of human body to the implant, which evaluates the biocompatibility of a biomaterial [65]. The reactions deduced from the material and its deterioration in the body environment are the two main factors affecting biocompatibility. Understanding the direct effects of an individual alloying element is of prime importance since it can dissolve in the human body due to tough wear and corrosion, causing local and systemic toxicity, inflammation and immune response. When materials are implanted into human body, a series of reactions happen, and this describes the acceptability of these materials by our system. At present, issues concerning biocompatibility are thrombosis, including blood coagulation and adhesion of blood platelets to biomaterial surface, and the fibrous tissue encapsulation of biomaterials that are implanted in soft tissues. To examine this above-mentioned performance, various tests are introduced into the research extracting from the material, offering screens for genotoxicity, carcinogenicity, reproductive toxicity, cytotoxicity, irritation, sensitivity and sterilization agent residues [66]. Biological safety of metals including cytotoxicity of pure metals and the relationship between polarization resistance and biocompatibility of pure metals, Co-Cr alloy and stainless steels is shown in Figure 3.

Figure 3. Biological safety of metals (a) cytotoxicity of pure metals; and (b) relationship between polarization resistance and biocompatibility of pure metals, Co-Cr alloy and stainless steels [18]. Reprinted with permission from [18]. Copyright 1998 Elsevier.



It is concluded that Ti, B, Mg, Si, P, Ca, Sr, Zr, Nb, Mo, Pd, In, Sn, Ta, Pt, and Au are biocompatible elements [67], while harmful elements include Be, Al, V, Cr, Mn, Fe, Co, Ni, Cu, Zn, and Ag [67]. The toxicity of V has been widely reported. Al is a questionable element on certain disease. The cytotoxicity of pure metals and the relationship between biocompatibility and polarization resistance of typical pure metals and surgical implant materials have been reported by Steinemann [18]. The high cytotoxicity of V and tissue response of capsule (scar tissue) type due to Al has been demonstrated, while Ti, Nb, Ta and Zr exhibit excellent biocompatibility and belong to the loose connective vital group in the type of tissue reaction. Kawahara has also reported that metallic V and Fe are cytotoxic elements, while Ti, Nb, Ta, Zr and Sn are low cytotoxic elements [18]. These trends reported by Steinemann and Kawahara are shown in Figure 3. Ninomi *et al.* [61] have shown that the cell viability of Ti-29Nb-13Ta-4.6Zr is much superior to the Ti-6Al-4V alloy. The non-toxic elements like Nb, Ta, Zr, Mo and Sn were selected for designing new β -type Ti-based alloys with lower elastic modulus, greater strength and corrosion resistance.

Human body is a complicated electrochemical system composed of an aggressive corrosion environment for implants. Because body fluids contain different kinds of corrosive substances and implants are exposed to them. Corrosion resistance is one of the principal properties an implant should possess. The success of an implant depends on the serious inspection of this property which is directly related to its capacity in reacting with the severe body environment. Bad corrosion resistance in the body fluids will cause the release of incompatible metal ions from the implant, which is a main factor leading to allergic and toxic reactions [68]. The consequences of corrosion are the disintegration of the implant and the harmful effect on the surrounding tissues and organs is produced. Surface roughness will increase the functioning area of an implant and raise total amount of corrosion. Therefore, surface finishing is an important element in improving corrosion resistance and consequently biocompatibility of the implant [69]. Besides, wear resistance mainly determines the service period of an implant, for low wear resistance results in implant loosening and wear debris and causes reactions in the tissue where they are deposited [70]. Ti-based alloys with a high coefficient of friction can lead to formation of wear debris and thus result in inflammatory reaction and loosening of the implant [71]. In summary, development of implants with high corrosion and wear resistance is of great importance for the longevity of a biomaterial in our human system. The inability of an implant surface to integrate with the adjacent bone and other tissues due to micromotions can also result in implant loosening [72]. A fibrous tissue is formed between bone and implant, if the implant is not well integrated with the bone [72]. Hence, materials with an appropriate surface are highly essential for the implant to integrate well with the adjacent bone. Surface chemistry, surface roughness and surface morphology all act a critical role in good osseointegration.

Long-term performance of surgical implants is often restricted by their surface properties. Tribological property of titanium and its alloys can be enhanced to a large extent by suitable surface coatings. Surface modification techniques such as physical deposition methods like ion implantation and plasma spray coating, and thermo chemical surface treatments such as nitriding, carburization and boriding have been used to improve the surface hardness of Ti-based alloys [61]. TiN coated hip and knee implants have been found to possess increased wear resistance and good compatibility [73]. However, various coating techniques are under investigation to achieve good adhesion and other required properties [74].

Waviness and porosity of the implant also play a vital role in bone integration. Bone ingrowth into porous surface can cause strong interlocking of surrounding bone tissue with the implant, resulting in improved biomechanical compatibility and high resistance to fatigue loading [42,75]. The size of the pores should be in the range of 100–200 μm for better osseointegration [61]. In addition to porous coatings, development of porous biomaterials to enhance long-term fixation and bone growth have also been tried with great interest. The porous biomaterial is expected to lead to strong interface between the bone and the implant and also the modulus of such porous biomaterial is very low, and thus these materials are expected to overcome the stress shielding effect and loosening of the implants.

A nanosurface seems to be advantageous from the biocompatibility and biomechanical compatibility points of view [61]. Nanocrystalline titanium surface enhances cell growth and exhibits excellent wear resistance due to high hardness and strength. The grain size of metal implant also affects osteoblast adhesion. *In vitro* studies using ultrafine-grained CP Ti (grade 2) and Ti-6Al-4V alloy exhibited increased cell adhesion when compared to conventional coarse-grained (CG) materials. This increase in cell adhesion is attributed to the increase in surface energy at the grain boundaries.

Biomedical implants require a strength level greater than that of bone and an elastic modulus close to that of human bone. Therefore, biomedical Ti-based alloys must exhibit a low elastic modulus combined with enhanced strength, good fatigue resistance and good workability required in hard tissue replacement. The above discussions lead to a strong belief that the new β -type Ti-based alloys are more promising from the wear, corrosion and biocompatibility aspects for biomaterial applications.

2.2. Market and Application Prospects of Ti-Based Alloys for Biomedical Applications

Biomaterials are used in different parts of human body as artificial valves in the heart, stents in blood vessels, replacement implants in shoulders, knees, hips, elbows, ears and dental structures [24,76–78]. It is also used as cardiac simulator and for urinary tract reconstruction. Amongst all these, the number of implants used for spinal, hip and knee replacements are extremely high.

2.2.1. Practice and Current Situation of Ti-Based Alloys in Biomedical Application

Different types of fracture repair mechanisms are known in medical practice. The surgical treatments of bone osteosynthesis are divided into external fracture fixation and internal fracture fixation. With external fracture fixation, the bone fragments are held in alignment by pins placed through the skin onto the skeleton, structurally supported by external bars. With internal fracture fixation, the bone fragments are held by wires, screws, plates, and/or intramedullary devices [79].

Surgical wires are used to reattach large fragments of bone provisionally or permanently to guide large screws during insertion. Screws are the most widely used devices for fixation of bone fragments. The bone immediately adjacent to the screw often undergoes necrosis initially, but if the screw is firmly fixed, permanent secure fixation may be achieved [80]. This is particularly true for Ti-based alloy screws or screws with a roughened thread surface, with which bone ingrowth results in an increase in removal torque [80]. Plates are intended to facilitate fixation of bone fragments. They range from the very rigid to the relatively flexible. The effect of the material on the rigidity of the plate is defined by the elastic modulus of the material for bending, and by the shear modulus for twisting [81]. Thus, given the same dimensions, a Ti-based alloy plate will be less rigid than a stainless steel one, since the elastic modulus

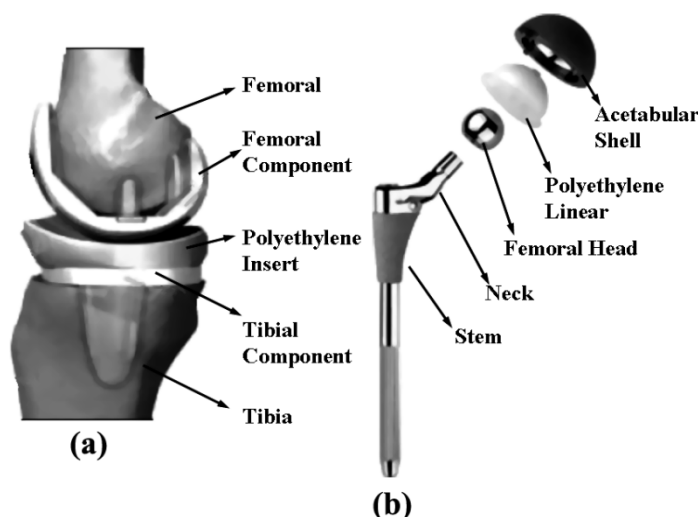
of each alloy is 110 and 200 GPa, respectively. Intramedullary devices (nails or rods) are used as internal struts to stabilize long bone fractures. Nails are better positioned to resist multidirectional bending than a plate compared to plates, since they are located in the center of the bone. However, their torsional resistance is less than that of the plate [81].

The design of an implant for joint replacement should be based on the kinematics and dynamic load transfer characteristic of the joint. Overloading the implant-bone interface or shielding it from load transfer may result in bone resorption and subsequent loosening of the implant [82].

The prosthesis for total knee replacement (TKR) consists of femoral, tibial, and/or patellar components, Figure 4a. Compared to the hip joint, the knee joint has a more complicated geometry and movement mechanics, and it is not intrinsically stable. The eccentric movement of the knee helps distribute the load throughout the entire joint surface [83]. TKRs can be implanted with or without cement, the latter relying on porous coating for fixation. The femoral components are typically made of Co-Cr alloy and the monolithic tibial components are made of ultra-high molecular weight polyethylene (UHMWPE). In modular components, the tibial polyethylene component assembles onto a Ti-based alloy tibial tray. The patellar component is made of UHMWPE and a Ti-based alloy back is added to components designed for uncemented use.

The endoprosthesis for total hip replacement (THR) consists of a femoral component and an acetabular component, Figure 4b. The femoral stem is made of Ti-based alloy or Co-Cr alloy. The femoral head is made of Co-Cr alloy, aluminum, or zirconium. Although Ti-based alloy heads function well under clean articulating conditions, they have fallen into disuse because of their low wear resistance to bone or cement particles. The acetabular component is generally made of UHMWPE.

Figure 4. Titanium orthopedics medical devices: (a) Total knee replacement; (b) Total hip replacement.



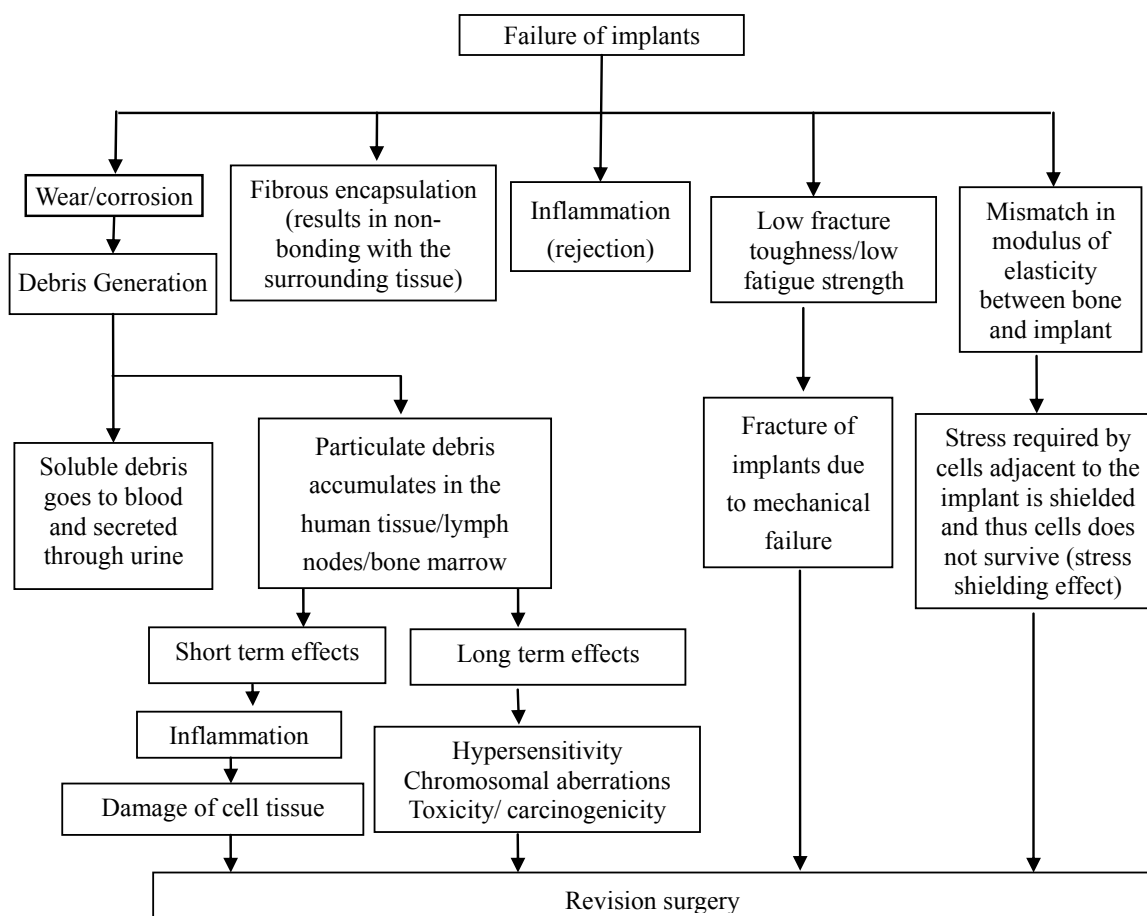
For maxillofacial osteosynthesis in the cranio-facial and mandibular areas, titanium plate and screw systems are preferred. In order to make them pliable, many of the plates are made from CP Ti sheet that is in the soft-recrystallized condition. The corresponding screws are either made from CP Ti or alloy and can be as small as 1 mm in diameter [84].

Traditionally, researchers have used already available materials that had been developed for aerospace or automotive applications, instead of developing new materials tailored specifically for biomedical needs. A typical example is THR, in which a dense metal is used that has a significantly higher density, stiffness and strength than natural bone which is a porous material. The typical lifetime of a THR is 7–12 years, and this lifetime has remained almost constant over the past 50 years, even though significant research and development have gone towards understanding the problem.

Presently, the materials used for these applications are 316L stainless steel, Co-Cr alloys, and Ti-based alloys. Unfortunately, these materials have exhibited tendencies to fail after long-term use due to various reasons depicted in Figure 5. Therefore, there is an increasing demand for improved implants which can perform for a longer lifetime *in vivo*.

The scenario has changed due to the advancements in medical technology. In addition, the prognosis is better for those who are physically traumatized due to sports or incorrect or over exertive exercise habits or due to road traffic and other accidents. Thus, the implants are now expected to serve for much longer period. The development of appropriate material with high longevity and excellent biocompatibility is highly essential.

Figure 5. Various causes for failure of implants that lead to revision surgery [75]. Reprinted with permission from [75]. Copyright 2013 Elsevier.



2.2.2. Market and Application Prospects

Nowadays, THR and TKR surgeries are being carried out with a higher rate on younger and older patients. The revision surgeries of hip and knee implants have also increased. The data collected on total joint replacements surgery estimates that by the end of 2030, the number of THRs will rise by 174% (572,000 procedures) and the number of TKRs is projected to grow by 673% from the present rate (3.48 million procedures) [85]. The total number of hip revision surgery is expected to increase by 137% and knee revision surgery by 607% between 2005 and 2030 [85]. It is projected that approximately 272,000 THRs will be performed annually by 2030. Additionally, approximately 12.8% of the 152,000 THRs performed in 2000 involve revisions of previous hip replacements. Therefore, there is a tremendous demand for the new long-lasting implants.

There are several reasons motivating improvements in joint replacements. Firstly, continual aging of population has brought an ever-increasing need for materials specifically for human body. It has been estimated 90% of population over the age of 40 suffers from degenerative diseases and the aged people population has increased tremendously recently. The United States Census estimates that the total number of people of age 65 and above has increased from 4.9 to 39.7 million between 2002 and 2010; Second, the age range has been broadened to include older patients who have greater incidence of co-morbidities over the last decade; Finally, THRs are now routinely performed on younger patients whose implants would be exposed to greater mechanical stresses due to the more active lifestyle.

An acceptable reason for the increasing number of revision surgeries is due to the higher life expectancy of the implant vs. the ever-increasing life expectancy of the patient. Consistently, over 30% of those requiring THRs have been below the age of 65 and even those over the age of 65 now have a life expectancy of 17.9 years. With normal implant longevity of 12–15 years, the majority of those that receive hip implants at the age of 65 will require at least one revision surgery. So the fact that such a high percentage of joint replacements performed every year are revision surgeries, although troubling, is not surprising.

Human joints suffer from degenerative diseases such as osteoporosis (weakening of the bones), osteoarthritis (inflammation in the bone joints) and trauma. The degenerative diseases lead to degradation of bone due to excessive loading or absence of normal biological self-healing process. Musculoskeletal disorders are most widespread human health problem which costs around 254 billion dollars to the society [86]. Artificial biomaterials are the solutions for these problems, as surgical implantation of the biomaterials of appropriate shapes help in restoring the function of the otherwise functionally compromised structures. These revision surgeries are very expensive and also their success rate is rather small. Moreover, there is still a lack of bone replacement material that is appropriate for restoring lost structure and function, particularly for load-bearing applications. Thus, a very high boom in implant manufacturing is expected in coming years. Ever-increasing demand for implants makes it imperative that development efforts on biomaterials have been accelerated. Among several materials that are currently in use as biomaterials, Ti-based alloys are fast emerging as the first choice for biomedical applications.

Ti-based alloys exhibit low elastic modulus favorable for homogeneous stress transfer between implant and bone [87]. Presently, Ti-based alloys composed of biocompatible alloying elements are being developed mainly for biomedical implants to be used as implant devices replacing failed hard

tissues and dental products, for example, artificial hip joints, artificial knee joints, bone plates, dental implants, crowns, dentures, artificial tooth roots, and screws, *etc.* Ti-based alloys are also expected to be used to fix soft tissue such as blood vessels [88].

3. Low Modulus β -Type Ti-Based Alloys

The development of Ti-based alloys has considered not only the safety of alloy constituent elements but also their mechanical biocompatibility for biomedical applications.

A brief introduction to physical metallurgy of Ti-based alloys is provided as a background for better understanding. Ti exists in two allotropic forms and the microstructure diversity of Ti-based alloys is a result of an allotropic phenomenon. Ti undergoes an allotropic transformation at 882.3 °C. Below this temperature, it has a closed packed hexagonal crystal (HCP) structure, known as α phase, while above 882.3 °C it has a body centered cubic (BCC) structure termed β phase. It may form solid solutions with a number of elements and hence, α phase and β phase equilibrium temperature may be modified by alloying Ti with interstitial and substitutional elements.

Two basic phases in Ti-based alloys are α phase and β phase. After thermal treatment such as annealing, solution treatment, quenching or aging treatment, the β phase can be turned into ω , α' , α'' or undercooling β phase fast cooling from high temperature. ω phase is not desired because it has the highest elastic modulus and α'' is desired for shape memory alloys. The addition of alloy elements can exert significant influences on phase composition and mechanical properties of Ti-based alloys. The concentrations of alloying elements should be less than 20 wt%, as further increase may lead to increase in phase precipitation such as ω phase, which can increase strength and elastic modulus of β -type Ti-based alloys [61].

A systematic study on deformation behavior of Ti-Nb-Ta-Zr alloys with varying composition of Nb and Ta was carried out by Nobuhito *et al.* [20,89–91]. It was shown that behavior of stress-strain in these alloys depends upon Nb and Ta content. The deformation mechanism in Ti-30Nb-XTa-5Zr alloys that contains less than 10 wt% of Ta is identified as stress induced martensite (SIM), while above 10 wt%, it is identified as slip [89]. The concentration of Ta is very critical and has to be maintained within a limited range, because they tend to increase the elastic modulus if varied marginally. Nobuhito *et al.* [20] have observed high elastic modulus of Ti-based alloys with 0 and 20 wt% of Ta and very low elastic modulus for an alloy with 10 wt% of Ta addition (Figure 6). This irregular variation viz., the high modulus of the alloy with 0 wt% of Ta was attributed to the presence of ω phase, while the low elastic modulus of the alloy with 10 wt% Ta was ascribed to the presence of only β phase in the microstructure. Although, the alloy with 20 wt% Ta had only β phase, it exhibits high elastic modulus because the high concentration of Ta in Ti-based alloy tends to behave like pure tantalum metal rather than Ti-based alloy and exhibits elastic modulus equivalent to that of Ta metal itself. It was noted that the tensile strength for 0 and 5 wt% Ta additions were low (Figure 7) in spite of the fact that the microstructure consisted of ω phase in β matrix, possibly due to SIM in these alloys.

Ti-Nb binary alloys with different compositions of Ti-36, 40%, and 44% Nb (wt%) were prepared by arc-melting with a nonconsumable electrode in an argon atmosphere [92]. The arc-melted buttons were cold rolled to 4 mm thickness and homogenized in vacuum at 1423 K for 24 h. The annealed plates were again cold rolled to 1.5 mm thickness and solution treated at 1223 K for 30 min in an evacuated quartz

tube, and then quenched in ice water. Composition dependence of Young's modulus in quenched binary Ti-Nb alloys exhibits a minimum arising from athermal ω phase formation at lower alloying contents, and an increase in β phase stability at higher alloying contents. Young's modulus increases by isothermal ω formation on aging at 573 K, as shown in Figure 8. A minimum in Young's modulus vs. Nb content plot is clearly seen after aging.

Figure 6. Effect of Ta addition on elastic modulus of Ti-30Nb-XTa-5Zr alloy [89]. Reprinted with permission from [89]. Copyright 2005 Elsevier.

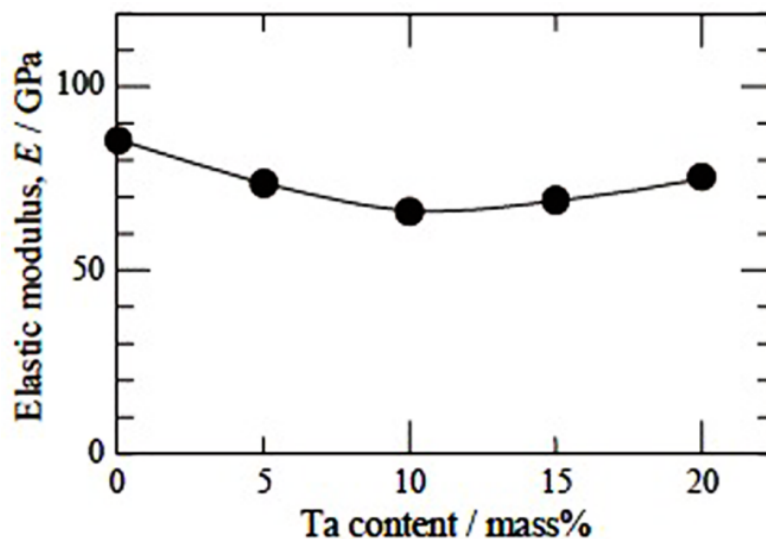


Figure 7. Effect of alloying addition on tensile strength of Ti-XNb-XTa-5Zr [89]. Reprinted with permission from [89]. Copyright 2005 Elsevier.

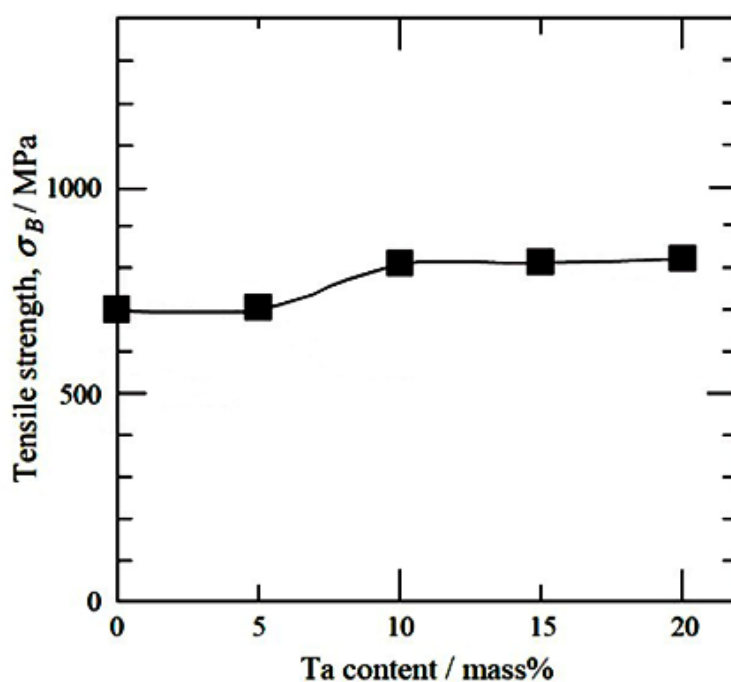
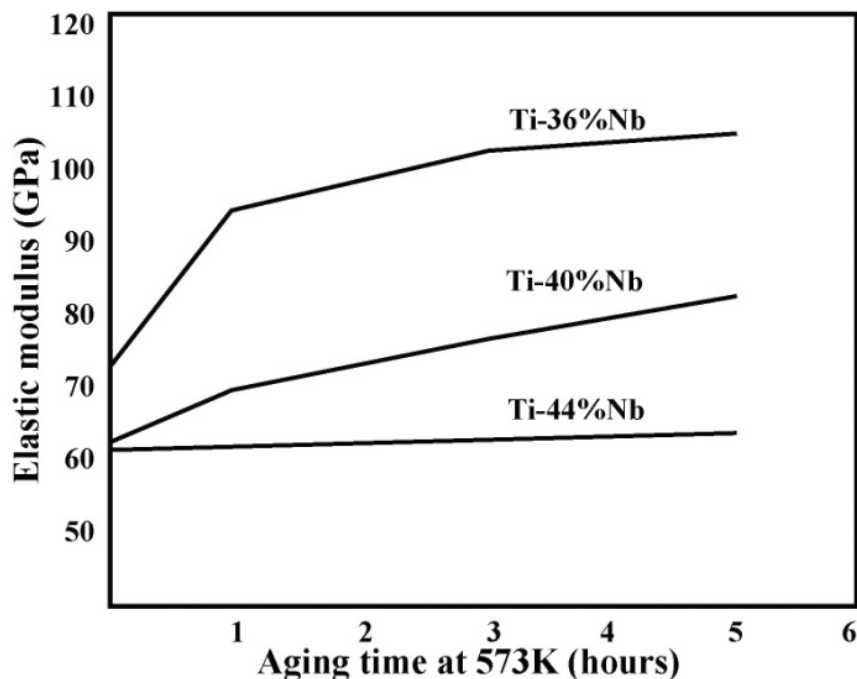


Figure 8. Aging time dependence of Young's modulus of Ti-36, 40%, and 44% Nb binary alloys at 573 K ([92], modified). Reprinted with permission from [92]. Copyright 2005 ASM international (for individual use).



These elastic properties can be reached using both lowering of the intrinsic modulus by specific chemical alloying and superelastic effects. The thermoelastic martensitic transformation from the high temperature bcc- β phase to the orthorhombic α'' phase gives rise to superelastic and shape memory behavior. For the vast majority of superelasticity and shape memory applications in biomedicine, Ti-Ni-based alloys are utilized. However, the long-term contact of Ni with human body is associated with adverse effects, such as allergic reactions. Thus, alloys with α'' phase are potential candidates to replace TiNi alloys [93].

The properties of Ti-based alloys are sensitive to their phases/crystal structure, and certain phases may be stabilized by the addition of alloying elements [94]. A good candidate for alloying is Zr, which is a neutral element when dissolved in Ti and it can enhance strength and improve elasticity of alloys [95]. On the other hand, zirconium is a material of interest for surgical implants because it shows acceptable mechanical strength, satisfactory biocompatibility, good osseointegration and good corrosion resistance [96]. More studies comparing zirconium and titanium implants showed that the degree of bone implant contact is actually higher in the case of Zr [97]. Both Zr and Ti belong to the same group in the periodic table of elements and the Ti-Zr system shows as a complete solid solution [98]. Nb, acting as a β -phase stabilizing element and a biocompatible element, has attracted much attention to take great deal of efforts on it and it has been added to many β -type Ti-based alloys and near β -type Ti-based alloys.

Ti alloying elements fall into three class: α -stabilizers, β -stabilizers and neutral. The alloying elements (Al, O, N, *etc.*) that tend to stabilize α phase are called α -stabilizers and the addition of these elements lead to an increase in the allotropic transformation temperature (ATT), while elements that stabilize β phase are known as β stabilizers (Nb, Ta, Mo, Mg, V, W, Fe, Ni, Cr, Co, Mn, Cu, *etc.*) and addition of these elements depresses the β transus temperature. If no significant change in the ATT is observed, the alloying elements are defined as neutral elements (Zr, Sn and Si). Addition of α and β stabilizers to Ti gives rise to a field in the corresponding phase diagram where both α and β phase may coexist. According to the nature of their microstructure, Ti-based alloys may be divided as α -type alloys, β -type alloys and $\alpha + \beta$ -type alloys. β -type alloys may be further classified into near β and metastable β alloys. Microstructure contains HCP α phase can be divided into CP titanium alloys, α titanium alloys and near α titanium alloys.

Analysis of slip systems in different crystal structures reveals that plastic deformation is easier in BCC crystal structure than in HCP structure. It explains enhanced ductility of β phase when compared to α phase. Since HCP structure exhibits a higher slip distance than BCC structure, it is possible to conclude that the atomic planes slip or the plastic deformation is easier in BCC structure than HCP structure. Hence, β -type Ti-based alloys present the best formability and ductility among the Ti-based alloys. The low modulus of β -type alloys is caused by the fact that the elastic modulus of BCC β phase is lower than that of HCP α phase. Since high modulus of $\alpha + \beta$ -type Ti-based alloys results in bone resorption and implant loosening, lower modulus alloys that retain a single β phase microstructure are attracting a great deal of interest.

It is of utmost importance that porous materials have a biocompatible chemical composition to avoid adverse tissue reaction. This is a feature of clinical significance for materials implanted in long-term clinical situations in both human and veterinary medicine as there have been some links between prolonged exposure to non-biocompatible materials and neoplastic tissue responses [99]. Toxic elements which can cause adverse body reactions include Be, Al, V, Cr, Mn, Fe, Co, Ni, Cu, Zn, and Ag, as shown in Figure 3. Alloys containing elements such as Nb, Zr, Ta, Pt, and Ti are being extensively evaluated since these are the only five elements that have been identified as producing no adverse tissue reaction [24,100]. Therefore, β stabilizing elements which can be used for implants are mainly Nb, Ta, Mo and Mg. Neutral elements such as Zr and Sn are good biocompatible elements and often considered as β alloying elements. In Ti-based alloys, Nb is a β -stabilizer [5]. The addition of Nb could improve the strength keeping the elastic modulus low [101]. In particular, Wang *et al.* [102] have fabricated a porous Ti-10Zr-10Nb alloy with a porosity of 69% which exhibits an elastic modulus of 3.9 GPa and a compressive yield strength of 67 MPa, resembling the mechanical properties of cortical bone. However, as mechanical properties of human bone are highly variable according to species, age, anatomical site, liquid content, *etc.* Once the porosity of the implant is selected, it is useful to study the possibility to adjust the values of the modulus and compressive yield strength by changing the amount of a minority element, as Nb, in the Zr-Ti alloys given that they are promising biomaterials because of their biocompatibility.

The mechanical properties of typical α -, $\alpha+\beta$ - and β -type Ti-based alloys are listed in Table 4. The β -type Ti-based alloys possess more excellent combination of high strength and low modulus as well as higher plasticity compared with α - or $\alpha+\beta$ -type Ti-based alloys. The authors [103] have confirmed the advantage of biomaterials with a low modulus with regard to bone healing and remodeling by using

rabbits, and finally prove that the low modulus β -type Ti-based alloys can better improve the stress transmission between the bone and the implant. It is effective in inhibiting bone resorption and enhancing the remodeling of bones. This has stimulated biomedical researchers to develop an optimized prosthesis that mimics human bone and the development of low modulus β -type Ti-based alloys with biocompatible alloying elements [18,24].

In recent years, a large number of biomaterial researchers have produced various β -type Ti-based alloys, among which Ti-Mo-based, Ti-Nb-based, Ti-Zr-based, Ti-Ta-based alloys are the systems that had been studied intensively [104–106]. The Ti-Nb-based alloys are attracting more researchers to study due to their low modulus, good biocompatibility and shape memory effect [61]. Zou *et al.* [107] produced TiNbZrTaFe alloy and achieved compressive elastic modulus as low as 52 GPa with yield strength of 2425 MPa and distinct plasticity. Very recently, the low cost β -type Ti-based alloys composed of low cost elements such as Fe, Cr, Mn and Sn have been proposed to reduce the consumption of high cost elements such as Nb, Ta and Zr. Examples of these alloys include Ti-Mn [108], Ti-Mn-Fe [109], Ti-Sn-Cr [110], Ti-Cr-Sn-Zr [111], Ti-(Cr, Mn)-Sn [112], Ti-Zr-Sn-Mo-Nb [113], Ti-12Cr [114] and Ti-31.0Fe-9.0Sn [115]. Among the early low modulus β -type Ti-based alloys [116], Ti-13Nb-13Zr, Ti-15Mo and Ti-12Mo-6Zr-2Fe have already been registered, while Ti-15Mo-5Zr-3Al has been registered in JIS T 7401-6, and Ti-35Nb-7Zr-5Ta will be registered in the ASTM standardization. Besides, new β -type Ti-based alloys with high strength and low modulus, for example, Ti-29Nb-13Ta-4.6Zr [117], Ti-24Nb-4Zr-7.9Sn [118], $\text{Ti}_{65.5}\text{Nb}_{22.3}\text{Zr}_{4.6}\text{Ta}_{1.6}\text{Fe}_6$ [107], are also being investigated for biomedical applications.

Ti-based alloys display a variety of properties which are connected to chemical composition and metallurgical processing [119–125]. The details of phase transformation and processing-microstructure-property relationships are reviewed in several papers and books [20,89,126–128]. Selected low modulus β -type Ti-based alloys newly developed for biomedical applications are given in Table 5. The elastic modulus is also shown in Table 5, together with an indication of the processing methods employed. The elastic modulus corresponds to the stiffness of a material and is associated to interatomic forces in the crystal structure. Addition of β -stabilizers allows β phase stabilization and hence causes low elastic modulus. While CP Ti shows elastic modulus values close to 105 GPa, Ti-6Al-4V α + β -type alloy presents the value of about 110 GPa, and β -type Ti-based alloys may present the values as low as 52 GPa [107]. When compared with common alloys used as biomaterials, such as 316L stainless steel (190–210 GPa) and Co-Cr alloys (210–253 GPa) [61], low elastic modulus Ti-based alloys display a more compatible behavior to human bone [17]. The mechanical, wear and corrosion properties of a material are largely dictated by its microstructure, grain size and are directly related to its composition. This makes Ti-based alloys highly amenable to tailor its properties as specific requirements. Though the structure property correlations have been well developed and addressed for structural Ti-based alloys, the effect of grain size and texture on properties is sparsely addressed. Hence, the variations in properties of the Ti-based alloys based on the grain size and texture will be discussed in detail in the next section.

Table 4. Mechanical properties of typical α -, $\alpha+\beta$ - and β -type Ti-based alloys for biomedical applications.

Alloy Designation (wt%)	Tensile Strength (MPa)	Yield Strength (MPa)	Elongation (%)	Elastic Modulus (GPa)	Standard
α-type					
CP Ti grade 1 [120] (annealed)	240	170	24	102.7	ASTM F 67 (ISO 5832-2) [3]
CP Ti grade 2 [120] (annealed)	345	275	20	102.7	ASTM F 67 (ISO 5832-2) [3]
CP Ti grade 3 [120] (annealed)	450	380	18	103.4	ASTM F 67 (ISO 5832-2) [3]
CP Ti grade 4 [120] (annealed)	550	485	15	104.1	ASTM F 67 (ISO 5832-2) [3]
$\alpha+\beta$-type					
Ti-6Al-4V ELI [120] (annealed)	860–965	795–875	10–15	101–110	ASTM F 136 (ISO 5832-3) [3]
Ti-6Al-4V [120] (annealed)	895–930	825–869	6–10	110–114	ASTM F 1472 (ISO 5832-3) [3]
Ti-6Al-7Nb [120] (wrought)	900–1050	880–950	8.1–15	114	ASTM F 1295 (ISO 5832-11) [3]
Ti-5Al-2.5Fe [120] (cast)	1020	895	15	112	ISO 5832-10 [3]
β-type					
Ti-13Nb-13Zr [120] (aged)	973–1037	836–908	10–16	79–84	ASTM F 1713 [116]
Ti-12Mo-6Zr-2Fe [120] (annealed)	1060–1100	1000–1060	18–22	74–85	ASTM F 1813 [116]
Ti-15Mo [120] (annealed)	874	544	21	78	ASTM F 2066 [116]
Ti-15Mo-5Zr-3Al [120] (solution treated/aged)	852–1100	838–1060	18–25	80	JIS T 7401-6 [116]
Ti-35Nb-7Zr-5Ta [120] (annealed)	597	547	19	55	Task Force F-04.12.23 [116]
Ti-16Nb-10Hf [120] (aged)	851	736	10	81	–
Ti-29Nb-13Ta-4.6Zr [120] (aged)	911	864	13.2	80	–
Ti-15Mo-2.8Nb-0.2Si [120] (annealed)	979–999	945–987	16–18	83	–
Ti-24Nb-4Zr-7.9Sn [118] (hot-rolled)	830	700	15	46	–
Ti-24Nb-4Zr-7.9Sn [118] (hot-forged)	755	570	13	55	–
Ti-24Nb-4Zr-7.9Sn [118] (selective laser melting)	665	563	14	53	–
Ti-35Nb-7Zr-5Ta-0.4O [75] (annealed)	1010	976	19	66	–
Ti _{65.5} Nb _{22.3} Zr _{4.6} Ta _{1.6} Fe ₆ [107] (sintering/960 °C/0 min)	–	2425	6.91	52	–

Table 5. Selected low modulus β -type Ti-based alloys newly developed for biomedical applications.

β -type Ti-based alloys	Preparation method	Modulus/GPa
Ti-29Nb-13Ta-4Mo [18]	Melting/Solutionized/Aged	50–80
Ti-29Nb-13Ta-6Sn [18]	Melting/Solutionized/Aged	65–70
Ti-29Nb-13Ta-4.6Sn [18]	Melting/Solutionized/Aged	55–78
Ti-29Nb-13Ta-2Sn [18]	Melting/Solutionized/Aged	45–48
Ti-30Nb-10Ta-5Zr [90]	Sintering/Hot-forged and swaged/HT	66.9
Ti-35Nb-4Sn [129]	Melting/Cold rolling/HT	42–55
Ti-30Zr-3Cr-3Mo [130]	Solution treated/Cold rolling	66/78
Ti-12Mo-3Nb [131]	Melting/Solubilized	105
Ti-12Mo-5Ta [131]	Annealed	74
Ti-50Ta [132]	Solution treated/Aged	77/88/93
Ti-50Ta [132]	Solubilized	88
Ti30Zr (5,6,7)Mo [133]	Solution treated	75/63/66
Ti30Zr (5,6,7)Mo [133]	Cold rolling	59/61/73
Ti-36Nb-2.2Ta-3.7Zr-0.3O (at%) [134]	High pressure torsion	43–65
Ti-31.0Fe-9.0Sn [115]	Cast	147
Ti-39.3Nb-13.3Zr-10.7Ta [115]	Cast	71
Ti-25Nb-11Sn [135]	Swaged	53
Ti-12Mo-5Zr [136]	Solution treated	64
Ti-25Nb-2Mo-4Sn [137]	Cold rolling/aged	65

4. Thermal Treatment, Grain Size, Microstructure and Mechanical Properties in Ti-Based Alloys

4.1. Effect of Thermal Treatment on Grain Size and Texture and the Influence of Grain Size and Texture on Cells

In general, the elastic modulus decreases, so does the mechanical strength. Mechanical strength may be increased by adding alloying elements or through heat treatments, which may lead to solid solution strengthening or even, precipitation of second phases. For example, CP Ti has yield strength between 170 and 485 MPa, while Ti-based alloys may reach 2500 MPa [107]. Besides, by using ageing processes, metastable structures obtained by rapid quenching from β field may give rise to fine precipitates, which considerably increases the mechanical strength. Ti-based alloys present a high specific strength, which is higher than most steels.

Heat treatment is mainly applied to $\alpha + \beta$ and β -type Ti-based alloys due to the α - β transformation (typically in the β isomorphous titanium alloy group). Strength of the annealed alloys increases gradually and linearly with increasing alloy contents. Quenching from the β phase field gives a martensitic transformation with improved strength (depending on composition). For lowly alloyed Ti-based alloys, rapid quenching from the β phase field gives maximum strength at M_f . For highly alloyed Ti-based alloys, rapid quenching from β phase field gives lowest strength but after ageing, the maximum strength is obtained.

Representative properties for several β -type Ti-based alloys together with their microstructures are presented in Table 6. Alloy chemistry, structural constituent and microstructure as well as grain size appear to have significant influence on properties of Ti-based alloys. In metastable β -type Ti-based alloys, β phase is usually retained on quenching and very fine α precipitates are retained on aging at lower temperatures, which leads to extremely high strength in these alloys. The β -type Ti-based alloys are generally solution treated in the β phase field and aged to decompose the metastable phases to achieve high strength. In spite of the fact that a variety of microstructures can be formed in β -type Ti-based alloys by appropriate heat treatments, in particular, equiaxed structure in the β alloys is tried with great interest, as equiaxed structure are found to possess best combination of mechanical properties in $\alpha + \beta$ -type Ti-based alloys [138,139].

Table 7 shows equiaxed microstructures provide high strength and ductility and relatively low fracture toughness, whereas lamellar structure provides good fracture toughness but with some compromise on strength and ductility [140–142]. The lamellar structure listed in Table 7 was typically produced following solution treatment above the β transus, followed by air cooling, and aging between 700 and 800 °C. Solution annealing below the β transus between 800 and 925 °C resulted in an equiaxed structure. Finally, the bimodal structure might be developed by solution treatment below the β transus, typically between 900 and 950 °C followed by air cooling and aging below 700 °C. In these Ti-6Al-4V alloys, the equiaxed microstructure has high tensile strength and ductility, and excellent resistance to fatigue crack initiation, while the Widmanstätten microstructure has high creep strength, fracture toughness, and excellent resistance to crack propagation [141]. Bimodal microstructure has the highest fatigue strength followed by the equiaxed structure, and the lamellar microstructure has the lowest fatigue resistance [140]. Within each of these microstructure categories, finer microstructures result in higher fatigue strength [140].

Recently, some plastic processes have been attempted to develop fine-grained structure in grade 2 CP Ti [140], which resulted in enhanced hardness, higher yield strength (increase by 140%) and higher fatigue strength (increase by 100%) compared to its CG counterpart as shown in Table 8. The strengthening of grade 2 CP Ti listed in Table 8 utilized equal channel angular pressing (ECAP) in combination with other deformation processes. Procedures examined included ECAP (8 passes) at 400 °C (#1), ECAP + 65% cold rolling (#2), and ECAP + rolling followed by annealing at 300 °C for 1 h (#3). He *et al.* [143] also revealed that combination of high strength and low modulus can be obtained in Ti₆₀Cu₁₄Ni₁₂Sn₄Nb₁₀ alloy by proper combination of composition design and production method. A novel combination of bimodal microstructure composed of a micrometer-sized dendritic bcc- β -Ti(Nb,Sn) phase and a nano/ultrafine structured matrix is obtained in this alloy by using different fabrication methods which are casting, melting, and casting and subsequent 700 °C annealing, respectively. The matrix is composed of B2, β -Ti, γ -TiCu, and a few intermetallics. A summary of the mechanical properties of these samples is listed in Table 9. This bimodal structure possessed high strength of the nano/ultrafine-structure and the good ductility of the BCC-structured dendrites.

The Ti-29Nb-13Ta-4.6Zr following water quenching from the β -phase field displays a mixture of β phase and orthorhombic martensite (α'') and has an elastic modulus of 65 GPa [144,145]. The average β grain size and the volume fraction of martensite have an important influence on this material's mechanical properties (Figure 9). Study shows that ultrafine-grained titanium alloys exhibit higher abrasion resistance than CG titanium [144].

Table 6. Phases formed in β -type Ti-based alloys under different heat treatments. (SA: single aging; DA: double aging; ST: solution treated; WQ: water quenched; AC: annealed condition; HT: heat treated).

Alloy composition	Heat treatment history	YS (MPa)	Modulus (GPa)	Microstructure
Ti-35Nb-7Zr-5Ta-(0.06-0.07)O[61]	β ST/WQ + aging	530	–	β phase with average grain size of about 60 μm
	Low temperature aging (SA)	630	–	Fine ω phase
	Double aging at low temperature (DA)	1202	–	Fine α and ω phase
Ti-30Nb-10Ta-5Zr [61]	HT/850 °C/30 min/AC	804	66.9	Equiaxed β phase with grain diameter of 62.3 μm
Ti-13Nb-13Zr [100]	$\alpha+\beta$ ST/WQ	–	80	Primary alpha and transformed beta
	WQ from β field	–	65	Metastable β phase and orthorhombic martensite
Ti-29Nb-13Ta-4.6Zr [100]	β ST/WQ	250	63	Metastable orthorhombic martensite
	β ST at still lower temperature/WQ	400	62	Metastable orthorhombic martensite
	Lower temperature aging	1100	97	Metastable orthorhombic martensite
Ti _{65.5} Nb _{22.3} Zr _{4.6} Ta _{1.6} Fe ₆ [107]	HT/960 °C/0 min	2425	52	dual β structure with average grain size of 200–300 nm

Table 7. Tensile properties of the Ti-6Al-4V alloys [61]. Reprinted with permission from [61]. Copyright 2009 Elsevier.

Microstructure	Yield Strength (MPa)	Ultimate Tensile Strength (MPa)	Elongation (%)	Reduction in area (%)	K _{1C} (MPa·m ^{1/2})
Equiaxed (Std)	951	1020	15	35	61
Lamellar (Std)	884	949	13	23	78
Equiaxed (ELI)	830	903	17	44	91
Equiaxed (CMG)	1068	1096	15	40	54

Std: wt(Al)% = 5.5%–6.75%, wt(V)% = 3.5%–4.5%, wt(Fe)% = 0.30 Max%, wt(O)% = 0.15%–0.20%, wt(N)% = 0.05 Max%, wt(C)% = 0.10 Max%, wt(H)% = 0.015 Max%; For ELI Grade: lower oxygen and aluminum contents, wt(O)% = 0.13 Max%, wt(Al)% = 5.5%–6.2%; For CMG Grade: higher oxygen content, wt(O)% = 0.18%–0.20%.

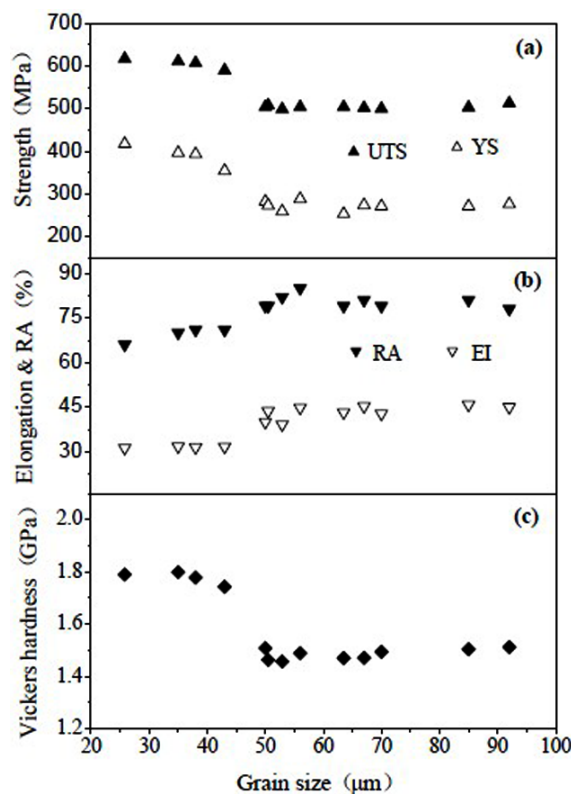
Table 8. Microhardness, tensile mechanical properties and fatigue limit of grade 2 CP Ti in different states [140]. Reprinted with permission from [140]. Copyright 2006 Elsevier.

State (structure type)	HV (MPa)	UTS (MPa)	YS (MPa)	EI (%)	RA (%)	Fatigue Limit (MPa)
Original coarse-grained	1800	460	380	26	60	238 ± 10
Ultrafine-grained #1 (Equiaxed, submicron-grained)	2700	710	625	14	60	403 ± 8
Ultrafine-grained #2 (Fibrous, with high dislocation density)	2821	960	725	10	45	434 ± 5
Ultrafine-grained #3 (subgrained with internal cells)	2850	110	915	9	40	500 ± 8
Ti-6Al-4V ELI (annealed)	–	965	875	10–15	25–47	515

Table 9. Summary of the compressive test data: elastic modulus E , yield strength σ_y , strain at the yield point ϵ_y , ultimate compression stress σ_{max} , and plastic strain ϵ_p [143]. Reprinted with permission from [143]. Copyright 2005 Elsevier.

Fabrication methods	Status	E (GPa)	σ_y (MPa)	ϵ_y (%)	σ_{max} (MPa)	ϵ_p (%)
As-cast	Φ3 mm-diameter cylinder	66	1312	2.2	2401	14.1
As-arc melted	50 g bar	59	1052	2.0	2345	21.1
As-cast/700 °C annealing	Φ3 mm-diameter cylinder	111	1620	1.7	2072	1.4

Figure 9. Effect of grain size on (a) yield strength and ultimate tensile strength; (b) on elongation and reduction in area; and (c) on vickers hardness of Ti-29Nb-13Ta-4.6Zr ([144], modified). Reprinted with permission from [144]. Copyright 2002 Springer.



The first report on the effect of thermomechanical treatment on the development of equiaxed structure in Ti-13Nb-13Zr (T1) came out from the work of Geetha *et al.* [146]. Their work consisted of development of equiaxed structure in two other new near β -type Ti-based alloys, namely Ti-13Nb-20Zr (T2) and Ti-20Nb-20Zr (T3) [127]. The three alloys T1, T2 and T3 were prepared by non-consumable vacuum arc melting technique and melting was repeated six to seven times to ensure chemical homogeneity. The pancakes were thereafter subjected to hot-rolling. The T1 alloy was hot-rolled in $\alpha + \beta$ phase field at 680 °C from 12 to 4 mm thickness. On the other hand, the alloys T2 and T3 were initially rolled in the β phase field at 800 °C from 12 to 9 mm and thereafter rolled in the $\alpha + \beta$ phase field at 620 °C to 5 mm thick sheets. Hot-rolling in $\alpha + \beta$ phase field leads to the formation of equiaxed structure in all the three alloys. The selection of appropriate processing for Ti-13Nb-20Zr and Ti-20Nb-20Zr alloys resulted in fine equiaxed structure, while a mixture of coarse equiaxed and elongated grains was observed in the case of Ti-13Nb-13Zr alloy. The presence of Nb in these alloys enabled working of these alloys at low temperatures, which led to the formation of fine equiaxed structure [127,146].

Recently, a material forming method by coupling powder consolidation with crystallization of amorphous phase was introduced to obtain equiaxed ultrafine-grained structure in $\text{Ti}_{65.5}\text{Nb}_{22.3}\text{Zr}_{4.6}\text{Ta}_{1.6}\text{Fe}_6$ alloy with an excellent combination of strength and ductility [107]. This developed biomedical alloy has a dual β -type structure, namely hard bcc β -Ti matrix surrounding soft bcc FeTi reinforcing phase. This alloy displays excellent combination of high fracture strength of 2650 MPa and fracture strain of 8.2% as well as extreme low elastic modulus of 52 GPa. As expected, they should have better biocompatibility than that of their CG counterparts [147].

The elastic modulus of β -type alloys depends on the amount of β phase present in the structure. Besides, the origin of α phase and other microstructural feature also decides mechanical properties. The presence of fine α phase is not always associated with increase in strength and modulus. For example, aging of Ti-34Nb-9Zr-8Ta results in low strength and modulus and this is attributed to dissolution of the ordered B2 phase [23]. The B2 phase in homogenized conditions possesses higher hardness than the aged condition. In contrast, in Ti-13Mo-7Zr-3Fe alloy, both strength and modulus increase upon aging due to precipitation of fine α from ω in the β native [23]. Interestingly, in case of another alloy Ti-15Mo, the strength decreases due to the absence of nanometer scale ω phase on aging and the modulus increases due to high volume fraction of fine α [23]. Besides, the elastic modulus depends on the crystal orientation. Therefore, the elastic modulus of low modulus β -type Ti-based alloys can be lowered by control the texture. A single crystal of the low modulus β -type Ti-based alloy Ti-29Nb-13Ta-4.6Zr oriented in the $\langle 100 \rangle$ direction exhibits a lower elastic modulus (35 GPa) than those oriented in other directions, such as $\langle 111 \rangle$ and $\langle 110 \rangle$ [148]. In this case, the elastic modulus is similar to the top of the range for bone (around 30 GPa).

The addition of alloy elements can also exert significant influences on mechanical properties of Ti-based alloys. Variation in the mechanical properties of Ti-Nb-Ta-Zr system with varying alloying concentrations could be attributed to various deformation mechanisms operating in these alloys (Table 10). The Nb/Ta ratio *versus* Zr content of the Ti-35Nb-7Zr-5Ta alloy is represented in a two-dimensional diagram (Figure 10) that assumes a four-component alloy system based on the alloy development work by the principal investigators [149], so as to obtain a minimum elastic modulus (steep iso-contour lines of constant moduli in Figure 10).

In addition, the introduction of oxygen, which is usually thought of as an important interstitial element, must be controlled in a fairly narrow range for little addition of oxygen content is able to greatly influence mechanical properties, aging and phase transformation behaviors of Ti-based alloys. O is a strong α stabilizer [150]. The intrinsic properties of an alloy with a practical chemical composition of about Ti-35Nb-7Zr-5Ta-(0.05–0.68) O are investigated [151]. Ti-35Nb-7Zr-5Ta with 0.06 wt% O, has much lower elastic modulus, 55 GPa, than the more recently developed alloys [152]. Table 11 illustrates the tensile properties achievable in this alloy after different aging treatments for three different oxygen contents. These materials were hot forged, rolled to 16 mm diameter rods, solution treated at 850°C (0.06 wt% O), 840°C (0.46 wt% O), and 900°C (0.68 wt% O) for 1 h, water quenched, and aged at 427°C or 538°C for 8 h followed by air cooling. Additional samples were pre-aged at 260°C for 4 h prior to aging at 427°C for 8 h to examine what benefits might be accrued by duplex aging. Yield strength can be increased at fixed oxygen content, either by single or duplex aging, and this increase is accompanied by a slight decrease in tensile elongation. An increase in the oxygen content from 0.06 wt% to 0.46 wt% O also increases the solution treated yield strength from 530 to 937 MPa with a slight decrease in elongation from 21% to 19%. It is notable, however, that this increase in the yield strength is accompanied by an increase in the elastic modulus, 63 GPa [152]. Additionally, this increase in the oxygen content also increases the fatigue strength of the alloy in the solution treated condition from 275 to 450 MPa (Figure 11). The oxygen content of Ti-35Nb-7Zr-5Ta strongly influences its aging behavior and hence its mechanical properties. Qazi *et al.* [153,154] have recently carried out extensive studies on the influence of oxygen (ranging from 0.06 wt% to 0.68 wt%) and duplex aging on the phase transformation behavior of the Ti-35Nb-7Zr-5Ta alloy. They observed that 0.68 wt% O completely suppresses the ω phase formation and concluded that the high yield strength of the alloy was due to the presence of the fine α precipitates only. Increasing oxygen above a certain (>0.46 wt%) level inhibits ω phase formation by oxygen occupying the interstitial sites within the β and resisting atomic displacements that can lead to ω formation. In addition, increase in α precipitates in the absence of ω phase has been attributed to the formation of oxygen rich clusters within the prior β grain boundaries and these clusters act as nucleation sites for a precipitation.

Table 10. Effect of alloying addition on the mechanical properties of β -type Ti-Nb-Ta-Zr alloys [61]. Reprinted with permission from [61]. Copyright 2009 Elsevier.

Alloying addition	Tensile strength (MPa)	Yield strength (MPa)	Elongation (%)	Reduction in area (%)	Elastic modulus (GPa)
Ti-30Nb-XTa-5Zr (0–20 Ta)	698–823	572–798	19.3–43.8 (decreases with increase in Ta)	51.3–73.0 (decreases with increase in Ta)	74.8–85.2 (decreases with increase in Ta)
Ti-XNb-10Ta-5Zr (20–35 Nb)	742–806 (decreases with increase in Nb)	704–779 (decreases with increase in Nb)	11.6–22.6	19.0–62.4	–
Ti-XNb-13Ta-4.6Zr (29–39 Nb)	612–715 (decreases with increase in Nb)	590–600	15–22	–	–
Ti-35Nb-7Zr-5Ta-XO (0.06–0.68)	590–1074	–	21–27	47–69	–

Figure 10. Modulus map for Ti-35Nb-7Zr-5Ta based on Nb/Ta ratio vs. Zr content [151]. Reprinted with permission from [151]. Copyright 2006 ASTM International.

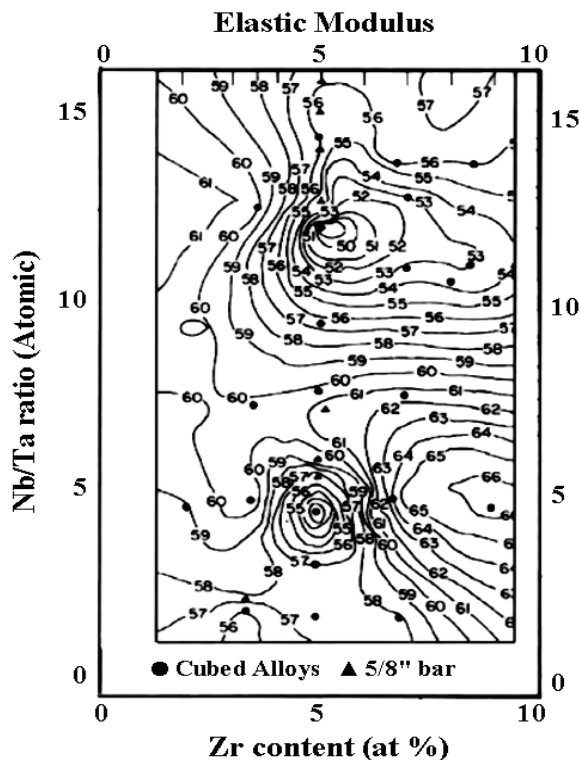
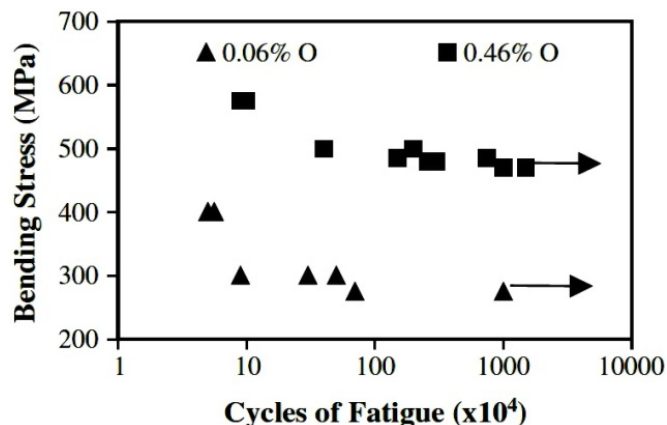


Table 11. Tensile properties of Ti-35Nb-7Zr-5Ta ([140], modified). Reprinted with permission from [140]. Copyright 2006 Elsevier.

Alloy composition	Thermal treatment	Yield strength (MPa)	Ultimate tensile strength (MPa)	Elongation (%)	Reduction in area (%)
Ti-35Nb-7Zr-5Ta-0.06O	ST	530	590	21	69
	427 °C/ 8 h/AC	630	686	17	42
	538°C/ 8 h/AC	493	537	21	52
	260 °C/4 h/AC/ 427 °C/ 8 h/AC	693	753	15	35
Ti-35Nb-7Zr-5Ta-0.46O	ST	937	1014	19	55
	427 °C/ 8 h/AC	1007	1055	12	27
	538°C/ 8 h/AC	806	929	11	22
	260 °C/ 4 h/AC/ 427 °C/ 8 h/AC	1202	1244	8	16
Ti-35Nb-7Zr-5Ta-0.68O	ST	1081	1097	21	50
	427 °C/ 8 h/AC	1222	1252	9	13
	538°C/ 8 h/AC	1036	1180	9	11
	260 °C/ 4 h/AC/ 427 °C/ 8 h/AC	1234	1260	7	9

ST: Solution treated, at 850°C (0.06 wt% O), 840°C (0.46 wt% O), and 900°C (0.68 wt% O) for 1h, water quenched; AC: Air cooled.

Figure 11. Stress-controlled fatigue response for Ti-35Nb-7Zr-5Ta with two different oxygen contents [155]. Reprinted with permission from [155]. Copyright 1999 Elsevier.



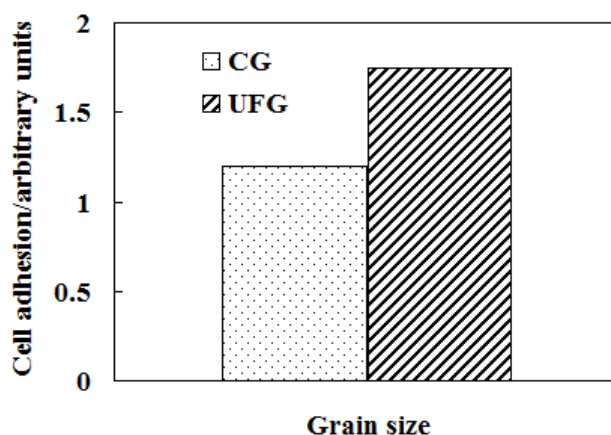
A broad range of properties is achievable for Ti-35Nb-7Zr-5Ta simply by increasing or decreasing the oxygen content [151]. The influence of oxygen as an interstitial strengthening element in Ti-based alloys is well known. It is also known and accepted that metastable β -type Ti-based alloys have a generally higher affinity for interstitial elements such as oxygen. Further, it is a fact that the β -type Ti-based alloys are generally much more highly alloyed than $\alpha+\beta$ -type Ti-based alloys and the metastable Ti-based alloys are generally more ductile than $\alpha+\beta$ -type Ti-based alloys [151].

In recent years, the research on Ti-Mo alloys with various Mo content has been developed and investigated extensively with the emphasis on microstructure, mechanical properties and electrochemical behavior. Ho *et al.* [156] and Oliveira *et al.* [157] have studied the structure and properties of a series of binary Ti-Mo alloys with Mo content ranging up to 20 wt%. The analysis shows that the crystal structure and morphology of the as-cast Ti-Mo alloys is sensitive to the Mo concentration. When Mo content was 6 wt%, a fine, acicular martensitic structure of orthorhombic α'' phase was observed. When Mo content was 7.5 wt%, the entire alloy was dominated by the martensitic α'' structure. When Mo content is increased to 10 wt% or higher, the retained β phase becomes the only dominant phase. Among all β phase alloys (with 10 wt%–20 wt% Mo), Ti-10Mo has the optimal mechanical properties. Oliveira and Guastaldi [158,159] have evaluated the electrochemical behavior of the as-cast Ti-Mo alloys containing 4 wt%–20 wt% Mo in Ringer's solution. The results indicate that all alloys present spontaneous passivation and do not exhibit pitting corrosion, suggesting that Ti-Mo alloys can be used as suitable alternative materials for orthopaedic devices. Capela *et al.* [160] have confirmed that the addition of Mo to the Ti-Mo alloys increases both the corrosion potential and the polarization resistance, and decrease the oxidation tendency in the following order: CPTi > Ti-6.5Mo > Ti-8.5Mo > Ti-10Mo. Alves *et al.* [161] have evaluated the corrosion behavior of Ti-10Mo alloys subjected to different treatments in fluoridated physiological serum and compared with that of Ti-6Al-4V alloy. The results indicate that the as-cast Ti-10Mo alloy exhibits the lowest passive current density.

Compared with conventional microcrystalline titanium and its alloys, nanostructured/ultrafine-grained Ti-based alloys have increased osteoblast adhesion [147] (Figure 12) and possess excellent properties with a good combination of high strength, low modulus, high hardness and excellent plasticity [162], which are highly expected for biomedical implants for good biocompatibility of Ti-based alloys is a prerequisite for biomedical human implant [107]. Kshang [163] and Webster [164] investigated the

effect of grain size on the behavior of cell adhesion and biocompatibility and the results showed that the nanostructured/ultrafine-grained material had better cell adhesion behavior than the fine-grained one. Therefore, the grain size is the most important factor affecting the behavior of cell adhesion and biocompatibility of biomaterials [61]. Moreover, it is an inevitable trend in the development of biomedical materials to prepare the nanostructured/ultrafine-grained Ti-based alloys.

Figure 12. Enhanced osteoblast adhesion on ultrafine-grained (UFG) CP Ti compared to CG CP Ti [147]. Reprinted with permission from [147]. Copyright 2004 Elsevier.



Therefore, based on above discussions it is evident that proper selection of alloying elements with right compositions and an appropriate thermomechanical treatment are highly essential to have high strength and low modulus for Ti-based alloys. The effect of each alloying element on phase transformation and resultant microstructure should be well understood in designing an implant material to achieve optimum properties.

4.2. Limitations of Current β -Type Ti-Based Alloys and Development Trends for Biomedical Materials

However, there are shortcomings in current β -type Ti-based alloys: (i) elastic modulus is still higher than that of human bone. The formation of ω phase and precipitation of α phase are the important factors causing elastic modulus increase; (ii) β -type Ti-based alloys mainly include β -stabilizers of Nb or Ta and neutral elements like Zr or Sn. Titanium, niobium, zirconium and tantalum are difficult to melt homogeneously due to limited cooling rate, high melting point and big difference in specific gravity. Besides, alloys produced by traditional melting method have coarse grains (typically larger than 30–40 μm) [18,61,128] and chemical macrosegregation [165], which may lead to bad biocompatibility and weak properties; (iii) it is difficult to obtain a microstructure composed of single equiaxed β phase. Thermomechanical processing can be used to improve the microstructures. However, alloys always display acicular or lamellar β after heat treatment above the β transus temperature. When these alloys are mechanically processed below the β transus (or $\alpha+\beta$ phase field) and then heat treated in $\alpha+\beta$ phase region, the microstructure consists of a mixture of equiaxed α and β phase. Equiaxed structure in Ti-based alloys is found to possess a better combination of high strength and low modulus than the acicular or lamellar structure [139]. Although different structures can be obtained by appropriate thermal treatment, single equiaxed β phase is difficult to achieve. Therefore, new β -type biomedical Ti-based alloys with lower elastic modulus, high strength and single equiaxed β phase with ultrafine grain size is

an urgent task. This may be achieved by appropriate design of alloy composition, proper selection of fabrication methods and precise control of processing parameters.

Metallic implants have a much higher stiffness and their linear stress-strain characteristics do not match the yield behavior of human bone. Most research results have confirmed the possibility of producing Ti-based alloys with superelasticity due to reversible β to α' martensitic transformation [166–170]. These materials have joined the family of previously developed low modulus near β and metastable β -type Ti-based alloys composed of nontoxic elements such as Nb, Ta, Mo, Zr and Sn. These aforementioned mismatches mainly include two aspects, *i.e.*, the biomechanical compatibility mismatch and functional mismatch, blocking further application of these alloys. Until now, the elastic modulus as low as 30 GPa has been achieved in some β -type Ti-based alloys [61]. However, compared with cancellous bones (0.2–2.0 GPa) [63], β -type Ti-based alloys are still stiffer. Also, it is very difficult to realize human tissue ingrowth due to the dense and rigid surface of Ti-based alloys. The second problem with dense titanium implants lies in the weak interfacial bond between implant surface and living tissue. Fibrous tissue encapsulation is of concern due to excessive relative micromovement of the device that can occur at the bone-implant interface because of poor interfacial bonding.

To meet practical requirements of bone ingrowth and long-term implantation, it is necessary to develop new implants with low elastic modulus that mimic the architecture and, in the meantime, encourage bone to grow into the pores [171]. A material with a porous structure is a promising implant to meet the abovementioned requirements and could eliminate the problem of interfacial instability with the host tissue [172]. An ideal implant should have mechanical properties close to natural bone and should bond well with human tissue.

Therefore, intrinsic problems of dense Ti-based alloys are mainly attributed to lack of osseointegration capacity and mismatches of mechanical properties, a suggestion to overcome this drawback could be the use of porous materials. Porous Ti-based alloys in arthroplasty implants are increasingly attracting widespread interest of researchers as a method of reducing stiffness mismatch and achieving stable long-term fixation by means of full bone ingrowth. The appearance of porous Ti-based alloys has brought new expectation for better hard tissue replacement and implantation, in particular for femur implantation and hip repair. The pore structure of porous Ti-based alloys can offer adjustable mechanical properties, light weight and improved biocompatibility to promote the tissue ingrowth, drug delivery and nutrition exchanges.

5. Porous Ti-Based Alloys

5.1. Introduction

Porous Ti-based alloys are able to provide adequate macro/micro pores for bone ingrowth, vascularization, and flow transport of nutrients and metabolic waste [173,174]. Calculations indicate that the introduction of porous (closed-cell or open-cell porosity) structure in dense materials might bring not only relatively high strength and larger plasticity but also lower elastic modulus [175,176]. According to $E_{foam} \propto (\rho_{foam}/\rho_{bulk})^2$ (E_{foam} is elastic modulus of porous materials, ρ_{foam} and ρ_{bulk} are the density of porous and dense materials, respectively) [177], the elastic modulus of porous materials can

be adjusted over a relatively wide range. Numerous researchers [175,178,179] have concluded that a porous matrix may be used as implant if it meets the following requirements:

- Interconnected porous structure to provide necessary space for cell ingrowth and vascularization and body fluid transport.
- High porosity (>50%) and the optimal macro-pore size in the range of approximately 300–400 μm or 200–500 μm for attachment, differentiation and growth of osteoblasts and vascularization [178]. Otherwise, the new tissue cannot develop an effective blood supply.
- The elastic modulus and compressive strength of human bones range from 0.01 to 30 GPa and 0.2 to 200 MPa, respectively. Porous samples are not load-bearing samples and they do not have to be as strong as alloys for plates and screws.
- Alloys composed of nontoxic and nonallergenic elements.

Fabrication methods of porous biomedical alloys have been investigated extensively, including space holder method, combustion synthesis, freeform fabrication, *etc.* [175,176]. Recent studies show the potential of using these techniques to control pore size, shape, orientation and distribution, including the creation of hierarchical and functionally-graded pore structures [175,180,181]. However, porous alloys fabricated through conventional sintering methods have coarse grains. Besides, it is hard to obtain single equiaxed β phase. For example, by using blended elemental powders together with space holder method, porous Ti-10Nb-10Zr alloys obtained at a sintering temperature of 1200 °C for 10 h under a high vacuum condition (10^{-4} – 10^{-5} Torr) consist of lamellar α and β phases with grain size above 10 μm [175].

5.2. Influence of Microstructural Configurations on Performance of Porous Ti-Based Alloys

Porous structure is helpful to reduce elastic modulus mismatch between implant and bone tissue. This is able to alleviate stress shielding effect to achieve stable long-term fixation. Extensive body fluid transport through open porous matrix is possible, which can trigger bone ingrowth if substantial pore interconnectivity is established [31]. Although porosity and pore size increase is obviously preferential for new bone ingrowth [37], it should be kept in mind that another consequence of the porosity and pore size increase is reduction of the implant mechanical properties. Thus depending on the intended application, a balance between mechanical properties and biological performance should be found.

The properties and requirements for success of porous materials have been studied extensively. The mechanical properties of porous Ti-based alloys are dependent on porosity, pore morphology, pore size distribution and microstructure. The nature of the pores or cell-walls together with the holistic architecture constructed by the pores is crucial for macro-mechanical behaviors of porous titanium and its alloys. Plastic collapse deformation of pores occurs in alloys with high plasticity under compression, while brittle alloys have brittle damages in pores. This shows that microstructure can exert great influence on yield strength. Both porosity and pore size play a critical role in bone ingrowth [37].

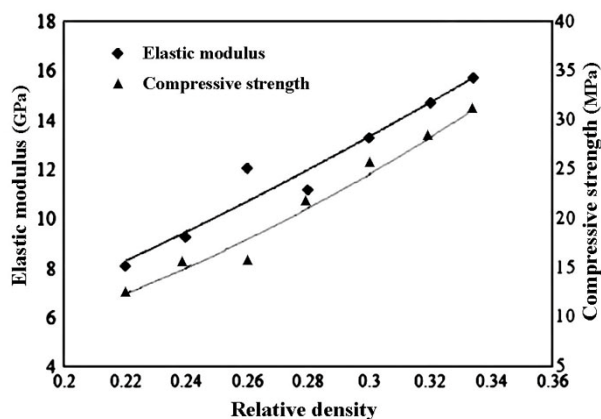
The relationship between mechanical properties and porosity has already been established empirically. It can be expressed as the well-known Gibson-Ashby Equation (1) [182]:

$$\begin{cases} \frac{E^*}{E_S} = C_1 \left(\frac{\rho^*}{\rho_S} \right)^{n_1} \\ \frac{\sigma^*}{\sigma_S} = C_2 \left(\frac{\rho^*}{\rho_S} \right)^{n_2} \end{cases} \quad (1)$$

For Equation (1), E , σ and ρ denote elastic modulus, strength and density, respectively. The superscript “*” indicates the value of porous material, and the subscript “s” indicates the value of dense material. C_1 and C_2 are constants related to material and experimental conditions, n_1 and n_2 are exponentials related to porous structure. It is clear that both strength and elastic modulus of porous materials decrease with porosity increased. A contradiction is that low elastic modulus (*i.e.*, comparable to cortical bone) corresponds to low strength. Porous titanium and its alloys with low elastic modulus are too weak to be used in load-bearing implants considering the defects and contaminations in the porous matrix. To enhance the strength will be a challenge in the real orthopedic application especially for resistance to tensile stress and impact load. Both elastic modulus and compressive strength of sintered specimens increase linearly with density increased (Figure 13).

It is well known that the properties of porous materials depend on their relative density and internal geometrical structure. Various methods have been developed to predict the structure-dependent mechanical performance of porous materials [183–185]. Analytical models can calculate the overall material response under idealized conditions or simplified assumptions, *e.g.*, modeling cell walls as beams or plates as proposed by Gibson and Ashby [182]. In contrast, finite element models are able to consider more realistic structures, such as randomly generated porous material [183,186]. The macrostructure is considered in the above two models, thus they cannot capture effects associated with the microscale structure that is present in partially sintered materials. In this case, the microstructure of the cell walls can significantly influence resulting properties of porous materials [187]. The porous materials made by the space holder technique have two types of pores, *i.e.*, macropores obtained by elimination of the space holder material and micropores obtained by partial sintering of titanium powder matrix. In this aspect, a two scale model for predicting elastic properties of porous titanium and its alloys formed with space holders was proposed by Niu *et al.* [188] to investigate the effect of relative density, pore shape, pore distribution on macromodulus and the effect of microdensity on micromodulus.

Figure 13. Influence of density on mechanical properties of porous Ti-10Mo alloys ([189], modified). Reprinted with permission from [189]. Copyright 2013 Elsevier.



To describe the dependence of mechanical properties of porous materials on their porosities, various empirical and theoretical relations have been proposed. Theoretical model, such as cross sectional or minimum solid area (MSA) [190], has been proposed to characterize mechanical properties of porous materials. The MSA model was developed for ideal bodies containing uniform spherical or cubical pores, aligned cylindrical pores and solid spherical particles, which cannot directly be applied to real porous materials with nonuniform pore distribution and pore shape. Besides, in the MSA model purely geometrical reasoning is used to predict the properties, and the microstructures involved and their contributions are not clearly illustrated [190]. The model proposed by Gibson and Ashby for elastic properties, toughness and strength of porous materials are basically load-bearing area models and neglect stress concentrations [182]. In Ti-based alloys, the type of phases present, grain size and microstructure determine various properties and deformation characteristics [191]. Thus, the degree of sintering, the porosity content and the type of microstructure have a direct influence on the mechanical properties of porous materials.

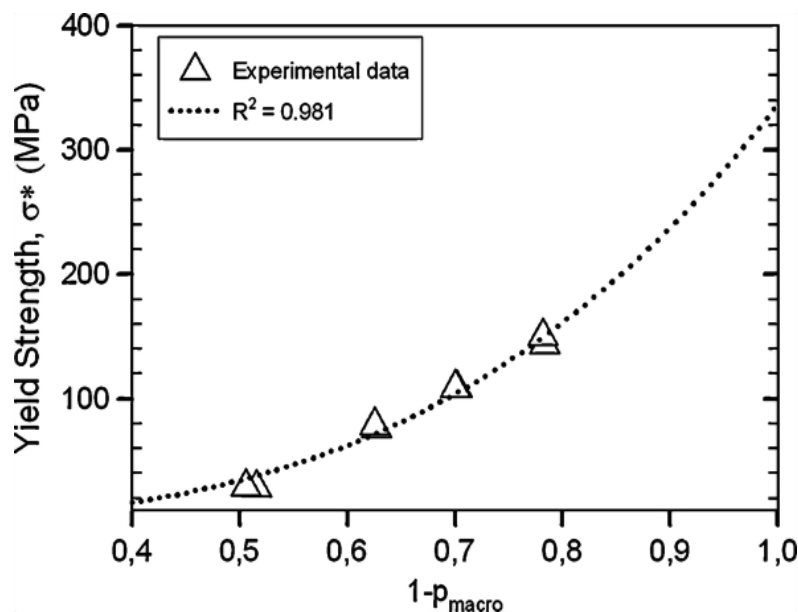
When load is applied to a porous material produced by powder metallurgy techniques, the resultant deformation localizes on the load-bearing contacts or necks between the particles and specimens with larger necks are expected to have higher strength values. Sintering usually results in reduced porosity and increased average inter-particle bond. Porosity and pore geometry also affect the materials' mechanical properties, stress shielding effect and fatigue strength [192,193].

The sintering operation involved in making porous titanium and its alloys requires a non-oxidizing environment to achieve good bonding, which typically means the need for a high vacuum oven (10^{-5} mbar) and sintering temperatures of around 1250 °C. Particle contamination (by oxidation or some other surface contaminant) would hinder particle bonding. The pore size, volume fraction, morphology and distribution throughout the sample thickness and the inter-particle neck size have a major impact on mechanical properties of the resulting material.

The production technique utilized to manufacture porous material affects pore shape, size, distribution, and cell wall/edge structure, which in turn determines mechanical properties, *i.e.*, yield strength and elastic modulus of porous materials. Liquid processing techniques were used extensively in production of low melting point metal porous materials such as Al, for example, the cell wall/edges are non-porous or bulky, whereas powder metallurgy processed porous materials contain micro-porous cell walls/edges in addition to macropores obtained as a result of expansion of an inert gas or by removal of spacer particles. Accordingly, the resultant mechanical properties of porous materials are sensitive to the cell edge/wall structure as well as the content and shape of macropores (Figure 14).

Powder metallurgy technique provides a high degree of freedom and allows one to produce structures varying in a wide range. However, this high degree of freedom brings along a high number of processing parameters, affecting structural, chemical and thus mechanical properties simultaneously. For instance, compaction and sintering behavior of powder mixtures composed of powders with different morphology and deformability change with size and proportion of the constituents. This induces a structural difference in pore walls. Another example could be the relationship among free surface area of the porous materials, the impurity content and its effects on mechanical properties.

Figure 14. Yield strength change of manufactured porous materials with macro porosity fraction [194]. Reprinted with permission from [194]. Copyright 2011 Elsevier.



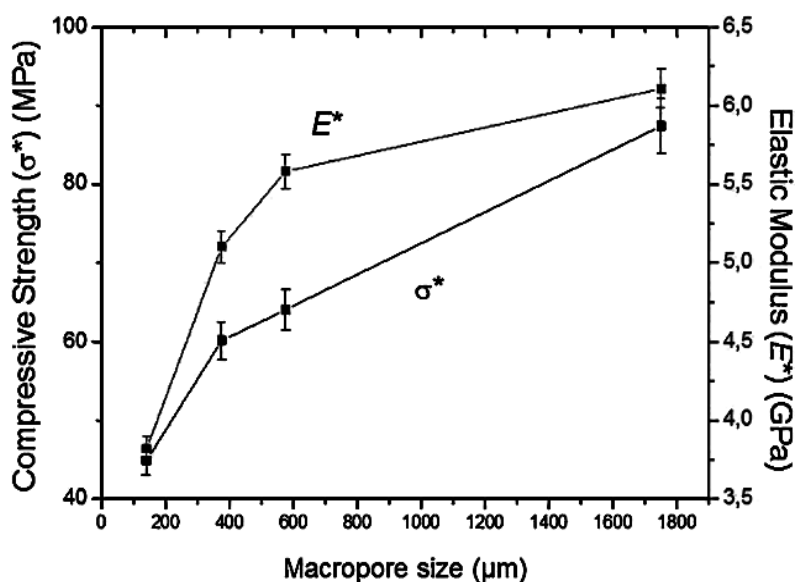
Many documents have been published on powder processing of porous titanium materials and the main interest in this field seems to be the correlation between porosity and mechanical properties and the material's potential for implant applications [195]. Only a few of these studies focused on powder processing variables [196]. However, sintering behavior and micro-porosity within pore walls were hardly mentioned. Laptev *et al.* [196] used ammonium hydrogen carbonate spacers to be removed thermally and reported the effects of compaction pressure, spacer size and amount on green structures. The effects of processing parameters on compaction and mechanical properties of green powder compacts were reported. Li *et al.* [197] investigated the effect of spacer amount, sintering temperature and sintering time on densification and pore wall hardness of porous titanium material, and also investigated structure-property relationship via experimental and statistical approaches. The structural characterization data were correlated with compressive properties of produced porous titanium material. For example, there are contradicting reports regarding pore size effect on mechanical properties in literature. While some researchers reported that pore size is inversely proportional to compressive strength and elastic modulus [198], others claimed that these properties increase with pore size increased [199] as well as that pore size does not affect mechanical properties [182].

When microstructure features varying with spacer size were considered, larger pores were expected to reduce strength due to more pore walls. On the other hand, their smoother pore faces and thicker pore walls were considered to enhance compressive properties. Relationship between relative density and mechanical property in porous titanium material with 64% porosity and different pore sizes showed that strength and modulus tend to increase with pore size increased (Figure 15). Based on mechanical test results, when architectural properties changing with pore size were considered, increased pore wall thickness and decreased pore face roughness in coarser-pored porous titanium material were found to have the most dominant effect on enhanced strength and modulus [200]. Spacer size has a considerable effect on physical properties of final product. Increasing spacer size decreases strut density due to poor compaction and sintering. It also decreases mean interconnection size and specific surface area of a

given relative density but increases pore wall thickness. When the architectural and mechanical measurements were correlated, pore wall thickness and pore face roughness were found to have a more dominant effect on strength and stiffness than pore wall porosity.

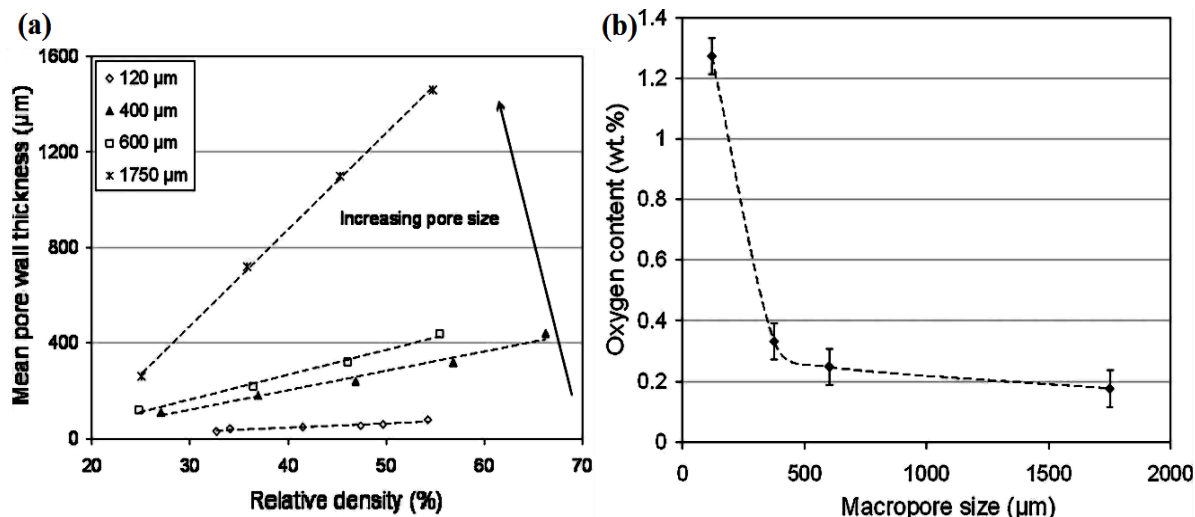
CP Ti with porosities ranging between 35% and 75% and pore sizes between 100 μm and a few millimeters were produced via powder metallurgy with spacers [200]. The use of coarser space holders resulted in thicker pore walls and a wider pore wall thickness distribution. The results indicated that strength and stiffness tend to increase with pore size increased. Among structural features, spacer size altered, pore wall thickness and pore face roughness were found to be the most dominant effect on strength and stiffness.

Figure 15. Compressive strength and elastic modulus variation with varying macropore size in porous titanium material with 64% porosity [200]. Reprinted with permission from [200]. Copyright 2011 Elsevier.



Pore wall thickness distributions calculated with granulometry on 3D images showed that mean pore wall thickness increases with spacer size increased for the same relative density (Figure 16a). This is an important design consideration where there is a risk of ligament rupture in machining or service. It should also be noted that porous titanium material with finer pores would capture more oxygen during cutting operation compared to the coarser-pored ones. Nevertheless, the results presented show a clear trend, which implies that increased free surface due to the use of fine spacer resulted in an increase in overall oxygen content by enhancing oxygen pick up during sintering cycle (Figure 16b). High oxygen interstitial content in titanium and its alloys is known to increase elastic modulus and strength [201]. However, it is not realistic to interpret on expected compressive properties of the porous titanium material produced since it was not identified whether the oxygen measured was on the surface or within the crystal structure.

Figure 16. (a) Mean pore wall thickness values of the porous titanium material produced with different size spacers at various relative densities; (b) Oxygen content of porous titanium material with 25% relative density and varying macropore size [200]. Reprinted with permission from [200]. Copyright 2011 Elsevier.



However, the pores in porous metallic materials could make the stress concentration higher than the theoretical value calculated by effective area [202]. Li *et al.* [203] reported that the pores with an average size of 236 μm in aluminum alloys are more likely to initiate a fatigue crack and accumulate plastic strain. Similarly, Ti matrix can be weakened by the pores in porous Ti-based alloys. As the porosity of porous titanium and its alloys decreases, the strength and stiffness increase [48,51,182,195], and the yielding region in stress-strain curve starts to disappear [195]. Spoerke *et al.* [204] found that elastic modulus and yield strength of porous titanium with elongated and aligned pores are larger in the longitudinal direction than in the transverse direction. Shen *et al.* [205] analyzed the effect of microstructure on uniaxial compressive response in porous titanium with 12% porosity by 2D and 3D finite element models, and suggested that the orientation and arrangement (random *versus* periodic microstructure) of pores are very important for mechanical response, and the arrangement of pores impacts more on local properties like stress concentration than macroscopic properties like elastic modulus. According to the finite element predictions and the experimental data on the porous titanium with 50% porosity, Li *et al.* [206] showed that the randomization of pore size and spatial distribution have significant influence on both local properties and macroscopic compressive properties. Zou *et al.* [207] investigated compressive properties of porous titanium (with porosities ranging from 35% to 84% and pore sizes from 150 to 600 μm) manufactured by sintering titanium fibers and found that the inhomogeneous microstructure and the spiral structure of the porous titanium bring about the large difference between the experimental data and the data calculated by the Gibson-Ashby model.

A previous study [208] on microstructure evolution and tensile fracture behavior of porous titanium produced by powder metallurgy technique using PMMA as space holder has shown that: the porous titanium has two kinds of pores: open interpenetrated macropores with the size of 30–260 μm and micropores (with the average size of 9 μm and the porosity of 8%) on the ligaments of porous titanium. The stress-strain curves of solid and porous titanium both show the linear-elastic relation in tension right up to fracture at small strains (<3%). Porous titanium fails mainly by the brittle cleavage, although, a few

small shallow dimples and a small amount of transcrystalline fracture of similarly oriented laths in a colony are observed on the fracture surface. In contrast to porous titanium, the mixed failure mechanism of solid titanium involves cleavage fracture with laths and voids, local ductile failure by dimples of varying size and shape, and transcrystalline fracture along the colonies. Additionally, porous titanium fails with the formation of shear bands at 45° to the tensile axis and the cracking of the struts on porous titanium is controlled primarily by the macro-pores. Effect of pore structure on the compressive property of porous titanium produced by powder metallurgy technique was investigated [209]: as the porosity and macropore size increase, the yield strength and elastic modulus of porous titanium decrease dramatically. The experimental data could be well described by the Gibson-Ashby mode, while the Mori-Tanaka model is only applicable to low porosity metals with randomly oriented spheroids, *i.e.*, to the porous titanium with 10%–55% porosity and average macro-pore size of lower than $400\ \mu\text{m}$; The stress-strain curves of the porous titanium show the elastic-plastic features with linear elastic region, a long yield stage and a densification stage. The cracking of struts on the porous titanium is controlled primarily by the macropores. The cracks nucleate priorly in the weak pore walls with maximum stress concentration and propagate throughout the structure at 45° to the axis of the applied load.

The porous structure, microstructure and electrochemical properties of a selective laser sintered porous Ti-10Mo alloy were investigated [210]. As sintering temperature increased from 1100 to $1400\ ^\circ\text{C}$, the large and interconnected pores changed gradually to small and isolated ones, while the porosity and pore size decreased from 63% to 28% and from 178 to $56\ \mu\text{m}$, respectively. In addition to a large number of pores, sintered alloy showed characteristic $\alpha + \beta$ lamellar structure at room temperature. The β phase volume fraction increased slightly with sintering temperature increased. The corrosion behavior of porous alloy is dependent on its porous structure. With porosity decreased, the corrosion potential shifts towards positive direction and corrosion current density reduces, while the passive current density decreases and passivation range widens. The lower porosity, smaller pore size and slightly increased β phase fraction cause a superior corrosion resistance.

As known, appropriate pore size and porosity, as well as superelasticity are indispensable for biomedical applications. This can facilitate cells and tissues ingrowth and allow medicine transportation and afford larger deformation strain. The control of porosity, pore size and distribution is necessary to obtain implants with mechanical properties close to those of bone and to ensure their osseointegration. As Wen *et al.* [178] have revealed, porous titanium and its alloys are not only biocompatible but also their open cellular structure, with a mean pore size of 200 – $500\ \mu\text{m}$, permits the ingrowth of new bone tissue and the transport of body fluids. Moreover, the mechanical properties of porous structures can be adjusted by modifying the number, morphology, and size of the pores. The question arises: do the size, shape, topology and volume fraction of voids have any influence on the substitute colonization? There is no consensus in the literature about the optimal pore size to enhance bone ingrowth. Otsuki *et al.* [211] showed that the pores of the structure have to be interconnected in order to ensure the bone ingrowth. These authors also compared the type of tissue formed as a function of time and implant internal architecture. They tested two levels of porosity (50% and 70%) combined with two ranges of pore sizes (between 250 and $500\ \mu\text{m}$ and between 500 and $1500\ \mu\text{m}$) and concluded that the size of pores should range from 500 to $1500\ \mu\text{m}$ for both levels of porosity to get a tissue of good quality. Xue *et al.* [212] demonstrated that the bone colonization is impossible for a pore size under $100\ \mu\text{m}$. Chen *et al.* [213] tested the osteogenesis on structures with pores ranging from 100 to $400\ \mu\text{m}$ but did not speak out

against higher pore dimensions. Hollander *et al.* [214] tested porous structure with pore dimensions of 500, 700 and 1000 μm and concluded that the growth of human osteoblast is possible for all these types of porosities. Those authors did not indicate a maximal pore size either. Generally speaking, no clearly identified rule exists to allow the optimal design of implants or bone substitutes in porous titanium materials. *In vivo* results of porous titanium implants showed significant increase in osteoconductive properties with increase in total porosity, and increasing the pore size increased the amount of new bone ingrowth [215]. Similar influence of porosity on bone ingrowth has also been reported in porous bioactive titanium implants [211].

The pore size of the space holder engineered porous NiTi alloys increases with the size of sieved space holder ammonium hydrogen carbonate particles added. The use of sieved space holder particle can greatly facilitate the fabrication of porous NiTi alloys with more satisfactory pore features, improved pore size uniformity and distribution than that using non-sieved ammonium hydrogen carbonate powder, and accordingly the engineered porous NiTi alloys exhibit significantly increased mechanical properties including excellent linear superelasticity [216]. It is clear that the modulus of the porous NiTi alloys decreases with increasing porosity from 35.8% to 42.1%. These modulus values are very close to those of human bones and far lower than those of the traditional metallic biomaterials [217]. The trend is similar to the results described by others [182]. It is worth indicating that the modulus of the porous NiTi alloys is also directly related to the pore characteristics and porosity, and it can be well tailored using space holder technique. The strength of the porous alloys decreases linearly with increasing porosity, and the linear correlations of the least squares regression are concluded [216].

Owing to the toxicity of Ni [18], much research effort is currently dedicated to the development of new Ni-free Ti-based shape memory alloys (SMAs) with improved biological and biomechanical properties. The major problem facing the development of new biomedical SMAs is inducing shape memory (SM) behavior and superelasticity (SE) without using any harmful alloying additions. The ideal alloying additions for a biocompatible Ti-based SMA should not only improve SM and SE properties toward those of commercial Ti-Ni alloys but must also be biocompatible (*i.e.*, without Ni, V, Al, *etc.*) to avoid any adverse reaction of the human body. The SM effect and SE have been reported in Ti-Mo, Ti-V and Ti-Nb alloys [93]. However, the Ti-Mo based alloys are susceptible to ω phase embrittlement. The Ti-V alloys are not suitable for biomaterial because of the cytotoxicity of V [18]. Ti-Nb based alloys are versatile candidate materials for biomedical applications. Ti-Nb-based alloys can undergo different solid-state phase transformations during deformation and/or quenching. Depending on the degree of stabilization of the parent high-temperature bcc β solid solution the following phase transformations may occur upon rapid cooling: $\beta \rightarrow \alpha'$ and $\beta \rightarrow \alpha''$. The thermoelastic martensitic transformation from the high temperature bcc β -phase to the orthorhombic α'' -phase gives rise to superelastic and SM behavior. TiNi is being replaced by TiNb alloy [93].

The mechanical properties of metallic materials deteriorate drastically with increase of porosity [51,195]. At a porosity of approximately 30%, the modulus is nearly equal to that of cortical bone, while the yield strength is below 100 MPa. This deterioration may be caused by stress concentration near the pores. Therefore, the inhibition of stress concentration by filling the pores with certain materials may improve the mechanical properties of porous metallic materials. In such a case, any material with a low modulus could be selected as a filling material (e.g., PMMA [218]) in order to prevent an increase in modulus of the porous metallic materials. A versatile process for filling a medical

polymer into a porous metallic material has been developed using porous CP Ti and PMMA [218] and showed that the tensile strength of CP Ti can be improved by the PMMA filling, while the effect of the PMMA filling on the modulus of CP Ti is smaller than that on the tensile strength because the modulus of PMMA is considerably lower than that of CP Ti. The decrease in the strength of porous titanium can be effectively inhibited by combining it with a biocompatible polymer. The tensile strength of the porous titanium and PMMA composites is greater than that of porous titanium alone. The effect of the PMMA filling on the improvement in the tensile strength of CP Ti is likely to appear only in the low tensile strength range of CP Ti. The tensile strength of CP Ti/PMMA is dominated by that of PMMA. Furthermore, it is considered that biofunctionalities are easily added to porous titanium and polymer composites because the surface of porous titanium can be covered with polymer [219].

The elastic-plastic mechanical behavior of porous CP Ti with given characteristics of pore size and distribution has no evident dependence on thermal treatment [220]. The observed variations are probably caused by the heterogeneous porous materials' macrostructure. On the other hand, it appears that the mechanical properties of porous Ti-Nb-Zr alloys are significantly sensitive to thermal treatment. Generally speaking, for porous Ti-Nb-Zr alloys, the higher the annealing temperature, the lower the elastic modulus: the highest elastic modulus is observed with the as-sintered material (8–12 GPa) and the lowest after annealing at 600 °C (5–7 GPa). As for porous CP Ti, their apparent elastic modulus remains stable regardless of the heat treatment conditions: it varies between 10 and 14 GPa depending on the deformation mode.

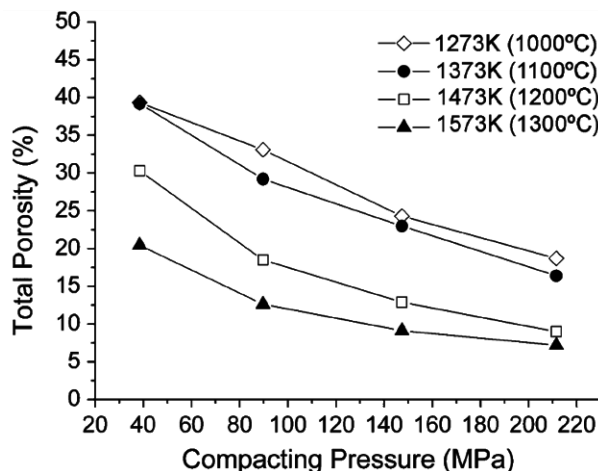
For porous materials, porosity has a prime impact on their mechanical properties compared with other factors [221]. Porosity percentage must be controlled to reduce the implant stiffness without any undesirable influence in mechanical resistance. Zhao [176] and Torres [222] investigated the influence of the main sintering conditions, compacting pressure and temperature, on both microstructural and mechanical properties of porous titanium materials obtained using conventional powder metallurgy (Figure 17). Highly porous titanium with a bioactive oxide layer by single step sintering in air at various different sintering temperatures were prepared by Wen *et al.* [223]. More than 90% of the pores were larger than 100 µm. Both total and open porosity decreases gradually with increasing sintering temperature. Higher temperatures lead to greater compressive strength and modulus due to the higher relative density or lower porosity of the porous materials. The samples sintered at 1000 °C possessed relatively higher compressive strength while there are no significant differences among the elastic modulus of the samples sintered at three different temperatures. This is because the oxygen diffusion attains a higher rate at higher temperatures, and hence gives faster densification kinetics during sintering.

Macro porous pure titanium with porosities of 30%–70% and pore sizes of 125–800 µm were prepared by using SPS and sodium chloride dissolution methods for bone implant applications [224]. The yield strength and elastic modulus agree with the Gibson-Ashby models, and coarsely obey linear declines with the pore size increase and exponential decays with the increase of porosity. Porous Zr-Ti-Nb alloys with nontoxic elements (Zr and Nb) and high porosity (between 60% and 70%) and average macropore size 260 µm were fabricated by space holder method [225]. Elastic modulus and compressive yield strength not only depend on the porosity but also on the amount of Nb in the porous material. Elastic modulus between 0.3 and 1.4 GPa and compressive yield strength between 11 and 32 MPa were obtained. It can be concluded that mechanical requirements can be accomplished

by changing the amount of the Nb, the minority alloying element. Oh *et al.* [51] have successfully fabricated porous titanium compacts by powder sintering with the porosity in the range of 5%–37.1%. Some of the compacts could achieve low elastic modulus comparable to human bone, but the compressive yield strengths are slightly lower than those of the bone. Recently, Nomura *et al.* [226] have tried to improve the strength by adding nitrogen into porous titanium compacts since N is known as one of strengthening elements for titanium and shows no toxicity to human body. Comparing nitrogen added titanium compacts to pure titanium compacts, both compacts show almost the same level of elastic modulus at the same porosity. However, the strength of nitrogen added compacts reached 144 MPa at the porosity of 29%, which is superior to that of pure titanium compacts. Thus, the strength of porous titanium compacts could be improved, while maintaining the elastic modulus comparable to human bone.

In summary, the pore characteristics and porosity as well as mechanical properties (including superelasticity) of the porous titanium and its alloys can be well designed and controlled by taking various abovementioned parameters into account. All these key macroscopic parameters are controlled by fabrication methods. Recently, a new series of highly porous Ti-based materials have been developed and released for use in orthopedic surgery through various fabrication methods, and these will be discussed in the next section.

Figure 17. Total porosity behavior as a function of both compacting pressure and sintering temperature [222]. Reprinted with permission from [222]. Copyright 2011 Springer.



5.3. Various Fabrication Methods for Porous Ti-Based Alloys

The methods fabricating porous metal materials are classified into four groups: liquid, solid, gas and aqueous solutions, among which there are mainly two basic manufacturing methods, liquid state processing and solid state processing [227]. The liquid state techniques have been extensively used for production of porous aluminium, zinc and magnesium due to simplicity of the processing and low reactivity and melting point [227]. However, they are unsuitable for the manufacture of porous titanium and its alloys. This is attributed to its high melting point (1660 °C) and extreme chemical affinity with atmospheric gases (e.g., oxygen and nitrogen). Hence, solid processing techniques seem more stable [228].

Powder metallurgy [229], a solid state processing, can produce porous titanium parts at much lower temperature and under less severe chemical reactivity constraints with more precise control of process variables and pore size. Besides, it has considerable advantages such as low cost, better control and the capability of near-net-shape production. Additionally, powder metallurgy techniques can provide a high degree of freedom and produce porous structures varying in a wide range. Therefore, fabrication methods of porous Ti-based materials are mostly based on powder metallurgy.

Powder conditioning is an important processing step in powder metallurgy and involves mechanical, thermal or chemical treatments or alloying of the powders [230]. The significance of powder treatment can be understood from the fact that the powder size, shape, and surface conditions have a significant influence on the subsequent processing. In powder conditioning, the powders prepared by various methods are subjected to a variety of treatments to improve or modify their physical or chemical characteristics. For instance, wet powders are dried to avoid any problems during subsequent processing, especially sintering. Physical characteristics like particle size, size distribution and shape may be varied by milling. Powders manufactured for powder metallurgy applications represent truly-engineered materials with precise control of physical and chemical characteristics. These powders are broadly classified into two major groups: elemental and prealloyed powders. Elemental powders refer to powders of a single metallic element. Elemental powders may be used in the case of iron for magnetic applications, or mixed with other elemental powders to form an alloy during sintering. Prealloyed powders consist of more than one element and are made by alloying elemental powders during the manufacturing process itself. In prealloyed powders, all the particles have the same nominal composition and each particle may be considered as a miniature ingot. Depending upon the nature of the powder, whether elemental or prealloyed, as well as on the type of application, majority of the powders are subjected to one or more treatments prior to compaction and sintering. These treatments are specific to a particular powder and may include a wide range of treatments like: (1) drying to remove moisture; (2) grinding/crushing to obtain fine sizes (e.g., powder agglomerates); (3) particle size classification to obtain the desired particle size distribution; (4) annealing to improve compaction; (5) mixing of different powders for premixes, and blending of powders and powder mixes to obtain a homogenous mix; (6) lubricant addition for compaction of powders; (7) powder coating. Most of these treatments are done by the powder producer.

The porous structure produced by powder metallurgy may have different types of pores [188]. For sintered porous materials fabricated without space-holders, there is only one type of pores namely micro-pores obtained by partial sintering of the titanium powder matrix. However, the porous state cannot be defined by a single parameter for those fabricated using space-holders. This is because there are two inherent length scales in this material, as listed below: Macro-scale pores—these are formed by elimination of the space-holder materials, which determines the size and morphology of these large pores; micro-scale pores—these arise due to incomplete sintering of the titanium powders. The size and morphology of these small pores are determined by the size of the constituent powder particles, and the level of compression and sintering.

Several mechanisms contribute to densification during hot-isostatic pressing (HIP) and this also reveals how the particles are connected during solid state processing [231]. When a pressure is applied to packed powder particles, it is transmitted through the powder bed as a set of forces acting across the particle contacts. The deformation at these contacts is at first elastic, but as the pressure rises,

the contact forces increase, causing plastic yielding and expanding the points of contact into contact areas. Once these contact areas can support the forces without further yielding, time-dependent deformation processes determine the rate of further densification: those we consider are power-law creep in the contact zones and diffusion from a grain-boundary source to the void surface. The contributions of other possible nondensifying processes, such as vapor transport, are usually insignificant because they are not enhanced by an applied pressure. During the initial stage (relative density < 0.9), the contacts between the initially-spherical particles grow in size and in number; throughout, the deformation is localized in and near the contact regions. The pores are cusp-shaped, and the individual particles and their contact regions can still be distinguished. Densification is determined by the deformation of the particle contacts. While the pressure is sufficient to cause plastic flow in the compact, densification is instantaneous; it ceases when the contact areas have grown to a size such that the yield stress is no longer exceeded. When yielding stops, the contact regions continue to deform by power-law creep. During the final stage (relative density > 0.9), the compact is considered as a homogeneous solid containing spherical voids, such that pores of equal size remain at each vertex of a tetrakaidecahedral particle (a good approximation for the particle shape at high compact densities). Densification is determined by the creep of the thick spherical shell surrounding each hole. Matter may be transported from the contact zones to the surface of a sintering neck by both grain-boundary and lattice diffusion. This mechanism is important in pressureless sintering and is enhanced in hot-isostatic pressing by the compressive traction acting on the grain boundary between the particles. Fine powders assist in densification in sintering. The simultaneous application of high pressure and high temperature are often used for high-performance components used in critical applications.

All the compression stress-strain curves of porous materials contained three regions of deformation: a linear elastic region; a yield stage; and a densification stage. This helps illustrate how the failure of the porous samples goes. During compression testing of porous metallic materials following the yielding, deformation bands perpendicular to the compression axis developed and cell collapsing took place together with the buckling and fracture of some cell walls and edges in the yield region. Compression stress-strain curves of manufactured Ti-6Al-4V porous materials were similar to those of elastic-plastic porous materials [194]. The porous materials' mechanical properties were found to be dependent on micro porous cell wall properties, which in turn depend on neck size between powder particles. The average size of macropores is found to be dependent on total porosity mainly due to interconnection of macropores in highly porous samples. In addition, it was detected that both total and macro porosity content increased as a result of increasing the amount of magnesium, however, a decrease is determined in micro porosity content since the volume occupied by cell walls and edges decreases. Thus, in addition to macropores formed as a result of magnesium evaporation, the mechanical properties of porous materials depend on strength of cell wall which in turn depends on underlying microstructure, powder packing characteristics and sintering degree [194]. In Gibson and Ashby model [182], for example, in which open porous structure and non-porous cell walls are considered.

5.3.1. Loose Sintering of Powder

The simplest fabrication technique for making porous titanium and its alloys is based on the partial sintering of metal powders. Compared with other technologies, this process is a simple, cost-effective

and most common powder metallurgical route. Except die wall lubrication if necessary, the process does not require a polymeric binder and hence minimize possible contamination associated with binder removal [51].

Oh *et al.* [51] sintered spherical unalloyed titanium powders with and without applied pressure by controlling sintering conditions and titanium powder sizes in a vacuum of 1×10^{-3} Pa, as shown in Table 12. Neck formation between titanium powder particles is observed in the porous sample 13. Only contacts between titanium powder particles are observed in the sintered sample 14. The porous sample 13 with about 30 vol% porosity shows elastic modulus of 25 GPa, bending strength of 115 MPa and compressive yield strength of 61 MPa. Porous compacts with porosity greater than 40 vol% cannot be fabricated when their particle sizes are in the range of 65–374 μm for the strength becomes almost 0 MPa. Porous titanium and its alloys fabricated by partial sintering of metal powders can achieve a low elastic modulus, but the compressive strength is low compared with human cortical bone [51].

For loose sintered powders, the pore size, volume fraction, shape and distribution throughout the sample thickness and the inter particle neck size have a major impact on the mechanical properties of the resulting material [51]. The porosity decreases with decreasing initial powder size and with increasing sintering pressure. In contrast, sintering temperature affects very slightly the densification of titanium compacts, as can be seen in Table 12.

Table 12. The total porosity and open porosity of porous Ti compacts sintered with various powder sizes and sintering conditions [51]. Reprinted with permission from [51]. Copyright 2003 Elsevier.

Sintering temperature (K)	Sintering pressure (MPa)	Powder size (μm)	Total porosity (%)	Open porosity (%)	Sample NO.
1173	0	374	37.1	100	1
		189	36.4	100	2
		65	34.7	93.2	3
	5	374	19.1	94.5	4
		189	8.7	84.0	5
		65	5.1	78.5	6
	10	374	19.0	94.3	7
		189	8.4	83.6	8
		65	5.0	73.2	9
1223	1	374	21.4	94.8	10
1373	0	374	36.2	100	11
		189	33.8	93.0	12
		65	32.4	92.7	13
1573	0	374	35.6	99.8	14
		189	33.6	91.2	15
		65	28.7	91.6	16

The porosity decrease by the decrease in powder size is attributable to the surface energy per unit volume. Smaller particles with high specific surface area have higher energy and thus they could be sintered faster in spite of lower sintering temperature. The elastic modulus, compressive yield strength

and bending strength decrease linearly with increasing porosity. Load–displacement curves obtained by three-point bending tests show almost linear elastic deformation followed by plastic yielding and strain hardening up to a peak stress. The crack propagates predominantly along interparticle boundaries. This suggests that plastic deformation occurs at bonded contact regions of powder particles. No catastrophic fracture occurs, although the compacts are strained up to a plastic strain of about 16%. The limitation of the conventional powder sintering approach is that pore size and shape are determined by the powder size and shape, which is difficult to control. Porosity is associated with the degree of particle interconnectivity and particle size. For spherical powder particles, the porosity is limited to 50% and pore shape is highly non-spherical [232,233]. Sintered loose titanium powders are often very brittle with poor toughness and are prone to crack propagation at low stresses, cracks are likely to initiate at the sintered necks of individual powder particles or along the interparticle boundaries, especially under fatigue conditions.

The influence of pore size and shape on mechanical properties of loose sintered powder and powder sintered with space-holders is different [38,51]. For powder sintered with space-holders, as introduced in Section 5.3.2, porosity amount, pore shape and macropore-size can be adjusted in a wide range by varying the shape, size and volume fraction of space holder materials, which also exerts great influence on the mechanical properties of the resulting porous material [178,195,196].

Zhuravleva *et al.* [38] prepared porous β -type nontoxic Ti40Nb alloy by compaction of mechanically alloyed powder mixed with NaCl (125–300 μm) or Mg (350–500 μm) particles as space-holder materials. The size ranges selection of the space-holder particles were based on the anticipated pore sizes. The Ti40Nb powder was consolidated to a green compact under pressure of 700 MPa for 2 h. The green compact was then sintered at 1273 K for 2 h and finally water quenched. For the preparation of porous samples with NaCl and Mg space-holders, they were sealed into argon filled quartz tubes for subsequent sintering. For removing the NaCl particles, the samples were then immersed in distilled water kept at 353 K for 4 h. The Mg particles evaporated after sintering. The complete removal of the space-holder materials requires that the porosity of the sample is larger than 50%. Samples with addition of 50 vol%, 60 vol% and 70 vol% of NaCl powders were prepared. The macropores display the rectangular shape corresponding to the shape of the NaCl particles, since NaCl particles are not deformed by cold pressing. The final porosity of the sintered and washed compacts is about 62%, 70% and 80%, respectively. This means that there are about 10% micro-pores. The average pore size is around 208 μm for the macro-pores, which fits in the range of 200 to 500 μm recommended for biomedical applications [178]. For porous samples prepared with 50 vol% Mg powder. The macro-pores resulting from evaporation of Mg particles have a slightly ellipsoidal shape because of the deformation of the initially spherical Mg particles during uniaxial pressing. The micro-pores have irregular sizes and shapes and are hard to control. The porosity of the sample is \sim 62%. It can be suggested that the micro-porosity fraction due to incomplete sintering of the Ti40Nb particles was \sim 12%. The mean macropore size is \sim 410 μm which also fits to the range of 200 to 500 μm recommended for biomedical applications [178]. The distribution of macro-pore size can be further controlled by careful sieving of the starting Mg powders. The big macro-pores are interconnected via small micro-porosity channels and thus the total porosity is interconnected. The porous samples show almost spherical shape and homogenous distribution of pores throughout a cross-section. Single micro-pores are present in the compact structure of Ti40Nb sample without space-holders and the porosity is \sim 36%. Compression tests

were carried out for samples produced with NaCl as a space-holder. The elastic modulus as well as the strength decreases with porosity increased. Stress–strain curves of these porous samples are alike the ones for cancellous bone. So it can be suggested that the samples deformation behavior follows the same three stages: at first some small number of walls, formed by sintered powder particles, fail; then slight hardening takes place; after that at the third stage a densification of broken walls occurs. The compression curves, where the maximum strain is only $\sim 2\%$, suggest a brittle fracture of the samples. The compacts with porosity of 36%–80% demonstrated a very low elastic modulus of $\sim 1.5\text{--}3$ GPa and compression strength of $\sim 10\text{--}35$ MPa, which is suitable for potential implant material application. The very low elastic modulus is a result of both high porosity of the samples and almost pure β phase composition of the alloy.

5.3.2. Space Holder Method

Space holder method, namely powder metallurgy technique using space holder materials, comes into action with its advantages like adjustable porosity amount, pore shape, and pore size distribution [178,195,196], which depend on the shape, size and volume fraction of space holder used for synthesizing porous titanium and its alloys. The process consists of five major steps: powder selection, mixing, compaction, sintering and spacer removal. First, metal and spacer powders must be selected. After selection, they must be mixed completely to assure the homogeneity of the mixture. The next step is compaction of the powders into a mold under controlled pressure to form a green body. The next stage can be either sintering or removal of the space holder depending on what kind of space holder is used in the process [178]. Figure 18 shows the schematic process of space holder method. By choosing the size, shape and quantity of the space holder, the mechanical properties as well as the pore diameter, morphology and porosity level of the porous metal can be adjusted under relatively low temperatures with low reactivity [178,234–236]. It can produce porous metal samples with greater porosity (Figure 19).

Several materials have been attempted by various investigators as temporary space holders, including urea [178], ammonium hydrogen carbonate [48,196], tapioca starch [237], sodium chloride [238], polymer granules [239] and magnesium [195,240]. In some cases, water soluble spacers such as sodium chloride, potassium chloride, potassium sorbate, or a mixture thereof [241] have been utilized to produce porous titanium and its alloys. Temporary space holders are selected primarily on the basis of different criteria: (i) reaction with titanium; (ii) residue left; and (iii) easy processibility.

Figure 18. The schematic fabrication process for porous titanium by space holder method.

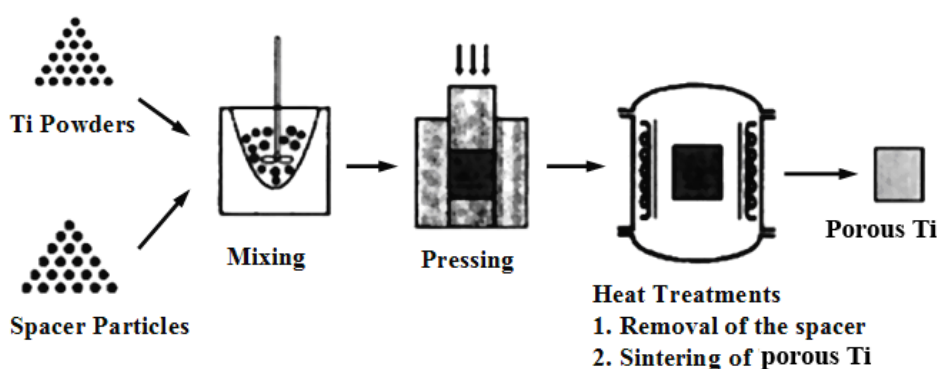
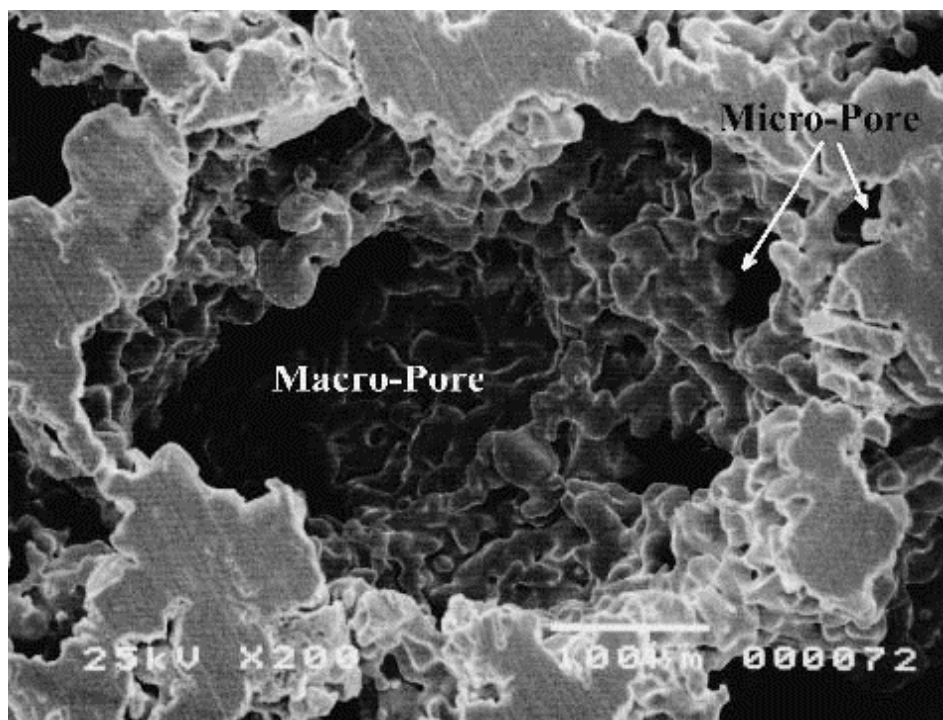


Figure 19. Scanning electron microscopy (SEM) micrograph of porous titanium with a relative density of 0.30 fabricated using space holder method [48]. Reprinted with permission from [48]. Copyright 2002 Cambridge University Press.



However, a general difficulty of this method is the removal of large quantities of space holder material and what kind of space holder material should be chosen. For biomedical applications, any residue left should be either bio-inert or bio-compatible. There is a possibility of absorption of residues left in case of space holders like urea, ammonium hydrogen carbonate and starch by the bio-implants which could import detrimental effect. In fact, most of the space-holders are evaporated at low temperatures or are removed by a dissolution process, generally in water. It is understood that sodium chloride could be a better choice because sodium chloride residue can be easily removed through dissolution in water. Additionally, even if any residue of sodium chloride is left, it would not be toxic for bio-implants. Patnaik [242] presented the advantages of using sodium chloride as space holder, such as low cost, fast dissolution in water, reduced etching of metal during dissolution, as well as much lower toxicity from residual content. Kohl *et al.* [243] showed good adhesion and proliferation of cells, indicating that any residual sodium chloride did not affect the *in vivo* performance of porous NiTi. Thus, there is an increasing interest of extensive research on the synthesis and characterization of porous titanium with sodium chloride as temporary space holder. The space holder method, which was first employed by Zhao and Sun [244], was used to fabricate porous Al by using sodium chloride as temporary space holder. Then porous titanium and its alloys with varying porosities (40%–80%) and macro-pore size ($>200\ \mu\text{m}$) were prepared using sodium chloride as space holder through powder metallurgy [176]. Urea and ammonium hydrogen carbonate were utilized for porous titanium and magnesium production for the first time by Wen *et al.* [178]. Torres [245] focused on finding the optimum sodium chloride percentage used as space holder, and finding an improved procedure to eliminate the salt before the sintering step and concluded the optimum conditions for salt dissolution

were: water temperature between 50 and 60 °C, maximum immersion time per cycle (4 h) and without agitation. These conditions ensure a faster route to salt dissolution, as well as to the best structural integrity of samples. The most important factors in controlling dissolution rate were: salt content, water temperature and immersion time per cycle.

In recent years, temporary space holders such as ammonium hydrogen carbonate or urea have been used to adjust porosity and pore structures [246]. However, the rapid decomposition of ammonium hydrogen carbonate at a lower temperature led to an imprecise control of porosity and pore structures, as well as an unsatisfactory repeatability of mechanical properties of porous alloys. In addition, the presence of sharp corners or notches of the pores in the alloys, which are due to the needle-like or flake ammonium hydrogen carbonate space holder particles, can obviously result in stress concentration and thus deteriorate mechanical properties [216]. Besides, the spacer particles, like urea and ammonium hydrogen carbonate, which have relatively low melting/dissociation temperature, are removed by thermal treatment and thus may cause oxidation resulting degradation of mechanical properties. Additionally, they may leave residue and cannot be removed completely, which makes them useless for many residue free requiring applications.

Porous Ti-10Nb-10Zr (wt%) alloy, with macropores of 300–800 µm and micropores of several micrometres, was successfully fabricated by space holder method [175]. The blended TiNbZr powder was firstly mixed with ammonium hydrogen carbonate (NH₄HCO₃), which was used as the space-holder material. The size of space-holder particles was 500–800 µm. The mixture of Ti, Nb, Zr powder and NH₄HCO₃ was then cold pressed into green compacts in a 50 ton hydraulic press. The green compacts were sintered in a vacuum of 10⁻⁴–10⁻⁵ Torr in two steps. The first step was carried out at 175 °C for 2 h to burn out the space-holder particles. In the second step the compacts were heated up to 1200 °C and held for 10 h. Porous TiNbZr alloys with porosities of 42%, 50%, 59%, 69% and 74% were fabricated by adding 20 wt%, 30 wt%, 40 wt%, 50 wt% and 60 wt% ammonium hydrogen carbonate to the powder mixture. Porous Ti-10Nb-10Zr alloy with 59% porosity exhibited an elastic modulus and yield strength of 5.6 GPa and 137 MPa, respectively, displaying significantly higher strength than unalloyed titanium scaffolds of the same porosity. Porous titanium was fabricated by powder metallurgy using urea as spacer material, heat treated at 180 °C/2 h in air to eliminate the spacer particles, sintered at 1200 °C/1 h under a vacuum (10⁻⁷ torr), exhibited three dimensionally interconnected pores. The average pore size was 480 (±210 µm) and total porosity was 36% (±2.4%) [247]. The microstructure showed interconnected pores and small isolated pores. Bram *et al.* [248] used urea powders as space holders, which could be removed at temperatures below 200 °C and had minimal contamination of titanium powders. Subsequent sintering at 1400 °C for 1 h resulted in porous titanium with porosities in the range of 60 vol%–70 vol% and pore diameters in the range of 0.1–0.24 mm, depending on the urea particle size. Wen *et al.* [178] used ammonium hydrogen carbonate as space holder with decomposition temperature of 200 °C and a sintering temperature of 1200 °C for 2 h. The resulting porous titanium had a porosity of 78% and exhibited a compressive strength of 35 MPa, whilst elastic modulus was 5.3 GPa. These values were a close match to those for cancellous bone. Porous Ti-10Mo alloy was successfully prepared from mechanical alloying particles and then consolidated by sintering using ammonium hydrogen carbonate as space holder [249]. Elemental metal powders of Ti were blended at Ti:Mo weight ratio of 9:1 in ball milling system and then milled for 5 h with a weight ratio of ball to powder of 20:1 and rotation rate of 300 rpm. The ball milling was carried out under a high pure argon atmosphere. The

blended Ti-10Mo powder was mixed with ammonium hydrogen carbonate (NH_4HCO_3). The mixture powders were cold compressed under 500 MPa for 1 min to form a green compact. Then, the resultant green compacts were heated to 175 °C to burn out the spacer-holding particles in air. After that, they were sintered at 1200 °C for 5 h in a highvacuum furnace and then cooled in the furnace. The compressive strength and elastic modulus had been tailored in the range of 174–646 MPa and 20.2–43.7 GPa, respectively. There was a substantial increase in porosity, from 5.5% to 37.5%, in mean pore size, from 20 to 130 μm , with the addition of 0–25 wt% ammonium hydrogen carbonate.

Magnesium played an important role in preventing contamination due to thermodynamical conditions. Homogeneous porous TiNi alloys having porosities in the range 59%–81% have been produced using magnesium powder as pore forming agent [240]. Prealloyed TiNi and Mg powders (50%, 60%, 70%, and 80% Mg by volume, balance TiNi) were mixed for 30 min using 5 wt% polyvinyl alcohol (PVA) solution (2.5 wt% PVA + water) as the binder prior to compaction. Particle size of Mg powders was in the range 250–600 μm , averaging at 450 μm . Then the mixtures were compacted in a double ended steel die at 400 MPa using a hydraulic press. Subsequently, compacts 10 mm both in diameter and height were heated to 1100 °C in purified argon atmosphere at a rate of 10 °C/min which is low enough to allow debinding of PVA below 600 °C and simultaneous Mg evaporation and sintering at higher temperatures. Sintering time at 1100 °C was 1 h. Sintered porous specimens were cooled in the cold zone of the furnace at a rate sufficient to prevent formation of intermetallics. The processed alloys exhibited interconnected open pores spherical in shape and with an average macro-pore size around 400 μm . Elastic modulus values observed to extend from 0.5 to 9 GPa, while yield stresses were in the range 2.2–31.0 MPa and compression strength values were in a broad range between 5.8 and 93.2 MPa depending on porosity content were comparable to that of cancellous bone. Porous TiNi alloys with porosities in the range of 38%–59% and homogeneous pore distribution, using 20 vol%–50 vol% spherical magnesium with a mean diameter around 450 μm as space formers, were also fabricated through the same fabrication procedure [250]. The porous TiNi alloys consist of fully spherical pores free from stress concentrations. Partial superelasticity has been observed in as-sintered and aged conditions. Linear and complete superelasticity up to 5% has been achieved after stress cycling.

Porous Ti-6Al-4V alloy was synthesized by space holder method as a result of evaporation of magnesium to achieve desired porosity content [194]. Magnesium powder with a wide range of distribution (300–1500 μm) and an average particle size of 660 μm was used. In the space holder technique used for the production of porous Ti-6Al-4V, firstly, 5 wt% PVA solution was added as a binder to Ti-6Al-4V/magnesium powder mixtures containing 30 vol%, 40 vol%, 50 vol%, 60 vol% and 70 vol% magnesium and the powder mixture mixed thoroughly for 0.5 h to ensure a homogenous mixture. Then, the mixtures were cold pressed at around 500 MPa using a double-ended steel die to obtain green compacts 8 mm in height and 10 mm in diameter. Eventually, for debinding and removal of magnesium by evaporation, the compacts were slowly heated with a heating rate of 12 °C/min up to 1200 °C at which the samples were kept for 1 h under high purity flowing argon gas for sintering and complete removal of magnesium. Final products contained porosities in the range of 43%–64% with an average macro-pore size 485–572 μm , and calculated elastic modulus and yield strength were in the range 1.42–14.7 GPa and 28.2–150 MPa, respectively. A power law relation was obtained between compression yield strength, σ_y , and macro porosity fraction, P_{macro} , in the form of $A \times (1 - P_{macro})^n$, similar to commonly used minimum solid area models. The proportionality constant “A” in relation was

found to be 330 MPa and defined as the yield strength of porous cell walls. Similar to model of Nyce and Shaffer the strength of porous cell walls changes with the square of neck size ratio $(X/D)^2$, where X and D are the average neck and powder particle size, respectively, indicating a strong dependence of strength on neck size, which are actually the load-bearing areas of porous materials.

Porous titanium with an average macropore size of 200–400 μm and porosities in the range of 10%–65% was manufactured using polymethyl methacrylate (PMMA) powders with the size of 71–100 μm , 100–154 μm , 154–200 μm , 200–315 μm , 315–400 μm and 400–630 μm as spacer particles [209]. The mixtures containing 10 vol%–70 vol% PMMA and CP-Ti powders were compacted as a cylindrical rod (ϕ 10 mm \times 10 mm) under the uniaxial pressure of 500 MPa to form green bodies. The green compacts were heated up to 250–450 $^{\circ}\text{C}$ for 5 h in a vacuum furnace under the pressure better than 7×10^{-4} Pa to remove the space holders, and then sintered at 1300 $^{\circ}\text{C}$ for 2 h. The compressive strength and elastic modulus of resultant porous titanium were observed in the range of 32–530 MPa and 0.7–23.3 GPa, respectively. With the increasing of the porosity and macropore size, the compressive strength and modulus decreased as described by Gibson-Ashby model. Porous Ti-24Nb-4Zr-8Sn alloy was fabricated by space holder method also using 30 vol% PMMA with an average pore size of 244–372 μm and porosities in the range of 35%–43% [62]. The mixers were cold rolled to form green compacts. Then the compacts were heated to 400 $^{\circ}\text{C}$ for 2 h to remove the PMMA space-holders and finally sintered at 1100–1300 $^{\circ}\text{C}$ for 4 h under vacuum condition and cooled in the furnace. The compressive strength and dynamic modulus of resultant porous Ti-24Nb-4Zr-8Sn alloy were observed in the range of 21–260 MPa and 1.54–6.66 GPa, respectively, which match those of cortical bone. Porous titanium with 64%–79% porosities and open cellular 100–300 μm pore sizes by using starch through powder metallurgy was successfully fabricated [237]. The yield strength and modulus were 23–41 MPa, and 1.6–3.7 GPa, respectively.

The space holder method is more attractive to make highly porous titanium and its alloys compared with loose powder sintering, slurry foaming [251] and hollow sphere sintering [229], which results in limited porosity (<50%) in the porous body. The space holder method can yield porous parts with desirable pore size, shape, volume and distribution using an appropriate space holder material, usually removed at low temperature without excessive contamination.

5.3.3. Spark Plasma Sintering

Conventional sintering of titanium and its alloy requires compacting metal powders in a die at room temperature, and subsequently a high sintering temperature (1200–1400 $^{\circ}\text{C}$) in a high vacuum (4×10^{-4} Pa) for a long time (24–48 h) [252]. Not only are high pressures, high temperatures, and long times required, but in the case of reactive materials, such as titanium and its alloys, an inert atmosphere is also inevitably required. The high temperatures involved in these processes, however, result in detrimental changes in the microstructure and mechanical properties. The difficult sintering process limits the usage of sintered titanium and its alloys.

Recently, there has been a growing interest to create porous implants for orthopedic applications by using spark plasma sintering (SPS) [253,254], which involves the application of an external current to assist powder consolidation. This technique is known under different names, such as field assisted consolidation technique [255], electrical field activated sintering [256], plasma activated sintering [257],

and electrical discharge compaction [258]. All techniques have in common the combination of an electrical discharge with rapid heating and pressure application to achieve fast sintering of powders. SPS is a high efficient and energy saving powder consolidation and sintering technology. The SPS studies on porous Ti-based alloys were mainly using low temperature and low pressure to decrease the relative density of samples [259–263]. The aforementioned methods are useful in that they can easily sinter titanium and its alloy powders, because ionization in the plasma created by the high current discharge can melt the local oxide surface film on the particles, bringing the particles into contact with each other, and allowing junctions to be formed. Electrical discharge compaction has been used to produce porous CP titanium implants [232,264].

Porous CP titanium with porosities of 30%–70% and pore sizes of 125–800 μm were prepared by combining SPS with sodium chloride dissolution methods [224], as shown in Figure 20. The porous titanium sintered at 700 $^{\circ}\text{C}$ for 8 min under 50 MPa showed pure α phase. All the samples exhibited highly interconnected structure and uniform pore distribution, as shown in Figure 21. The macroporous titanium with yield strength 27.2–94.2 MPa and elastic modulus 6.2–36.1 GPa had a potential to be used as bone implants. Porous titanium and Ti-5Mn alloy were successfully prepared by using SPS technique at pressureless conditions using ammonium hydrogen carbonate in size 250–245 μm as well as blowing agent TiH_2 in size <44 μm at different temperatures for 5 min [256]. Experimental results showed that pure Ti sample, which sintered under pressureless condition at sintering temperature 1000 $^{\circ}\text{C}$ the porosity was 53% and elastic modulus was 40 GPa. The Ti5Mn alloy indicated a good pore distribution, and the porosity decreased from 56% to 21% by increasing the sintering temperature from 950 to 1100 $^{\circ}\text{C}$. Elastic modulus was increased from 35 to 51.83 GPa with increasing of the sintering temperatures from 950 to 1100 $^{\circ}\text{C}$. The elastic modulus data obey the Gibson-Ashby mode well.

SPS is a combination of strong electric field, stress field and temperature field under the action of consolidation method [265], with advantages of low sintering temperature, fast cooling rate, integration of sintering and heat treatment, etc. SPS can produce field effect between powder particles during sintering [265] and effectively inhibit grain growth with controllable structure, which is a kind of interface clean nanostructured/ultrafine-grained crystal material forming technology [107]. It should be noted that due to high melting point features of alloy components, fabrication of Ti-based alloys by traditional sintering method might bring some shortcomings, such as too high sintering temperature, too long sintering temperature, and too high vacuum condition. As an advanced materials forming technology, SPS can provide relatively low sintering temperature, short holding time, and rapid cooling during the whole process. Especially, an outstanding advantage is that SPS can provide a high heating rate to several hundred K/min. Therefore, alloys with controllable microstructures can be obtained by SPS due to its special sintering mechanism on powder particles [107]. SPS provides a new way of fabricating nanostructured/ultrafine-grained porous biomedical titanium and its alloys with excellent properties and provide an alternative method for synthesizing new biomedical materials.

Figure 20. Schematic illustration of the fabrication process by using SPS and sodium chloride dissolution: (a) sieving of the titanium and sodium chloride powders; (b) mixing of the titanium and sodium chloride powders; (c) processing by the SPS; (d) dissolution of the sodium chloride in water; (e) obtaining of the porous titanium.

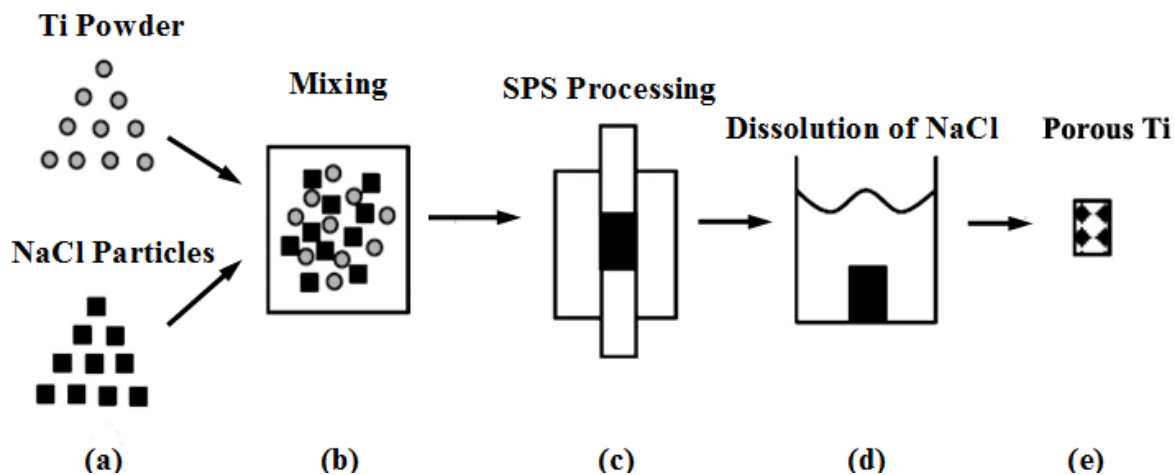
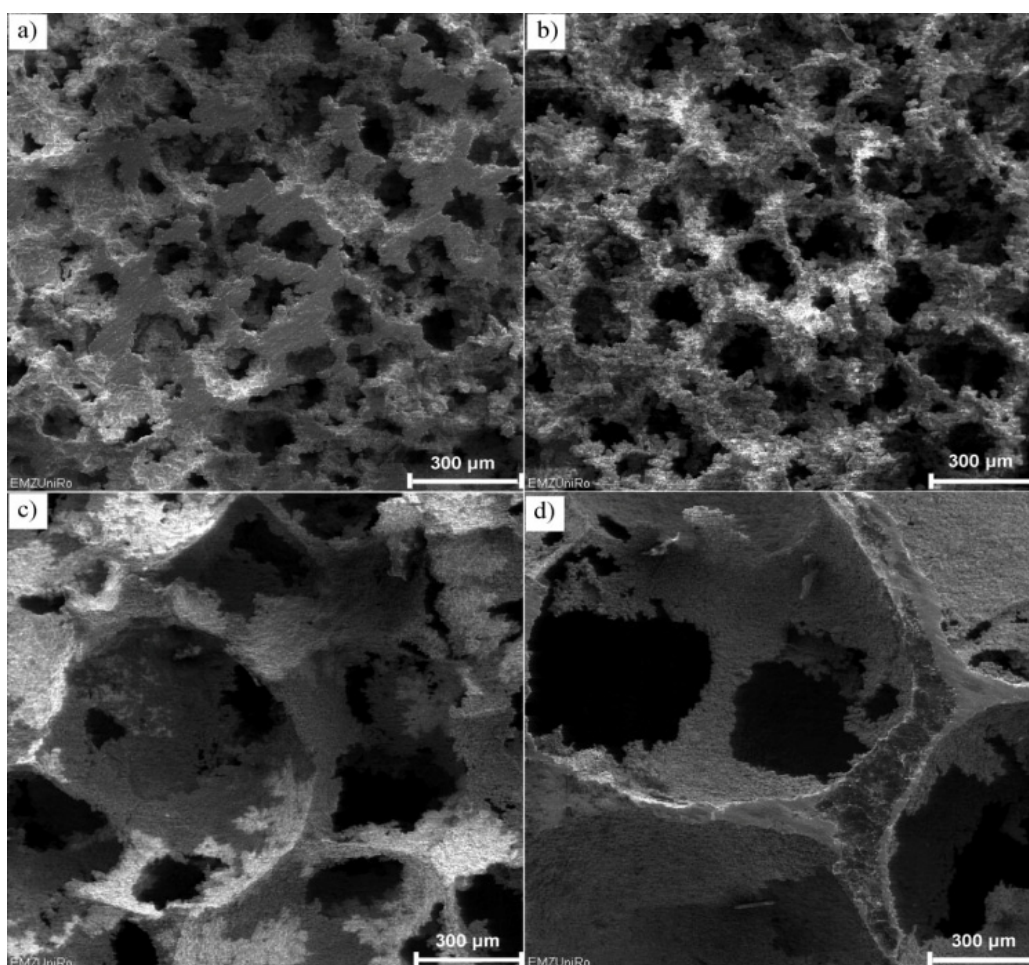


Figure 21. SEM micrographs of the porous titanium surfaces with the same porosity of 55% but different pore sizes of 125 (a); 250 (b); 400 (c); and 800 μm (d) [224]. Reprinted with permission from [224]. Copyright 2010 John Wiley and Sons.



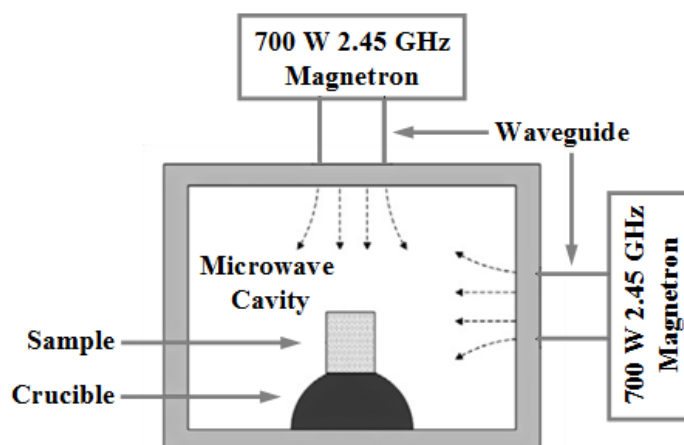
5.3.4. Microwave Sintering

Roy *et al.* [266–269] firstly obtained a fully sintered dense metal in a single-mode microwave cavity, after which microwave assisted powder metallurgy methods were developed for the sintering of metal alloys and their composites.

Tang *et al.* [270] fabricated porous Ti-6Al-4V alloy/TiC composites by the *in situ* formation of TiC from the reaction between multi-walled carbon nanotubes and titanium alloy powders, using the microwave sintering technique as shown in Figure 22. Ti-6Al-4V powders were mixed with 14.5 vol% of multiwalled carbon nanotubes (MWCNTs) and the particle size of Ti-6Al-4V was reduced to about 5 μm by ball milling. The MWCNTs acted as microwave susceptors as well as reactants for the rapid sintering of Ti-6Al-4V alloys. The green compact of the Ti-6Al-4V/MWCNTs powder was sintered in a 1.4 kW, 2.45 GHz bi-directional microwave emission furnace without using any protective gas environment. The microwave sintering was completed within 2 min. The surface temperature of the sample reached 1620 $^{\circ}\text{C}$ during sintering, as measured by a pyrometer. The processed porous composite had a porosity of approximately 25% and displayed compressive strength of 270.41 ± 24.97 MPa, yield strength of 145.48 ± 27.28 MPa, elastic modulus of 10.87 ± 2.46 GPa and compressive strain of $3.75\% \pm 1.11\%$. The Vickers hardness value in the TiC region (545.4 ± 13.9 HV) was significant higher than that in the titanium alloy region (435.9 ± 12.9 HV). An overall Rockwell hardness of 47 HRA was measured.

Traditional powder metallurgy processing of Ti-based alloys and their composites requires a long sintering time. Although a prolonged heating time can ensure complete sintering, it also increases the chance of impurities formation, such as oxides. In such cases, the sintering needs to be performed in either a protective gas atmosphere or in a vacuum [271]. Microwave heating has been used for the processing of materials such as ceramics, metals and composites, taking advantage of time and energy saving, reduced processing cost, decreased sintering temperature, better production quality, and lower environmental hazards [272]. The transfer of microwaves to the materials directly can result in a faster generation of heat, thereby achieving rapid and uniform heating.

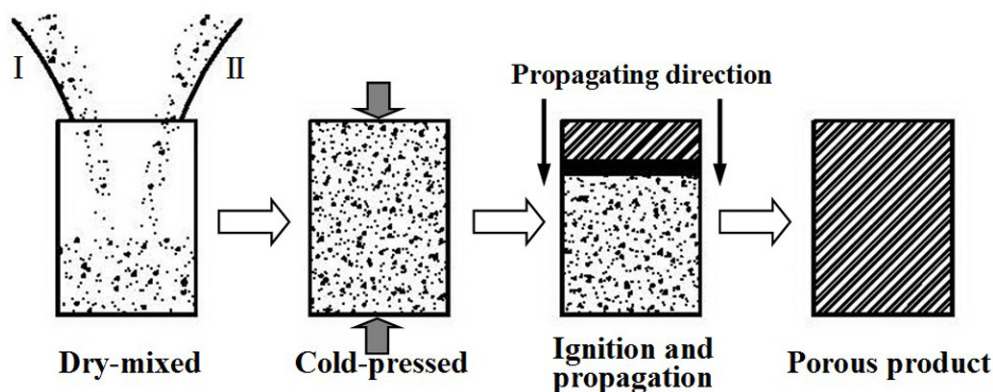
Figure 22. Schematic diagram showing microwave sintering [270]. Reprinted with permission from [270]. Copyright 2013 Elsevier.



5.3.5. Combustion Synthesis

A recently developed effective method of producing high purity porous alloy is a process known as combustion synthesis. Particle fusion is obtained through an extremely rapid self-sustaining exothermic reaction driven by the large heat released in the synthesis. The exothermic reaction can then be instigated under two different regimes: (a) the reactants are gradually heated until reactions take place simultaneously throughout the whole sample; and (b) self-propagating high-temperature synthesis (SHS), once ignited, a strong exothermic reaction propagates as a combustion wave through the entire mixture, without requiring additional energy. Various processing parameters such as the reactant particle size of powder, the use of a binder and the compaction pressure affect the final microstructure and porosity of the sample [273]. A schematic of the stages in this process is shown in Figure 23.

Figure 23. Schematic representation of the stages involved in combustion synthesis. The compaction acts as the trigger for initiating an explosion, which synthesizes the mix as it propagates ([232], modified).

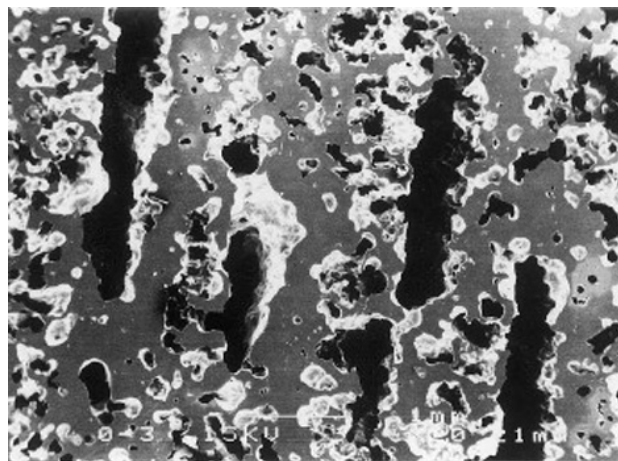


Several researchers have investigated the use of combustion synthesis in the fabrication of porous NiTi alloys [274–281]. Li *et al.* [282] successfully prepared porous NiTi alloys with anisotropic pore structure and porosity of 54 vol% by SHS. The mixed powder with a Ti: Ni atomic ratio 1:50 was cold pressed in a newly designed die. The green compact (ϕ 33 mm \times 80 mm), whose porosity is 40 vol% after being cold pressed with a pressure of 75 MPa, was placed in a reaction chamber and ignited at a preheating temperature of 550 °C. The NiTi SMA synthesized has an open porous structure, also its pores and channels with various size and shape are three-dimensionally interconnected. 100% Ni-Ti intermetallic compounds are formed in the SHS synthesized Ni-Ti SMA. A porous structure formed along the propagation direction of the combustion wave was shown in Figure 24.

Porous NiTi alloys were also fabricated by combustion synthesis of powders with the help of ZrH₂ as foaming agent and TiB₂ as endothermic agent [283]. 32.5 vol% TiB₂ and 0.5 wt% ZrH₂ were added in the NiTi mixture. Cylindrical compacts (ϕ = 15 mm, h = 15 mm, relative density = 0.7) were produced by cold pressing of the powder blend with compacting pressure of 165 MPa. The compact was placed inside a crucible and ignited in a chamber filled with argon gas. A thermocouple was inserted in the powder compact to measure its temperature during the combustion reaction. The powder size of Ni and Ti affected the ignition temperature of the combustion reaction, cell morphology and microstructure of this alloy. Porosity and pore diameter of samples decrease by increasing the powder size of Ni and Ti.

Porosity of combustion synthesized samples using different size Ni powder and Ti powder was 14.5%–60.0% and 42.6%–60.0%, respectively.

Figure 24. SEM micrographs of the longitudinal section of the porous Ni-Ti SMA with a banded structure showing channels along the propagating direction of combustion wave [282]. Reprinted with permission from [282]. Copyright 2000 Elsevier.



Propagating direction ⇨

This process can reduce the amount of energy required to fabricate porous materials with high melting points by utilizing the heat that was produced during combustion reaction. Also, it was found that in addition to an endothermic agent (TiB_2), a foaming agent was necessary to make such porous materials [284]. The heat of NiTi formation reaction was so high that the viscosity of molten NiTi during the reaction was very low. An advantage of this fabrication process is the high purity of the resulting porous materials, which is largely due to the expulsion of volatile impurities under the extremely high temperatures. *In vivo* studies suggest strongly that there is natural bone ingrowth with no apparent immune response in the composite materials produced in this process [273].

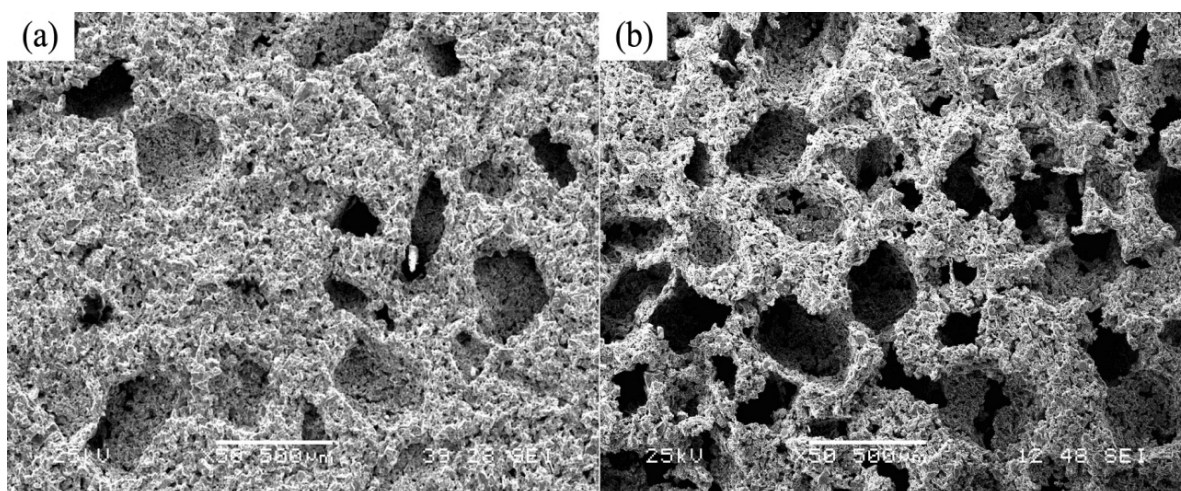
5.3.6. Metal Injection Molding

Metal injection molding (MIM) could be an attractive process combining the technique of polymer injection molding with the advantages of powder metallurgy. The possibility of near-net-shape production combined with a high potential for automation makes the MIM process suitable for the industrial production of porous titanium and its alloys. The MIM process starts with the mixing of metal powder with one or more polymers to produce a feedstock, followed by molding of the homogenized feedstock into shape parts, removal of polymer and final sintering.

Chen *et al.* [285] fabricated porous titanium by using MIM method with space holder sodium chloride. Mold temperature was 30 °C, injection temperature was 155 °C, and injection pressure was 100 MPa. The compacts were sintered at 1150 °C for 2 h under a vacuum of 1.33×10^{-3} Pa. Porous titanium powders with porosities in the range of 42.4%–71.6% and pore size up to 300 μm were obtained. Mechanical test showed that with sodium chloride content increased, compressive strength decreased from 316.6 to 17.5 MPa and elastic modulus decreased from 3.03 to 0.28 GPa. These mechanical properties were similar to those of cancellous bone. The microstructures of porous titanium

samples were shown in Figure 25. It could be seen there were interpenetrating macropores with size in the range of 50–300 μm which were formed by spacer holder removal. Macropores in sample with 42.4% porosity are mostly isolated (Figure 25a); those in sample with 71.6% porosity are well interconnected (Figure 25b). Simultaneously, the cell walls of the porous titanium are rough and honeycomb-like. The interconnected pore structure and rough wall-surface of macropores were appropriate for ingrowth of new bone tissues and transport of body fluids [286].

Figure 25. SEM microstructures of porous titanium by using MIM method with sodium chloride, sintered at 1150 $^{\circ}\text{C}$ for 2 h under a vacuum of 1.33×10^{-3} Pa: (a) 42.4%; (b) 71.6% [285]. Reprinted with permission from [285]. Copyright 2009 Elsevier.



5.3.7. Capsule-Free Hot Isostatic Pressing

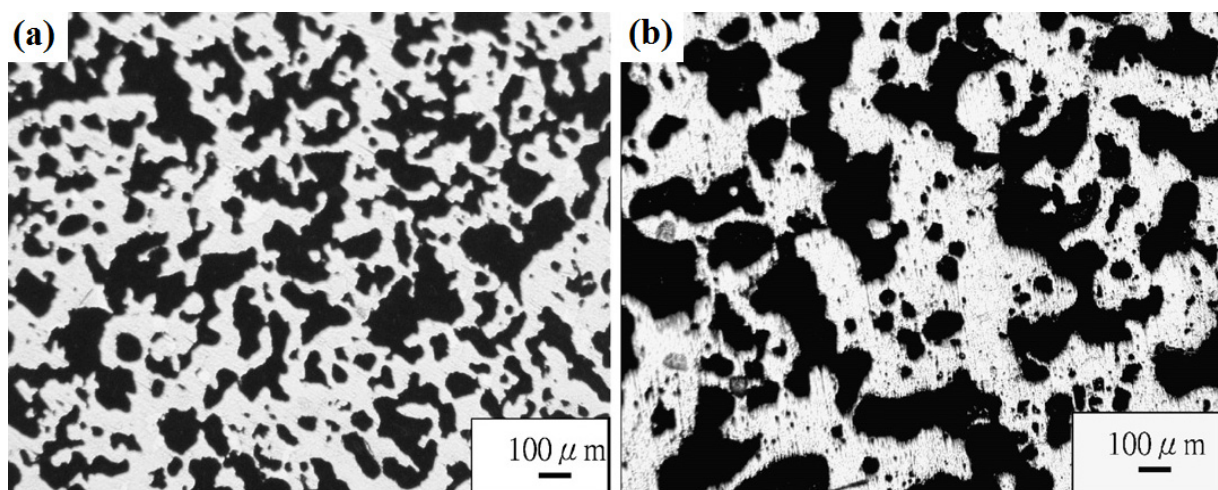
Porous NiTi alloys were initially fabricated by combustion synthesis [274,277,278,287]. However, the porous alloys fabricated by these this process showed inhomogeneous constituents and non-uniform pore distribution. These are not beneficial for tissue ingrowth. In addition, their mechanical properties are not as good as expected; in particular the shape memory effect (SME) and superelasticity (SE) deteriorate remarkably.

Recently, capsule-free hot isostatic pressing (HIP) process was developed to improve the quality of porous NiTi alloys [279,280]. This process can densify the dense part of the alloy and decrease sharp angles of open pores through extra high pressure argon gas [279]. Therefore, fabricated porous alloys showed nearly spherical pore shape with homogeneous pore distribution [279,280], and exhibited good SME and SE [279]. However, this process still has some problems, such as relatively low porosity and small pore size. For example, average pore size is 129 μm according to Weibull distribution calculation [280]. Although some research was carried out to improve the pore characteristics by using TiH_2 as the vesicant in fabrication of porous NiTi alloys [281], the pore size turned to be small after the addition of TiH_2 and use of TiH_2 is dangerous in fabrication process. More recently, a new process was reported by using sodium chloride as pore forming agent for fabricating near-net-shape porous NiTi parts [238]. The results showed that the porous alloys exhibited large pore size (355–500 μm) and sodium chloride did not deteriorate functional property of the alloys. However, the downside of this process was that

removing sodium chloride was relatively complicated, and most of pores were not connected, while high connectivity of pores is highly required for use as tissue implants.

Zhang *et al.* [288] reported a new attempt for fabricating porous NiTi alloys with adjustable and high porosity as well as large pore size by use of ammonium hydrogen carbonate and an updated capsule-free HIP process. Firstly, elemental Ti and Ni powders were mixed with ammonium bicarbonate. Then the mixed powders were blended by ball milling for 4 h. After that, the blended powders were cold pressed into cylindrical compacts of ϕ 15 mm \times 25 mm under a pressure of 100 MPa. The green samples were heated, under protection of high-purity argon, to a temperature of 200 °C for 30 min to decompose the pore forming agent. Then the treated green samples were sintered at 1050 °C (under protection of high-purity argon gas) in the furnace for 3 h under hot pressing pressure of 50 MPa. Finally, all samples were aged under 450 °C for 2 h, and then quenched into ice-water. The porosity of the fabricated porous alloys increased linearly from 30.4% to 48.4% with addition of 0–11.9 wt% ammonium hydrogen carbonate, and the alloys showed more uniform pore distribution with most pores larger than 300 μ m (Figure 26).

Figure 26. Optical microscopy (OM) micrographs of porous NiTi alloys with use of 0 (a) and 8.3 wt% (b) ammonium hydrogen carbonate [288]. Reprinted with permission from [288]. Copyright 2007 Elsevier.



5.3.8. Solid State Isothermal Foaming Technique

Nugroho *et al.* [289] have investigated the use of pressurized bubble entrapment in the manufacture of porous Ti-29Nb-13Ta-4.5Zr alloys, which were used instead of traditional prealloyed powders. Firstly, the elemental powders were blended for 30 min in a roller mixer. Following this, approximately 50 g of alloy powder was placed into a stainless steel can with an inner diameter and length of 28 and 30 mm, respectively. Each can was subsequently evacuated to approximately 10^{-2} Pa and then backfilled with 0.48 MPa of argon and sealed. The pressurized cans were then densified using hot isostatic pressing (HIP) at 1000 °C for 2 h or 1100 °C for 4 h under 100 MPa of argon and then furnace cooled. The HIP-ed billet specimens were then rapidly heated in a graphite element vacuum furnace to 1150 °C (for the 1000 °C HIP-ed specimens) or 1350 °C (for the 1100 °C HIP-ed specimens) and held for 10 h (isothermal foaming process). During this time the pressurised pores were expected to expand due to creep of the

surrounding metal. The resulting alloys were found to contain porosity and sizes ranging between 20%–40% and 20–200 μm , respectively, with some interconnected pores. Backscattered SEM and OM micrographs illustrating pore morphologies for the specimens foamed at 1150 and 1350 $^{\circ}\text{C}$ using a backfilled argon pressure of 0.48 MPa were investigated. The specimen foamed at 1150 $^{\circ}\text{C}$ was noted to contain approximately 30% porosity with uniform pore size and morphology. On the other hand, the pore size distribution in the specimen foamed at 1350 $^{\circ}\text{C}$ varied with the pores at the specimen center being discrete and mainly equiaxed with typical diameters of 20–50 μm ; the porosity in this region was found to be approximately 14%. In contrast, the pores close to the specimen surface had noticeably expanded with the porosity level achieving approximately 45% and pore sizes of typically 100–200 μm .

However, complex-shaped porous implants cannot be fabricated using the solid state isothermal foaming technique and the properties of the samples fabricated are mechanically inadequate.

5.3.9. Freeze Casting and Reverse Freeze Casting

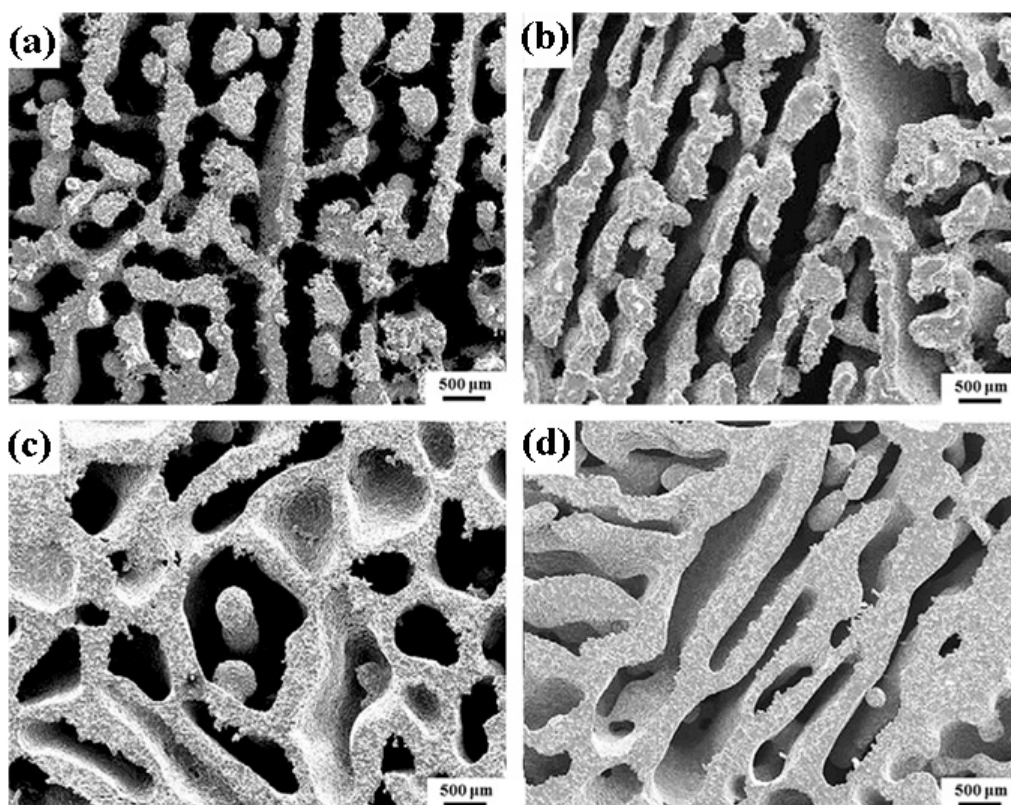
Among the prospective methods of fabricating porous metals, freeze casting (FC) has been widely studied with regard to mechanical performance of the scaffold. FC method is quite simple and offers the possibility to produce many parts. This method has great potential, as it can be employed for the fabrication of various kinds of porous materials (e.g., polymers, bioglass, ceramics and metals). In addition, a variety of structures can be produced for a fixed material composition by adjusting the process parameters, such as the freezing temperature and time, freezing direction, freezing vehicle, *etc.* [290]. By varying the processing conditions, wide variations in mechanical properties of freeze casting materials can be achieved [291–293]. The FC technique can lead to randomly distributed pores and enables a porous material with a compressive strength close to that of bone to be obtained, but its main drawback underlined by Yook *et al.* [293] is pore size does not exceed 300 μm for a long manufacturing time of 7 days. The control of the elastic properties anisotropy seems to be difficult. Jung *et al.* [294] used a new manufacturing technique called dynamic FC to create porous titanium scaffolds with a uniform porous structure and good ductility. Chino and Dunand [295] developed directional FC of aqueous titanium slurry, followed by ice sublimation and powder sintering. Porous titanium with aligned and elongated pores was created from this technique.

However, there are some limitations to FC method. Firstly, the degree of alignment is a critical issue when camphene is used as the freezing vehicle. It is difficult in practice to increase the length of aligned camphene dendrites, as the freezing rate of camphene is slower than that of water [296,297]; Secondly, most metal powders cannot be employed in the FC method; Thirdly, the maximum pore size for the existing FC method was 400 μm , which is the limit of the diffusion distance of the partially remelted frozen camphene; Finally, the merging and diffusion phenomena of the remelted camphene stopped when the thickness of the camphene dendrites reached 300 μm [293,298]. Therefore, a radically new solution was necessary in order to overcome the limitations of FC method.

Yook *et al.* [299] proposed a new method, referred to as reverse freeze casting (RFC), a suggested way to produce highly porous titanium with aligned large pores, and it was suggested that the powder particle size should not exceed 50 μm . The major concept of this method is based on the migration of raw powder, rather than the growth of camphene dendrites. Camphene-based slurries of titanium with adequate powder content (20 vol%) were prepared by ball milling at 60 $^{\circ}\text{C}$ for 6 h. After sufficient

unidirectional freezing of camphene, the slurry was poured onto the frozen camphene, followed by immediate quenching to $-20\text{ }^{\circ}\text{C}$. Thereafter, the resulting double layered material, consisting of the frozen camphene layer and the camphene–titanium slurry on top of it, was kept at $45.5\text{ }^{\circ}\text{C}$ for various periods of time (1–3 days). This allowed for sufficient migration of the raw powders down the channels within the directionally solidified camphene. The exposure temperature of $45.5\text{ }^{\circ}\text{C}$ was determined empirically by studying the solidification behavior of the slurries by means of DSC. After demolding, the green bodies were freeze dried for more than 10 h to remove the frozen camphene and then sintered at $1300\text{ }^{\circ}\text{C}$ in a vacuum furnace. After the freeze drying and sintering, all of the fabricated samples had long aligned pores up to $500\text{ }\mu\text{m}$ in size, as shown in Figure 27.

Figure 27. Cross sectional images of aligned porous structures for different casting times: (a) 20 h: columnar structure (74%); (b) 24 h: co-existing columnar and lamellar structures (69%); (c) 36 h: most columnar structures have turned into lamellar structures (59%); (d) 48 h: lamellar structure (51%) [299]. Reprinted with permission from [299]. Copyright 2012 Elsevier.



The average size of the aligned pores was $300\text{ }\mu\text{m}$, and their maximum length was 3 cm. The average porosity of titanium with highly aligned pores was controlled by tuning the casting time. With casting time increased, more titanium powder particles migrated downwards and the resulting columnar struts started to link up with one another. As the casting time increased from 24 to 48 h, the porosity was changed from 69% to 51% and the average wall thickness increased from $179\text{ }\mu\text{m}$ to $310\text{ }\mu\text{m}$; the compressive strength of the porous titanium scaffolds in the direction of pore alignment increased from 121 to 302 MPa and the elastic modulus of the samples was in the range of 2–5 GPa.

5.3.10. Slip Casting and Gel Casting

Researchers have been using ceramic techniques to fabricate near-net-shape porous titanium products and this has emerged as an attractive approach [300].

Slip casting is a conventional near-net-shape ceramic technique that is commonly used to manufacture dinnerware and sanitary ware. It is a filtration process in which solvent based powder slurry is poured into a plaster mold, creating capillary forces as a result of the porosity and these absorb the solvent from slurry. Over a period, the powder compact will be formed in the mold. Viscosity is a critical parameter in slip casting [301]. This process involves binder, plasticizer and dispersant for controlling the viscosity of slurry. Neirinck *et al.* [301] presented slip casting of a mixture consisting of slurry of titanium and titanium hydride powder to form a green compact through absorption of solvent by plaster mold, followed by sintering. However, safety is a major concern with this process due to the high reactivity of titanium hydride powder. Asthana *et al.* [302] indicated that too high or too low a viscosity slurry yielded poor quality sediment. A solvent is an important component to make a slip in the slip casting. This offers a media for powder interactions and the interaction between the powder and organics additives. Although an organic solvent is commonly used as a dispersion media in colloidal processing due to its excellent compatibility with organic additives, water is emerging as an alternative because it is environmentally friendly, low cost and safe [303]. Xu *et al.* [304] demonstrated that porous titanium compacts can be produced from water based titanium slurry using a slip casting approach. This opens up a simple and low cost manufacturing route for porous titanium production to shape titanium compacts with controlled levels of porosity. An important aim was the optimization of the water based titanium slurry formulation to minimize the content of organic additives. A lower organic additive content reduces the probability of carbon contamination in the sintered titanium products.

Gel casting process, also a near-net-shape ceramic processing technology [305], can be easily adjusted, and porosity and mechanical properties of porous titanium parts can be controlled by altering the parameters. Furthermore, the easy preparation of complex shaped products combined with the low costs of the molds make gel casting more appropriate for the fabrication of porous titanium implants, especially in personal medical treatment areas. In this process, the powders, organic monomer binder, dispersant and solvent are mixed together to first form slurry. Subsequently, a crosslinking reaction occurs when initiator and catalyst are added to form an *in situ* polymerization green body. After solvent evaporation, the polymer acts to bind the powders and retain the desired shape. By altering the solid loading of the slurry, the porosity and mechanical properties of porous titanium parts can be changed, therefore easily obtaining custom made performance. Erk *et al.* [306] demonstrated the feasibility of a gel casting process to fabricate porous titanium in complex shapes. A unique porous titanium screw for implant applications was fabricated with a 20% porous core and a higher porosity near the surface. Yang *et al.* [307] have used gel casting and subsequently sintering to prepare porous Ti-Mo and Ti-Nb alloys with three dimensionally interconnected porosity and good property. Schematic representation of the gel casting process is shown in Figure 28. Sintering temperatures of 900 to 1050 °C for 2 h were used to fabricate Ti-Mo and Ti-Nb alloys with varying porosity. The results showed that total porosity ranging from 39% to 50% and the pore size ranging from 5 to 120 μm can be achieved by changing the gel casting parameters. These porous Ti-Mo and Ti-Nb alloys have elastic modulus range from 5 to 18 GPa and compressive strengths in the range 141–286 MPa. The bending strengths are in the range

89–131 MPa for Ti-Mo alloys and 79–120 MPa for Ti-Nb alloys. Microstructure study indicated that the pores were irregular in shape with uniform pore size distributed in the two samples processed under the same processing parameters (Figure 29), promising for load-bearing implant. Also, Yang *et al.* [308–310] prepared porous Ti-Co and Ti-Mo alloys by gel casting. Sintering temperatures of 1000 and 1100 °C for 2 h in vacuum at 3.5×10^{-3} Pa were used and achieved open and closed three dimensional pore morphologies and total porosity ranging from 38.34% to 58.32%. In contrast to porous titanium fabricated by gel casting, the compression and bending strengths of porous Ti-based alloys were significantly increased by adding Co and Mo with elastic modulus ranging between 4 and 25 GPa and compressive strength from 82 to 333 MPa, which is close to that of human cortical bone. Moreover, the bending strengths are in the range 64–109 MPa for porous Ti-Co alloys and 89–204 MPa for porous Ti-Mo alloys.

Figure 28. Schematic representation of the gel casting process [307]. Reprinted with permission from [307]. Copyright 2012 Elsevier.

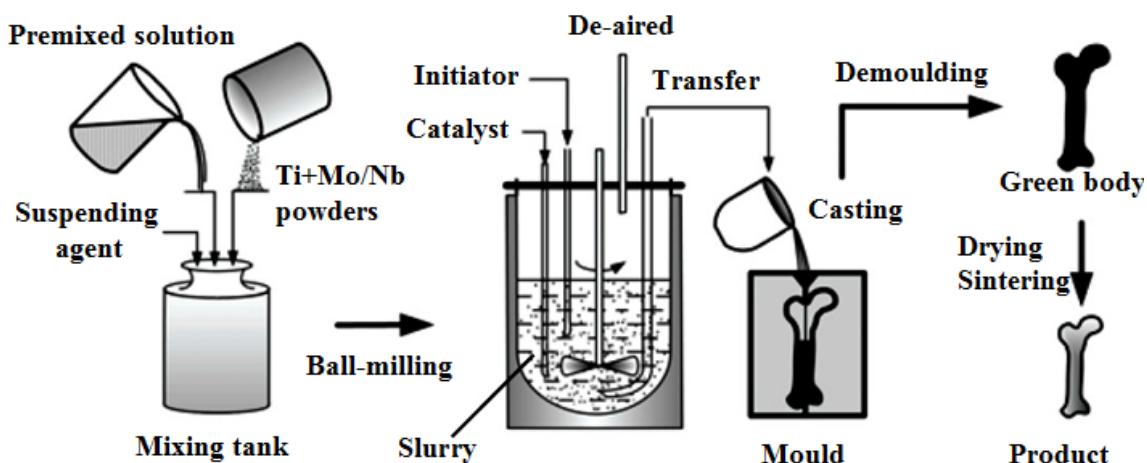
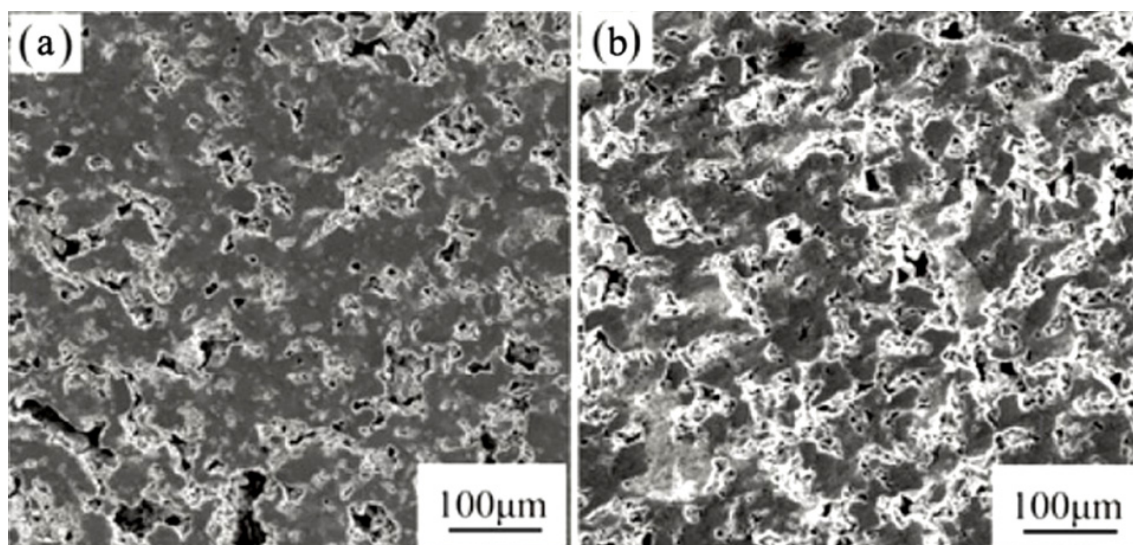


Figure 29. SEM microstructures of pore morphology and distribution in porous Ti-based alloys processed at 32% solid loading: (a) Ti-17.5Mo alloy; (b) Ti-35Nb alloy, respectively [307]. Reprinted with permission from [307]. Copyright 2012 Elsevier.



5.3.11. Slurry Foaming and Plasma Sprayed Coating

Figure 30 presents processing steps for fabricating porous titanium by slurry foaming method using H_2O_2 as forming agent [311]. The resulting porous titanium presented three dimensional structure (Figure 31) with porosity 58% and average pore size up to $460\ \mu m$. The compressive strength and elastic modulus were 190.7 MPa and 4.15 GPa, respectively. These values well matched those of human bone [312]. However, current techniques that use foaming agents, either in solid state sintering processes or in molten metal techniques, have inherent limitations, such as contamination, presence of impurity phases, limited and predetermined part geometries, and limited control over the size, shape and distribution of the porosity [51,178].

Plasma spraying method can be used to create rough solid surface textures, porous surface coatings on solid cores and also fully porous structures. Porous surface coatings on solid cores and fully porous structures whether they are open cell or closed cell, allow bone ingrowth into pores. A schematic description of the plasma spraying process is shown in Figure 32. Porous coatings with varying degrees of porosity can be created on the substrate by adjusting the spraying parameters [313].

Figure 30. Processing steps for fabricating porous titanium by slurry foaming [311]. Reprinted with permission from [311]. Copyright 2006 China Academic Journal Electronic Publishing.

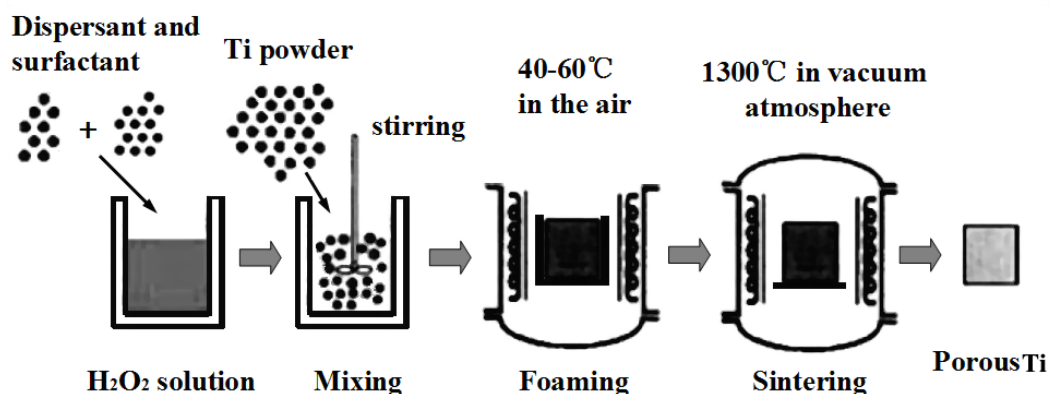
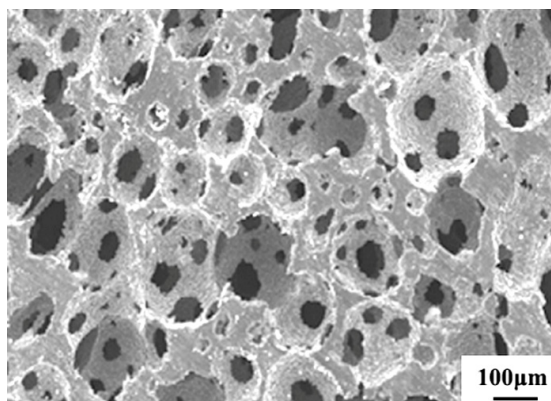
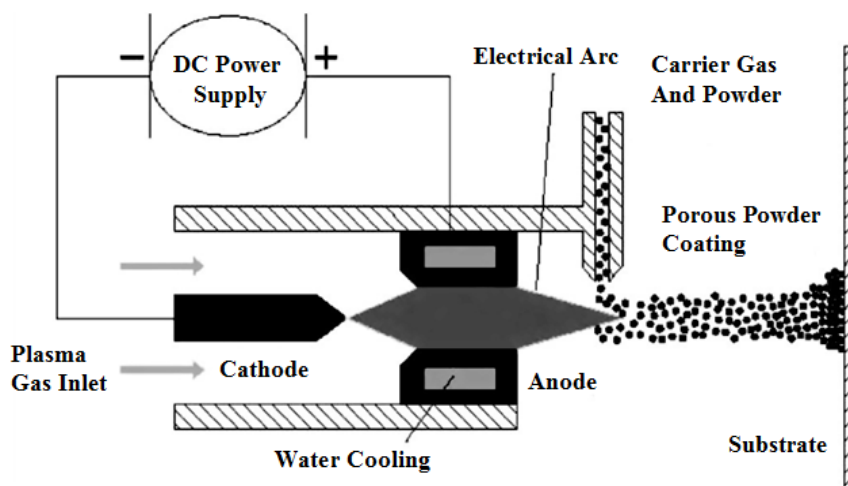


Figure 31. SEM microstructures of porous titanium fabricated by slurry foaming [311]. Reprinted with permission from [311]. Copyright 2006 China Academic Journal Electronic Publishing.



Hahn and Palich [44] first described titanium plasma sprayed coating for fabricating porous coated implants. By choosing an appropriate gun-to-substrate distance, a thin coating (approximately 900 μm thick) with porosity that varied from 0 at the substrate interface to about 50% at the coating surface was formed. However, coatings prepared with this method result in irregular and rough surfaces with some macro and micro pores and the pore interconnectivity is quite low compared to other techniques. Furthermore, it is difficult to form bulk structures with large pores ($>100 \mu\text{m}$). Due to short reaction time, deposited material is usually a composite of the starting material forming the matrix and *in situ* synthesized phases. This is indispensable for plasma spraying of titanium, which is a sensitive material prone to oxygen and nitrogen absorption [313].

Figure 32. Schematic representation of the plasma spraying process [232]. Reprinted with permission from [232]. Copyright 2006 Elsevier.



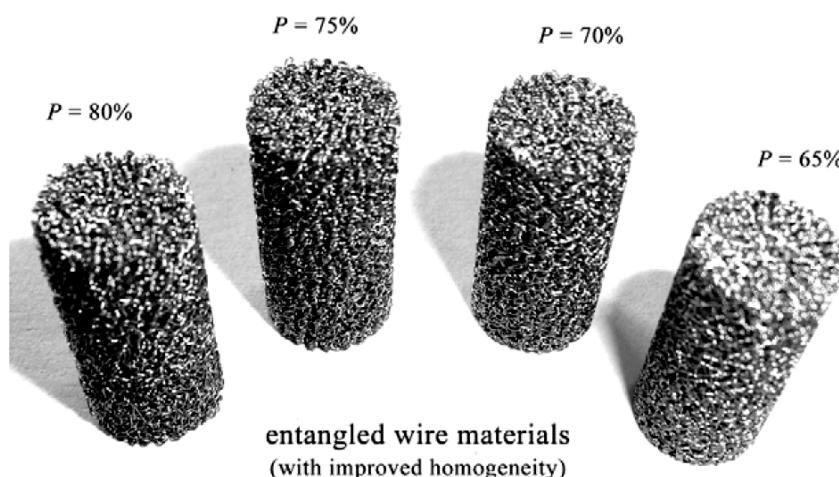
5.3.12. Entangled Titanium Wire Materials

A group of entangled titanium wire materials with nonwoven structure were fabricated by using 12–180 MPa forming pressure, which have porosity in the range of 48%–82% [57]. CP Ti (Grade 1) wires with diameters of 0.08 and 0.15 mm, respectively, are selected as raw materials. The spatial architecture constructed with wires is controlled by the wire-twisting methods and intertwisting procedures. A general procedure for forming nonwoven titanium wire materials is as follows: firstly the wire is entangled by winding and twisting to form a precursory bundle of twisted wires. Then the bundle is put into a specially designed steel mold for compaction and shaping. A high pressure in a range of 12–180 MPa is necessary. The holding time under certain pressure and at high temperature (around 650 °C) is about 10 min for avoiding wire-rebound and shape-finalizing. After that, the sintering temperature about 1200 °C and holding time 60 min were used. After the sintering a step-cooling followed with annealing at 650 °C is carried out for plasticity recovering of the titanium wires. The mechanical behavior of the porous titanium wire materials strongly depends on raw material (titanium composition, treatment status, and wire diameter), entangled wire architecture, and porosity. The pores in the resulted materials were irregular in shape, which had a nearly half normal distribution in size range. The yield strength, ultimate tensile strength, and elastic modulus were 75 MPa, 108 MPa, and 1.05 GPa, respectively, when its porosity was 44.7%. The low elastic modulus was due to the structural

flexibility of the entangled titanium wire materials. The average pore size depends on the porosity and the wire diameter. The larger porosity and the larger wire diameter lead to the larger average pore size. The quasi-ordered entangled wire materials are practically useful because they are more homogeneous in porous structure and easily mass manufactured [314]. Figure 33 showed some cylindrical samples of the quasi-ordered entangled wire materials with different porosities.

So far, several shapes such as cylinders, rectangular prisms, tubes, sheets, and flat dog-bones have been made [57]. This kind of material is very promising for implant applications because of good toughness, perfect flexibility, high strength, adequate elastic modulus, and low cost. It should be noticed that the entangled wire material is a kind of fiber or wire mesh, in which the entangled wire can be either stochastic (like nonwoven) [315] or ordered [314]. Originally, titanium wire or fiber materials were introduced for producing porous surfaced implants [316]. The relationship between the mesh structure and the mechanical properties has not been established. Furthermore, the basic aspects in terms of the fabrication techniques (especially for the three dimensionally porous titanium wire materials), the structure characterization, and the mechanical properties tailoring are still open for investigation.

Figure 33. Entangled metallic wire materials with improved homogeneity [57]. Reprinted with permission from [57]. Copyright 2012 Elsevier.



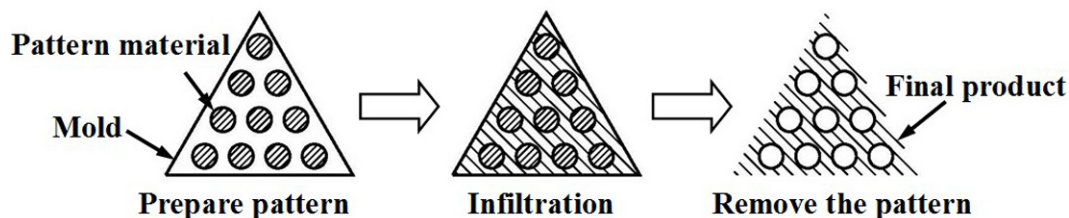
5.3.13. Replication Method

The sponge replication method seems to be effective because of its flexibility in producing different structures, and its simplicity and low cost [297]. Additionally, this method can achieve high porosity and good interconnection between pores [297,317], which is beneficial to human bone ingrowth and the vascularization of newly formed tissue [37]. These porous structures have many applications ranging from spinal fixation to acetabular hip prostheses, dental implants, permanent osteosynthesis plates, and intervertebral discs [246].

Highly porous titanium was prepared through sponge replication method [223]. Schematic representation of the three-step replication process is shown in Figure 34. The samples were slowly heated to 400 °C at a rate of 2 °C/min and maintained for 2 h to burn out the polyurethane foams and sintered at three selected temperatures (800, 900 or 1000 °C) for a hold time of 1 h at a heating rate of 20 °C/min in air in an electric furnace. The total porosity of the sintered porous titanium is larger than

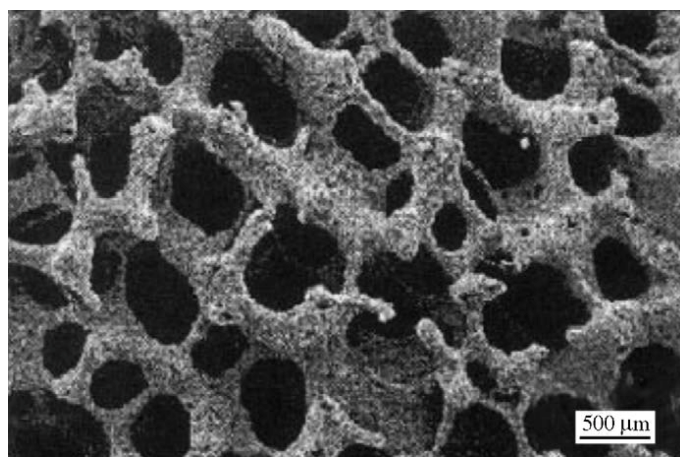
79%, and open porosity is larger than 74%. The open porosity ratio is in excess of 0.92, suggesting that most pores are interconnected. Moreover, the strength (6–10 MPa) and elastic modulus (0.4–0.6 GPa) of the sintered porous titanium conform to the basic mechanical property requirement of cancellous bone.

Figure 34. Schematic representation of the three-step replication process ([232], modified).



Li *et al.* [251] utilized this method to produce porous titanium and its alloy structures. Polyurethane porous materials were immersed in titanium slurry comprising Ti-6Al-4V powder (70 wt%), H₂O (20 wt%) and ammonia solution. The sample was subsequently dried and the process was repeated until all the struts of the polyurethane porous material were coated with Ti-6Al-4V powder. After thermal removal of the polyurethane scaffold and binder, samples were sintered at 1250 °C for 2 h in a vacuum furnace. A reticulated open cell porous material with hollow titanium struts remained, as shown in Figure 35. Open cellular pores are necessary for human bone ingrowth, and extensive body fluid transport through the porous scaffold matrix is possible, which can trigger bone growth if substantial pore interconnectivity is established [31,232]. The porous Ti-based alloy fabricated in this way was found to possess a porosity of 88% and compressive strength of about 10 MPa.

Figure 35. SEM microstructure of reticulated porous Ti-6Al-4V produced by sintering of powders deposited onto a temporary polyurethane scaffold [232]. Reprinted with permission from [232]. Copyright 2006 Elsevier.



It was found that the rheological properties of the titanium slurry played an important role in the impregnation process, governed by the particle size and shape of the raw powder, the type and content of the binder, *etc.* It was also discovered that a rapid drying process was important in maintaining a positive replica shape. It was later shown that a second deposition of powder slurry on a previously sintered porous material followed by a second sintering resulted in increased density (80%) and improved

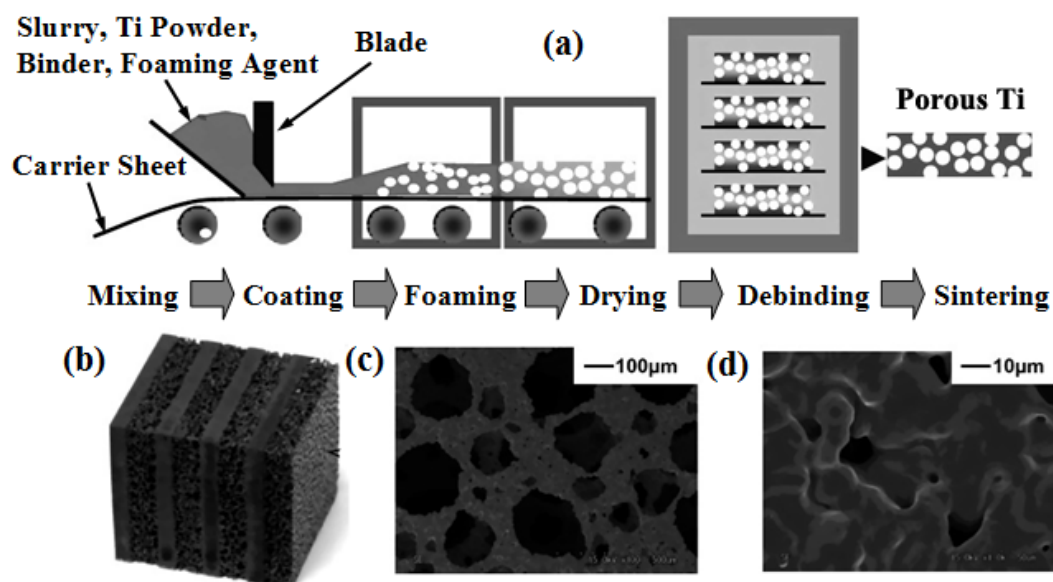
compressive strength (36 MPa), as a result of the correction of flaws in the titanium struts created during the first cycle [318].

5.3.14. Multilayer Porous Titanium

Although open pore structures have the advantages of low elastic modulus and bone ingrowth, leading to better fixation with bone, they have the disadvantage of insufficient mechanical strength compared with that of bulk structural materials [319]. As a result, the majority of these porous metals are applied as coatings on fully dense substrates [320].

Imwinkelried [321] reported the first application of a porous titanium device for human lumbar spine. However, the yield strength of this porous titanium with porosities of 63%–50% was 68–140 MPa under compression. This low mechanical property limited its application to the load-bearing devices for human lumbar spine. Therefore, porous metal fabrication technology ensuring adequate strength and tailorable open pore structure is assumed to be very important for orthopaedic implants. To achieve these contradictory requirements of adequate strength and high porosity with adequately open pore structure, some researchers developed novel porous titanium by stacking porous material sheets of different porosities layer by layer to create multilayer porous titanium (Figure 36). The resulting multilayer porous titanium exhibited an elastic modulus of 11–12 GPa and yield strength of 150–240 MPa in compression tests with porosities of 80%–17%.

Figure 36. (a) Illustration of the slurry foaming method; (b) photograph of a multilayer porous titanium sample; (c,d) SEM microstructures of the arrow surface of (b) in (c) low and (d) high magnification [322]. Reprinted with permission from [322]. Copyright 2013 Elsevier.



5.3.15. Rapid Prototyping

Rapid prototyping (RP) techniques, combining computer-aided design (CAD) with computer-aided manufacturing (CAM), are considered as a viable alternative for achieving extensive and detailed control over porous architecture [323,324], making it possible to build objects with predefined

microstructure and macrostructure [325] and controlled hierarchical structures [326]. The imperfection of conventional techniques has encouraged the use of RP technologies [310]. Since 1980s, RP technologies have emerged as a revolutionary manufacturing process with inherent capability to rapidly make objects in virtually any shape. Until now, RP developments mainly focused on polymer and ceramic materials [309,327]. The transfer of RP technologies to metal materials possesses a significant challenge, because there are few investigators on making metal scaffold for orthopedic and tissue engineering application by RP techniques [328]. A key requirement for RP technologies is tight control over the scaffolds' pore structure, including pore size, shape, volume and interconnectivity [329]. This enables an accurate assessment of the level of precision that the fabrication process can deliver.

Two methods were applied to make metal scaffold. One is indirect to make porous scaffolds by investment casting melt metal or metal powder slurry into a mold where the mold was made using RP [328]. Another is developing porous titanium scaffolds for tissue engineering using direct metal deposition [330]. Using investment casting technique, Lopez *et al.* [49] created a porous titanium scaffold with 100% interconnected structure and porosity around 60%. Hollander *et al.* [214] used a technique called direct laser forming to create porous Ti-6Al-4V alloy. Direct laser metal sintering proved to be an efficient way constructing dental implants with a functionally graded material [331]. Garrett *et al.* [332] adopted a multi-stage RP technique combining RP and powder metallurgy techniques, and successfully produced porous titanium scaffolds with fully interconnected pore networks and reproducible porosity and pore size. The scaffolds' porous characteristics were governed by a sacrificial wax template, fabricated using a commercial three-dimensional (3D) printer. Powder metallurgy processes were employed to generate the titanium scaffolds by filling the wax template with titanium slurry. Scaffolds with porosities of 66.8%–3.6% revealed compression strength of 104.4–22.5 MPa in the axial direction and 23.5–9.6 MPa in the transverse direction, demonstrating their anisotropic nature and potential ability employed in orthopaedic applications. By altering the wax design template, pore sizes ranging from 200 to 400 μm were achieved. 3D reconstruction enabled the main architectural parameters such as pore size, interconnecting porosity, level of anisotropy and level of structural disorder to be determined.

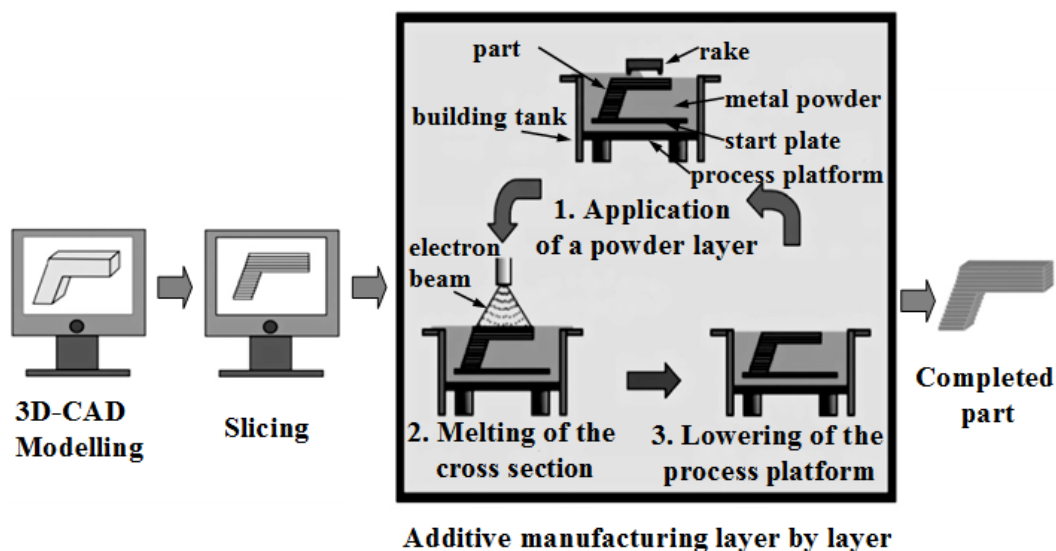
3D fiber deposition (3DF), also a RP technology, was successfully directly applied to produce novel 3D porous Ti-6Al-4V scaffolds with fully interconnected porous networks and highly controllable porosity and pore size [53] and thus meet the requirements of tissue engineering. Through a series of experiments, a nozzle diameter of 0.4 mm, a powder concentration of 66%, a fiber depositing pressure of 2.5 bar, a feeding speed of 350 mm/min, and an initial height of 0.25 mm, were found to be optimal parameters for fabrication of Ti-6Al-4V scaffolds. The scaffolds have a good attachment between layers, and a fully interconnected porous structure.

Selective laser sintering (SLS), as one of the RP technologies, can individually design and rapidly manufacture components with any complex geometry from powder materials based on CAD model [333]. In recent years, SLS technique has been explored to fabricate tissue engineering scaffolds and porous implants consisted mainly of biocompatible polymers and polymer/ceramic composites [334,335]. However, there is little information available on preparation of porous Ti-based alloys by SLS. Shishkovsky *et al.* [336] reported an original method to obtain porous NiTi alloy by a combination of SLS and SHS processes. Porous Ti-10Mo alloy was prepared from a mixture of elemental metal powders and polymer binders by indirect SLS [210]. When the sintering temperature increased to 1100 °C in a vacuum condition, the porosity and pore size were 63% and 178 μm , respectively. The

alloy comprised major α and minor β phases and meanwhile the alloy exhibited compressive yield strength of 95.59 MPa and an elastic modulus of 4.89 GPa at room temperature. SLM process was chosen to produce porous titanium with a particular periodic internal architecture. A porosity of 53% and pore size in the range of 860–1500 μm were finally adopted.

Selective electron beam melting (SEBM) was successfully used to fabricate novel porous Ti-6Al-4V structures with well-defined cellular structures for orthopaedic applications [55]. Firstly, a 3D CAD model is sliced into layers with constant thicknesses to provide layer information. The SEBM process starts with homogeneous application of a layer of metal powder on a process platform. After a preheating step, an electron beam scans the powder layer and creates a cross section of the part by fusing the loosely joined powder particles. Subsequently, the process platform is lowered by the thickness of one layer, and a new powder layer is applied and the process is repeated until the whole part has been built (Figure 37). The absorption of atmospheric gases should be effectively prevented because this might lead to a reduction in the ductility of titanium. Due to the layer-by-layer generation process, structures exhibited an interconnected porosity. Measurements gave a porosity of 80.5% and a mean pore size of 1.23 mm for the diamond structure, and 61.3% and 0.45 mm for the hatched structure, respectively, which is one of the most important requirements for tissue ingrowth. Thus, the structures exhibited porosities comparable to that of trabecular bone.

Figure 37. Schematic explaining the additive manufacturing by selective electron beam melting used to generate titanium bodies with a cellular structure [55]. Reprinted with permission from [55]. Copyright 2008 Elsevier.

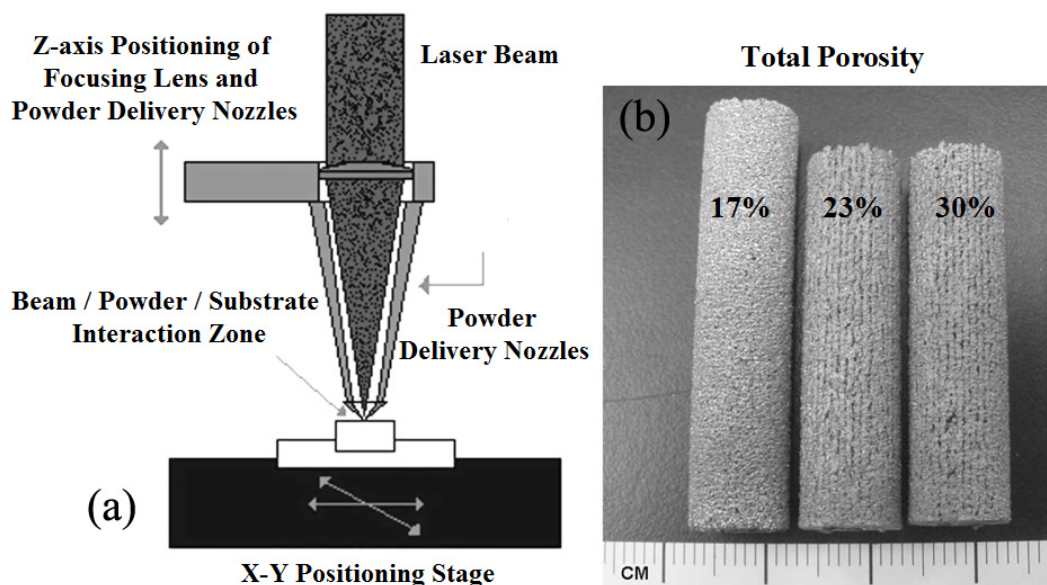


Laser engineered net shaping (LENS) is a solid freeform fabrication process that is primarily used to build near-net-shape metallic parts. Being a CAD and layer-based manufacturing process, LENS gives a significant advantage over conventional methods in terms of controlling the shape, size and internal architecture, particularly of porous structures. The schematic representation of the LENS process is shown in Figure 38a. First, a 3D model of a component is generated using CAD. Subsequently, a computer program slices the model into a number of horizontal cross sections or layers. These cross sections are sequentially created on a substrate, producing a 3D object. More detailed description of the

process is provided in Reference [221]. Previous work involving LENS has been focused on net shape manufacturing [337], alloy development [338], gradient structures [339,340] and coatings [341]. Recently, this process has also been used to fabricate net shape porous Ti-based alloys [221] with superior mechanical, physical, and biological properties.

As a CAD driven process, LENS opens the way for mass customization of metallic parts, such as bone implants. LENS produced titanium parts have a natural rough surface with a macroporous structure, which also eliminates the need for applying a thermally sprayed titanium coating on implants. Moreover, this technique allows us to control porosity, pore size and distribution to meet a variety of different application needs. Bandyopadhyay *et al.* [342] have fabricated porous Ti-6Al-4V alloy structures (Figure 38 b), and demonstrated that the advanced manufacturing technique can be used to fabricate low modulus and tailored porosity implants with a wide variety of alloys. The effective elastic modulus of Ti-6Al-4V alloy has been tailored between 7 and 60 GPa, and porous Ti-based alloys containing 23%–32% porosity showed elastic modulus equivalent to human cortical bone. Also, Bandyopadhyay [212] used this technology to successfully fabricate 3D interconnected porous titanium structures with controlled porosity and pore size for hard tissue replacement. Meanwhile, the porous titanium exhibited a high mechanical strength between 24 and 463 MPa and an elastic modulus between 2.6 and 44 GPa, which are better matched properties with bone tissue compared with dense titanium.

Figure 38. (a) Schematic depiction of the laser engineered net shaping (LENS) process; (b) typical porous Ti-6Al-4V samples fabricated using LENS [342]. Reprinted with permission from [342]. Copyright 2010 Elsevier.



Notwithstanding the advancements have been attained in porous titanium and its alloy scaffolds fabrication, the control over scaffold architecture using conventional sintering is highly process dependent. Over the past few years, novel direct fabrication processes of metallic components such as direct laser metal sintering [331], using metal powders to create functional parts with gradient porosity and cellular structures, can overcome the shortcomings of conventional methods. However, there are disadvantages such as high cost and low efficiency.

5.3.16. Advantages and Disadvantages of Various Preparation Methods

Many techniques have been applied to produce porous titanium and its alloy implants in recent years as above mentioned, but almost all the fabrication routes suffer from some problems stated to a certain extent.

Formation of secondary intermetallic phases, irregular pore shapes, inappropriate pore size, inhomogeneous pore distribution and the contamination during conventional powder metallurgy processing techniques, such as SHS, HIP, conventional sintering, SPS, MIM and space holder technique, limit their use. For example, when elemental powders are used in any of the powder metallurgy methods, undesirable nonequiatomic Ti-Ni phases leading to brittleness and inferior superelasticity often remain in the produced porous material. All these powder metallurgy processing techniques, especially MIM and space holder method, cannot avoid contamination during processing due to decomposition of binders and space filling materials which are mainly polymeric based or metallic salts. Although the combustion synthesis process can produce high purity porous materials, the complex shaped porous implants cannot be fabricated by the above-mentioned traditional methods. In addition, titanium and its alloys require very strictly controlled furnace atmospheres and they are extremely prone to react to interstitial elements such as O, C, N and H. As a result, contamination and more or less decrease in mechanical features are almost inevitable for all of the production routes. For example, through space holder method, homogenous pore structure can be produced with greater porosity, but nonmetallic inclusion tends to be introduced into the powders because of large quantities of space holder additions. Although higher pore sizes can be reached with the space holder technique, mechanical properties obtained may be lower than those of human bone [234]. In comparison, porous materials fabricated by powder sintering show high purity, but pore sizes and shapes are mainly predetermined by the raw powder characteristics, which makes pore structure difficult to control, while sintering of compacted loose powder normally results in low porosities. Meanwhile, fabrication technique of porous titanium and its alloys based on prealloyed starting powder generally contains lower levels of biocompatible elements and is expensive when compared to the use of elemental powders. Moreover, a common limitation of traditional processes is the inability of individually designing and manufacturing customized prostheses with complex and 3D framework. FC process mostly leads to randomly distributed pores whereas RP and laser processing are adopted when a controlled architecture is required. In both cases, the control of elastic properties anisotropy seems to be difficult.

A variety of powder metallurgy approaches have been developed to fabricate titanium products with tailored porosity. Wen *et al.* [178] used space holder method to create products with a large portion of open pores in an interconnected structure, which are created by the space holders. However, it is limited by high cost of molding dies, the limited complexity of compact shape and a variable density gradient. Chen *et al.* [285] employed metal injection molding, mixing titanium powders with space holders, to produce porous titanium compacts. MIM can be used to fabricate complex shapes, but the cost of molds and the problem of variable density gradient are important issues. In addition, a relatively large amount of binder is required for MIM, which raises concerns about binder residuals after the debinding stage, especially in the case of titanium.

A modified powder metallurgy technique called sponge replication [52] or impregnating method [343] has been used in fabrication of porous titanium and its alloys, by which pore size, shape, and distribution

can be well adjusted in a large scale. Some interconnected porous structures that perfectly mimic spatial morphology of cancellous bone can be easily reproduced by this method. However, the major drawback is the difficulty to avoid contamination and impurity phases in the titanium materials. In addition, sintered titanium struts likely contain cracks and other metallographic defects, and thus porous titanium materials cannot bear tensile stress and even exhibit brittle nature. This limitation implies a risk of the orthopedic applications of the porous titanium *in vivo* where a tensile or impact load may be applied on the implant.

In order to improve toughness and tensile strength of porous titanium, a novel porous titanium material called entangled wire material [314] has been developed. Its prominent advantage is that strong metal wires acting as struts construct spatial porous structure, so that the drawbacks of as-sintered/as-solidified struts (e.g., metallurgical defects, contaminations, *etc.*) can be completely overcome. Compared with brittle nature of conventional porous titanium, entangled titanium wire porous material is very tough and exhibits excellent superelasticity. Its superiority in mechanical properties supposes the potentials for orthopedic applications, such as hip joint implant and dental implant, *etc.* However, elastic modulus is too low due to structural flexibility of entangled titanium wire materials and is not suitable for load-bearing biomedical applications. The relationship between mesh structure and mechanical properties has not been established. Furthermore, basic aspects in terms of fabrication techniques (especially for the 3D porous titanium wire materials), structure characterization, and mechanical properties tailoring, are still open for investigation.

In recent years, RP technique has been utilized to fabricate porous titanium and its alloys by using laser power to sinter/remelt titanium powders [214]. It is of great benefit to accurately control pore shape, size and distribution by beforehand design and programming, so that an ideal porous architecture can be constructed. With alternative fabrication approaches, this technique has been developed into direct laser sintering [331] and selective laser melting [221,344]. The RP technique provides good feasibility and excellent flexibility for production of custom built metallic implants with complicated structures. Another advantage of RP is the case sensitive manufacturing according to the needs of specific patient. However, porous titanium production also suffers from impurities, inclusions and other defects associated with laser sintering or melting processing, which significantly deteriorate mechanical properties such as tensile stress resistance and toughness. In the view of physical metallurgy, the struts in porous titanium with as-sintered (laser sintering) or as-solidified (laser melting) microstructure usually exhibits much lower ductility than that of the wrought or plastically deformed counterparts. It is unlikely that laser sintered/melted porous titanium implants can stand against tensile and impact stress, though there are very few data published [214,221,331,344]. Apart from RP, a similar 3D deposition approach was also used to fabricate porous titanium, in which deposited 3D porous structure was strengthened by drying in air and sintering in high vacuum [53]. This approach does not need laser source and control system involved. Despite the fact that a good 3D mesh structure was constructed, its low tensile strength and low ductility can be expected due to the similar above reasons. Besides, this method is often time consuming because of the need to use pre-designed wax templates, and hence it is difficult to employ RP in mass production.

Therefore, there are still problems to be solved in current techniques for fabrication of porous titanium and its alloys for biomedical applications: the difficulty to create controlled pore characteristics such as porosity, pore size and distribution, *etc.*; contamination, presence of impurity phases, limited and

predetermined part geometries; the insufficient knowledge of porous structure-property relationships; the requirements of new sintering techniques with rapid energy transfer, and less energy consumption and so on. The growing demand for individualized treatment and excellent properties of a porous metallic implant requires the use of novel methods to fabricate near-net-shape implants, which likely could be achieved by combining the above-mentioned approaches. Fabrication methods for porous titanium and its alloys that can ensure uniform pore size, shape and distribution, mechanical properties and high levels of purity are in high demand [232]. Conventionally sintered porous titanium and its alloys are often very brittle and are prone to crack propagation at low stresses and usually suffer from loss of physical properties due to stress concentrations at porous interface, microstructures changes, and surface contamination from high temperature sintering process [51,178,232]. Influences of microstructural configurations on performance of porous titanium and its alloys will be discussed in the next section.

5.4. Prospects and Challenges of Porous Ti-Based Alloys: Current Status, Future Opportunities and Obstacles for Expanded Applications

Porous titanium and its alloys are considered as a new class of materials. This is mostly due to the fact that their applications have been discovered in the past two decades and are becoming more and more applicable and popular. The characteristics of porous Ti-based alloys are the combined properties of metals and porous materials. Metals are tough and strong. Porous materials have low weight and adjustable properties [227]. These combined characteristics have made the application of porous Ti-based alloys quite extensive. Each specific feature of porous materials is used in a separate application. Biomedical implants are among the most applications of porous Ti-based alloys [240].

Research on the biological behavior of metals has shown that the composition of implant biomaterials must be carefully selected to avoid adverse reactions. Ti, Zr, Nb, Mo, Ta, Sn *etc.* are non-toxic metals with a good compatibility. Because β -type Ti-based alloys themselves obtain high strength and low elastic modulus compared to pure titanium, they are also one of the promising candidates as a starting material for the improvement of mechanical properties of porous compacts.

To provide a way for living bone to attach itself permanently to an implant, an artificial bone should have a porous structure. It has been proven that porous titanium implants demonstrate an important gain in promoting tissue ingrowth and in the firm securing of an implant [345]. Several manufacturing techniques are capable of producing porous materials, such as sintering, SHS, *etc.* Some recent studies show the potential of using these techniques to control pore size, shape, orientation and distribution, including the creation of hierarchical and functionally graded pore structures [175,180,181]. Thus there is an increasing research interest in developing porous Ti-based alloys using non-toxic alloying elements. New generation porous Ti-based alloy scaffolds are expected to combine high mechanical strength and good biocompatibility.

Although fabrication of implants from materials with lower elastic modulus can reduce stress shielding effect, the modulus mismatch to bone is still substantial [346]. A suggestion to overcome this drawback could be the use of porous materials in stems. The clinical literature of the past 30 years records a variety of approaches to this end and several researchers have performed studies aimed at clarifying the fundamental aspects of interactions between porous metals and hard tissue. Porous

materials in arthroplasty implants are increasingly attracting the widespread interest of researchers as a method of reducing stiffness mismatches and achieving stable long-term fixation by means of full bone ingrowth.

6. Conclusions

Metallic biomaterials are still widely used, mainly for the reconstruction of failed hard tissue. Intense researches are still being pursued in the development of new Ti-based alloys with biofunctionalization (including mechanical biofunctionalization) closer to human bone, owing to their excellent mechanical strength and resilience when compared to alternative biomaterials, such as polymers and ceramics. Development of an appropriate microstructure with optimum mechanical properties is a challenging problem in the field of low modulus β -type Ti-based alloys. The interest in using porous Ti-based alloys for orthopaedic reconstructive surgery as a means of replacing autografts is of increasing interest and the large number of scientific reports confirm this trend.

Although great progress has been made with the various available fabrication processes in manufacturing porous structures, certain limitations continue to exist. The successful employment of porous titanium and its alloys relies on the same requirement that can ensure homogeneously distributed pores of similar size and shape, and cell walls of consistent thickness, and levels of purity, and absence of cracks or crevices, a multi-factorial design process that has to consider understanding of material properties, such as corrosion resistance, passivation levels and potential for bone adherence.

In spite of the fact the newly developed Ti-based alloys have modulus closer to bone and consist of highly compatible alloying elements, their mechanical properties such as wear resistance and strength under loading conditions are poor. Extensive research is presently being carried out to improve the properties of Ti-based materials. However, only compressive studies are carried out at different conditions of loading and environment.

Continued activity within this area will hopefully bring new materials and techniques improving the quality of patient care and lifestyle. In the future, success in this exciting endeavor will require an ever increasing cooperation of individuals with expertise in materials science, biomechanics and cell biologists in order to attain increased functional longevity of the implant in the human body.

Acknowledgments

This work was supported by the Guangdong Natural Science Foundation (No. S2013010012147), the Science and Technology Innovation Project of Higher School of Guangdong Province (No. 2012KJCX0010), the Fundamental Research Funds for the Central Universities (No. 2013ZZ0008), the Program for New Century Excellent Talents in University (No. NCET-11-0163), and the Excellent Young Talents of South China University of Technology.

Conflicts of Interest

The authors declare no conflict of interest.

References

1. Park, J.B. Biomaterials: Introduction. In *The Biomedical Engineering Handbook*; CRC Press: Boca Raton, FL, USA, 2000; Volume 1, pp. IV1–IV8.
2. Temenoff, J.S.; Mikos, A.G. *Biomaterials: The Intersection of Biology and Materials Science*; Pearson/Prentice Hall: Upper Saddle River, NJ, USA, 2008; pp. 235–258.
3. Hanawa, T. Recent development of new alloys for biomedical use. *Mater. Sci. Forum* **2006**, *512*, 243–248.
4. Lütjering, G.; Williams, J.C. *Titanium*, 2nd ed.; Springer: Berlin, Germany, 2003; pp. 20–22.
5. Long, M.; Rack, H.J. Titanium alloys in total joint replacement—A materials science perspective. *Biomaterials* **1998**, *19*, 1621–1639.
6. Bothe, R.T.; Beaton, L.E.; Davenport, H.A. Reaction of bone to multiple metallic implants. *Surg. Gynecol. Obstet.* **1940**, *71*, 598–602.
7. Leventhal, G.S. Titanium, a metal for surgery. *J. Bone Jt. Surg.* **1951**, *33*, 473–474.
8. Bannon, B.P.; Mild, E.E. Titanium Alloys for Biomaterial Application: An Overview. *Titanium Alloys in Surgical Implants*; ASTM: Philadelphia, PA, USA, 1983; pp. 7–15.
9. Oliveira, V.; Chaves, R.R.; Bertazzoli, R.; Caram, R. Preparation and characterization of Ti-Al-Nb alloys for orthopedic implants. *Braz. J. Chem. Eng.* **1998**, *17*, 326–333.
10. Zwicker, U.; Buhler, K.; Muller, R.; Beck, H.; Schmid, H.J.; Ferstl, J. Mechanical Properties and Tissue Reactions of a Titanium Alloy for Implant Material. In *Titanium'80, Science and Technology*; Kimura, I., Ed.; Metallurgical Society of AIME: New York, NY, USA, 1980; Volume 1, pp. 505–514.
11. Niinomi, M. Recent metallic materials for biomedical applications. *Metall. Mater. Trans. A* **2002**, *33*, 477–486.
12. Evans, F.G. Mechanical properties and histology of cortical bone from younger and older men. *Anat. Rec.* **1976**, *185*, 1–11.
13. Lindahl, O.; Lindgren, A.G. Cortical bone in man II. Variation in tensile strength with age and sex *Acta Orthop. Scand.* **1967**, *38*, 141–147.
14. Rho, J.Y.; Tsui, T.Y.; Pharr, G.M. Elastic properties of human cortical and trabecular lamellar bone measured by nanoindentation. *Biomaterials* **1997**, *18*, 1325–1330.
15. Lindahl, O. Mechanical Properties of Dried Defatted Spongy Bone. *Acta Orthop. Scand.* **1976**, *47*, 11–19.
16. Ding, M.; Dalstra, M.; Danielsen, C.C.; Kabel, J.; Hvid, I.; Linde, F. Age variations in the properties of human tibial trabecular bone. *J. Bone Jt. Surg.* **1997**, *79*, 995–1002.
17. Gross, S.; Abel, E.W. A finite element analysis of hollow stemmed hip prostheses as a means of reducing stress shielding of the femur. *J. Biomech.* **2001**, *34*, 995–1003.
18. Kuroda, D.; Niinomi, M.; Morinaga, M.; Kato, Y.; Yashiro, T. Design and mechanical properties of new β type titanium alloys for implant materials. *Mater. Sci. Eng. A* **1998**, *243*, 244–249.
19. Hao, Y.L.; Niinomi, M.; Kuroda, D.; Fukunaga, K.; Zhou, Y.L.; Yang, R. Aging response of the Young's modulus and mechanical properties of Ti-29Nb-13Ta-4.6Zr. *Metall. Mater. Trans. A* **2003**, *34*, 1007–1012.

20. Sakaguchi, N.; Niinomi, M.; Akahori, T.; Takeda, J.; Toda, H. Relationship between tensile deformation behavior and microstructure in Ti-Nb-Ta-Zr. *Mater. Sci. Eng. C* **2005**, *25*, 363–369.
21. Niinomi, M.; Akahori, T.; Katsura, S.; Yamauchi, K.; Ogawa, M. Mechanical characteristics and microstructure of drawn wire of Ti-29Nb-13Ta-4.6Zr for biomedical applications. *Mater. Sci. Eng. C* **2007**, *27*, 154–161.
22. Kuroda, D.; Kawasaki, H.; Yamamoto, A.; Hiromoto, S.; Hanawa, T. Mechanical properties and microstructures of new Ti-Fe-Ta and Ti-Fe-Ta-Zr system alloys. *Mater. Sci. Eng. C* **2005**, *25*, 312–320.
23. Nag, S.; Banerjee, R.; Fraser, H.L. Microstructural evolution and strengthening mechanisms in Ti-Nb-Zr-Ta, Ti-Mo-Zr-Fe and Ti-15Mo biocompatible alloys. *Mater. Sci. Eng. C* **2005**, *25*, 357–362.
24. Wang, K. The use of titanium for medical applications in the USA. *Mater. Sci. Eng. A* **1996**, *213*, 134–137.
25. Qazi, J.I.; Rack, H.J. Metastable beta titanium alloys for orthopedic applications. *Adv. Eng. Mater.* **2005**, *7*, 993–998.
26. Brailovski, V.; Prokoshkin, S.; Gauthier, M.; Inaekyan, K.; Dubinskiy, S.; Petrzhik, M.; Filonov, M. Bulk and porous metastable beta Ti-Nb-Zr (Ta) alloys for biomedical applications. *Mater. Sci. Eng. C Mater. Biol. Appl.* **2011**, *31*, 643–657.
27. Matsumoto, H.; Watanabe, S.; Hanada, S. Strengthening of low Young's modulus beta Ti-Nb-Sn alloys by thermomechanical processing. In *Proceeding of the Materials & Processes for Medical Devices Conference 2006*, Boston, MA, USA, 14–16 November 2006.
28. Gibson, L.J. The mechanical behavior of cancellous bone. *J. Biomech.* **1985**, *18*, 317–328.
29. Robertson, D.M.; Pierre, L.; Chahal, R. Preliminary observations of bone in growth into porous materials. *J. Biomed. Mater. Res.* **1976**, *10*, 335–344.
30. Cameron, H.U.; Macnab, I.; Pilliar, R.M. A porous metal system for joint replacement surgery. *Int. J. Artif. Organs* **1978**, *1*, 104–109.
31. Head, W.C.; Bauk, D.J.; Emerson, J.R. Titanium as the material of choice for cementless femoral components in total hip arthroplasty. *Clin. Orthop. Relat. Res.* **1995**, *311*, 85–90.
32. Schneider, E.; Kinast, C.; Eulenberger, J.; Wyder, D.; Eskilsson, G.; Perren, S.M. A comparative study of the initial stability of cementless hip prostheses. *Clin. Orthop. Relat. Res.* **1989**, *248*, 200–209.
33. Kujala, S.; Ryhanen, J.; Danilov, A.; Tuukkanen, J. Effect of porosity on the osteointegration and bone ingrowth of a weight-bearing nickel–titanium bone graft substitute. *Biomaterials* **2003**, *24*, 4691–4697.
34. Homsy, C.A.; Cain, T.E.; Kessler, F.B.; Anderson, M.S.; King, J.W. Porous implant systems for prosthesis stabilization. *Clin. Orthop.* **1972**, *89*, 220–235.
35. Pilliar, R.M. Porous-surfaced metallic implants for orthopedic applications. *J. Biomed. Mater. Res.* **1987**, *21*, 1–33.
36. Kienapfel, H.; Sprey, C.; Wilke, A.; Griss, P. Implant fixation by bone ingrowth. *J. Arthroplast.* **1999**, *14*, 355–368.
37. Karageorgiou, V.; Kaplan, D. Porosity of 3D biomaterial scaffolds and osteogenesis. *Biomaterials* **2005**, *26*, 5474–5491.

38. Zhuravleva, K.; Chivu, A.; Teresiak, A.; Scudino, S.; Calin, M.; Schultz, L.; Eckert, J.; Gebert, A. Porous low modulus Ti40Nb compacts with electrodeposited hydroxyapatite coating for biomedical applications. *Mater. Sci. Eng. C* **2013**, *33*, 2280–2287.
39. Simancik, F. Introduction: The Strange World of Cellular Metals. In *Handbook of Cellular Metals*; Degischer, K., Ed.; Wiley-VCH Verlag: Weinheim, Germany, 2002; pp. 1–4.
40. Weber, J.N.; White, E.W. Carbon-metal graded composites for permanent osseous attachment of non-porous metals. *Mater. Res. Bull.* **1972**, *7*, 1005–1016.
41. Klawitter, J.J.; Weinstein, A.M. The status of porous materials to obtain direct skeletal attachment by tissue ingrowth. *Acta Orthop. Belg.* **1974**, *40*, 755–765.
42. Sauer, B.W.; Weinstein, A.M.; Klawitter, J.J.; Hulbert, S.F.; Leonard, R.B.; Bagwell, J.G. The role of porous polymeric materials in prosthesis attachment. *J. Biomed. Mater. Res.* **1974**, *8*, 145–153.
43. Hirschhorn, J.; McBeath, A.; Dustoor, M. Porous titanium surgical implant materials. *J. Biomed. Mater. Res.* **1971**, *2*, 49–67.
44. Hahn, H.; Palich, W. Preliminary evaluation of porous metal surfaced titanium for orthopedic implants. *J. Biomed. Mater. Res.* **1970**, *4*, 571–577.
45. Karagiennes, M. Porous metals as a hard tissue substitute. *Biomater. Med. Dev. Artif. Organs* **1973**, *1*, 171–181.
46. Yoshikawa, H.; Myoui, A. Bone tissue engineering with porous hydroxyapatite ceramics. *J. Artif. Organs* **2005**, *8*, 131–136.
47. Rezwan, K.; Chen, Q.Z.; Blaker, J.J.; Boccaccini, A.R. Biodegradable and bioactive porous polymer/inorganic composite scaffolds for bone tissue engineering. *Biomaterials* **2006**, *27*, 3413–3431.
48. Wen, C.E.; Yamada, Y.; Shimojima, K.; Sakaguchi, Y.; Chino, Y.; Hosokawa, H.; Mabuchi, M. Novel titanium foam for bone tissue engineering. *J. Mater. Res.* **2002**, *17*, 2633–2639.
49. Lopez-Heredia, M.A.; Sohiera, J.; Gaillard, C.; Quillard, S.; Dorget, M.; Layrolle, P. Rapid prototyped porous titanium coated with calcium phosphate as a scaffold for bone tissue engineering. *Biomaterials* **2008**, *29*, 2608–2615.
50. Yamada, Y.; Shimojima, K.; Sagaguchi, Y.; Mabuchi, M.; Nakamura, M.; Asahina, T.; Mukai, T.; Kanahashi, H.; Higashi, K. Processing of cellular magnesium materials. *Adv. Eng. Mater.* **2000**, *2*, 184–187.
51. Oh, I.H.; Nomura, N.; Masahashi, N.; Hanada, S. Mechanical properties of porous titanium compacts prepared by powder sintering. *Scr. Mater.* **2003**, *49*, 1197–1202.
52. Li, J.P.; Li, S.H.; van-Blitterswijk, C.A.; de-Groot, K. A novel porous Ti6Al4V: Characterization and cell attachment. *J. Biomed. Mater. Res.* **2005**, *73A*, 223–233.
53. Li, J.P.; de-Wijn, J.R.; van-Blitterswijk, C.A.; de-Groot, K. Porous Ti6Al4V scaffold directly fabricating by rapid prototyping: Preparation and *in vitro* experiment. *Biomaterials* **2006**, *27*, 1223–1235.
54. Markaki, A.E.; Clyne, T.W. The effect of cell wall microstructure on the deformation and fracture of aluminium-based foams. *Acta Mater.* **2001**, *49*, 1677–1686.

55. Heinel, P.; Muller, L.; Korner, C.; Singer, R.F.; Muller, F.A. Cellular Ti-6Al-4V structures with interconnected macro porosity for bone implants fabricated by selective electron beam melting. *Acta Biomater.* **2008**, *4*, 1544–1536.
56. Hayashi, K.; Uenoyama, K.; Matsuguchi, N.; Sugioka, Y. Quantitative analysis of *in vivo* tissue responses to titanium-oxide and hydroxyapatite-coated titanium alloy. *J. Biomed. Mater. Res.* **1991**, *25*, 515–523.
57. He, G.; Liu, P.; Tan, Q.B. Porous titanium materials with entangled wire structure for load-bearing biomedical applications. *J. Mech. Behav. Biomed. Mater.* **2012**, *5*, 16–31.
58. Burstein, A.H.; Reilly, D.T.; Martens, M. Aging of bone tissue: Mechanical properties. *J. Bone Jt. Surg.* **1976**, *58*, 82–86.
59. Black, J.; Hastings, G. *Handbook of Biomaterial Properties*; Chapman & Hall: London, UK, 1998; pp. 16–21.
60. Vinz, H. Change in the mechanical properties of human compact bone tissue upon aging. *Mech. Compos. Mater.* **1975**, *11*, 568–571.
61. Geetha, M.; Singh, A.K.; Asokamani, R.; Gogia, A.K. Ti based biomaterials, the ultimate choice for orthopaedic implants—A review. *Prog. Mater. Sci.* **2009**, *54*, 397–425.
62. Wang, X.H.; Li, S.J.; Jia, M.T.; Hao, Y.L.; Yang, R.; Guo, Z.X. Porous Ti-24Nb-4Zr-8Sn alloy for biomedical applications fabricated by space-holder method. *Chin. J. Nonferr. Met.* **2010**, *20*, s967–s971.
63. Hrabe, N.W. Characterization of Cellular Titanium for Biomedical Applications. Ph.D. Thesis, University of Washington, Seattle, WA, USA, 28 May 2010.
64. Moyon, B.J.-L.; Lathey, P.J.; Weinberg, E.H.; Harris, W.H. Effects on intact femora of dogs of the application and removal of metal plates. A metabolic and structural study comparing stiffer and more flexible plates. *J. Bone Jt. Surg.* **1978**, *60*, 940–947.
65. Williams, D.F. On the mechanisms of biocompatibility. *Biomaterials* **2008**, *29*, 2941–2953.
66. Wataria, F.; Yokoyama, A.; Omorib, M.; Hiraic, T.; Kondoa, H.; Uoa, M.; Kawasakia, T. Biocompatibility of materials and development to functionally graded implant for bio-medical application. *Compos. Sci. Technol.* **2004**, *64*, 893–908.
67. Calin, M.; Gebert, A.; Ghinea, A.C.; Gostin, P.F.; Abdi, S.; Mickel, C.H.; Eckert, J. Designing biocompatible Ti-based metallic glasses for implant applications. *Mater. Sci. Eng. C* **2013**, *33*, 875–883.
68. Hallab, N.J.; Anderson, S.; Stafford, T.; Glant, T.; Jacobs, J.J. Lymphocyte responses in patients with total hip arthroplasty. *J. Orthop. Res.* **2005**, *23*, 384–391.
69. Shabalovskaya, S.A. Surface, corrosion and biocompatibility aspects of Nitinol as an implant material. *Biomed. Mater. Eng.* **2002**, *12*, 69–109.
70. Sargeant, A.; Goswami, T. Hip implants: Paper V. Physiological effects. *Mater. Des.* **2006**, *27*, 287–307.
71. Liang, P.G.; Ferguson, E.S.; Hodge, E.S. Tissue reaction in rabbit muscle exposed to metallic implants. *J. Biomed. Mater. Res.* **1967**, *1*, 135–149.
72. Viceconti, M.; Muccini, R.; Bernakiewicz, M.; Baleani, M.; Cristofolini, L. Large-sliding contact elements accurately predict levels of bone-implant micromotion relevant to osseointegration. *J. Biomech.* **2000**, *33*, 1611–1618.

73. Alves, C., Jr.; Guerra Neto, C.L.B.; Morais, G.H.S.; da Silva, C.F.; Hajek, V. Nitriding of titanium disks and industrial dental implants using hollow cathode discharge. *Surf. Coat. Technol.* **2005**, *194*, 196–202.
74. Brizuela, M.; Garcia-Luis, A.; Viviente, J.L.; Braceras, I.; Onate, J.L. Tribological study of lubricious DLC biocompatible coatings. *J. Mater. Sci. Mater. Med.* **2002**, *13*, 1129–1133.
75. Gepreel, M.A.; Niinomi, M. Biocompatibility of Ti-alloys for long-term implantation. *J. Mech. Behav. Biomed. Mater.* **2013**, *20*, 407–415.
76. Ramakrishna, S.; Mayer, J.; Wintermantel, E.; Leong, K.W. Biomedical applications of polymer-composite materials: A review. *Compos. Sci. Technol.* **2001**, *61*, 1189–1224.
77. Wise, D.L. *Biomaterials Engineering and Devices*; Humana Press: Berlin, Germany, 2000; pp. 205–319.
78. Park, J.B.; Bronzino, J.D. *Biomaterials: Principles and Applications*; CRC Press: Boca Rator, FL, USA, 2003; pp. 1–241.
79. Hulth, A. Current concepts of fracture healing. *Clin. Orthop.* **1989**, *249*, 265–284.
80. Hutzschenreuter, P.; Brümmer, H. Screw Design and Stability. *Current Concepts of Internal Fixation*; Springer-Verlag: Berlin, Germany, 1980; pp. 244–250.
81. Cochran, G.V.B. Biomechanics of Orthopaedic Structures. *Primer in Orthopaedic Biomechanics*; Churchill Livingstone: New York, NY, USA, 1982; pp. 143–215.
82. Sarmiento, A.; Ebramzadeh, E.; Gogan, W.J. Cup containment and orientation in cemented total hip arthroplasties. *J. Bone Jt. Surg.* **1990**, *72B*, 996–1002.
83. Burstein, A.H.; Wright, T.H. Biomechanics. In *Surgery of the Knee*, 2nd ed.; Insall, J.N., Windsor, R.E., Scott, W.N., Eds.; Churchill Livingstone: New York, NY, USA, 1993; Volume 7, pp. 43–62.
84. Perren, M.S.; Pohler, O.E.M.; Schneider, E. Titanium as Implant Material for Osteosynthesis Applications. In *Titanium in Medicine*; Brunette, D., Tengvall, P., Textor, M., Thomsen, P., Eds.; Springer-Verlag: Berlin/Heidelberg, Germany, 2001; pp. 772–823.
85. Kurtz, S.; Ong, K.; Lau, E.; Mowat, F.; Halpern, M. Projections of primary and revision hip and knee arthroplasty in the United States from 2005 to 2030. *J. Bone Jt. Surg. Am.* **2007**, *89*, 780–785.
86. Orthoinfo Homepage. Available online: <http://www.orthoinfo.aaos.org> (accessed on 24 October 2012.)
87. Niinomi, M. Recent research and development in metallic materials for biomedical, dental and healthcare products. *Mater. Sci. Forum* **2007**, *539–543*, 193–200.
88. Witcher, F.D. Simulation of *in vivo* loading conditions of nitinol vascular stent structures. *Comput. Struct.* **1997**, *64*, 1005–1011.
89. Sakaguchi, N.; Niinomi, M.; Akahori, T.; Takeda, J.; Toda, H. Effect of Ta content on mechanical properties of Ti-30Nb-XTa-5Zr. *Mater. Sci. Eng. C* **2005**, *25*, 370–376.
90. Nobuhito, S.; Niinomi, M.; Toshikazu, A.; Takashi, S.; Tadahiko, F. Effects of alloying elements on elastic modulus of Ti-Nb-Ta-Zr system alloy for biomedical applications. *Mater. Sci. Forum* **2004**, *449–452*, 1269–1272.
91. Sakaguchi, N.; Niinomi, M.; Akahori, T.; Saito, T.; Furuta, T. Effect of Nb content on microstructure, tensile properties and elastic modulus of Ti-XNb-10Ta-5Zr alloys for biomedical applications. *J. Jpn. Inst. Met.* **2003**, *67*, 681–687.

92. Ozaki, T.; Matsumoto, H.; Miyazaki, T.; Hasegawa, M.; Watanabe, S.; Hanada, S. Development of beta titanium alloys with low Young's modulus. *Adv. Mater. Process.* **2005**, *163*, 68–70.
93. Bönisch, M.; Calin, M.; Waitz, T.; Panigrahi, A.; Zehetbauer, M.; Gebert, A.; Skrotzki, W.; Eckert, J. Thermal stability and phase transformations of martensitic Ti-Nb alloys. *Sci. Technol. Adv. Mater.* **2013**, *14*, 055004:1–055004:9.
94. Ho, W.F.; Cheng, C.H.; Pan, C.H.; Wu, S.C.; Hsu, H.C. Structure, mechanical properties and grind ability of dental Ti-10Zr-X alloys. *Mater. Sci. Eng. C* **2009**, *29*, 36–46.
95. Zhen, T.Y.; Lian, Z. Influence of martensitic transformation on mechanical compatibility of biomedical β type titanium alloy TLM. *Mater. Sci. Eng. A* **2006**, *438–440*, 391–394.
96. Inoue, A. Stabilization of metallic supercooled liquid and bulk amorphous alloys. *Acta Mater.* **2000**, *48*, 279–306.
97. Guglielmotti, M.B.; Renou, S.; Cabrini, R.I. A histomorphometric study of tissue interface by laminar implant test in rats. *Int. J. Oral Maxillofac. Implant.* **1999**, *14*, 565–570.
98. Hsu, H.C.; Wu, S.C.; Sung, Y.C.; So, W.F. The structure and mechanical properties of as-cast Zr-Ti alloys. *J. Alloy. Compd.* **2009**, *488*, 279–283.
99. Schmidt, C.; Ignatius, A.A.; Claes, L.E. Proliferation and differentiation parameters of human osteoblasts on titanium and steel surfaces. *J. Biomed. Mater. Res.* **2001**, *54*, 209–215.
100. Niinomi, M. Recent research and development in titanium alloys for biomedical applications and healthcare goods. *Sci. Technol. Adv. Mater.* **2003**, *4*, 445–454.
101. Abdel-Hady, M.; Fuwa, H.; Hinoshita, K.; Kimura, H.; Shinzato, Y.; Morinaga, M. Phase stability change with Zr content in β -type Ti-Nb alloys. *Scr. Mater.* **2007**, *57*, 1000–1003.
102. Wang, X.; Li, Y.; Hodgson, P.D.; Wen, C. Biomimetic modification of porous TiNbZr alloy scaffold for bone tissue engineering. *Tissue Eng. A* **2010**, *16*, 309–316.
103. Niinomi, M.; Hattori, T.; Niwa, S. Material Characteristics and Biocompatibility of Low Rigidity Titanium Alloys for Biomedical Applications. In *Biomaterials in Orthopedics*; Yaszemski, M.J., Trantolo, D.J., Eds.; Marcel Dekker Inc.: New York, NY, USA, 2004; pp. 41–62.
104. Laheerte, P.; Eberhardt, A.; Philippe, M.J. Influence of the microstructure on the pseudoelasticity of a metastable beta titanium alloy. *Mater. Sci. Eng. A* **2005**, *396*, 223–230.
105. Yang, G.J.; Zhang, T. Phase transformation and mechanical properties of the $\text{Ti}_{50}\text{Zr}_{30}\text{Nb}_{10}\text{Ta}_{10}$ alloy with low modulus and biocompatible. *J. Alloy. Compd.* **2005**, *392*, 291–294.
106. Zhou, Y.L.; Niinomi, M.; Akahori, T. Decomposition of martensite α during aging treatments and resulting mechanical properties of Ti-Ta alloys. *Mater. Sci. Eng. A* **2004**, *384*, 92–101.
107. Li, Y.Y.; Zou, L.M.; Yang, C.; Li, Y.H.; Li, L.J. Ultrafine-grained Ti-based composites with high strength and low modulus fabricated by spark plasma sintering. *Mater. Sci. Eng. A* **2013**, *560*, 857–861.
108. Ikeda, M.; Ueda, M.; Matsunaga, R.; Ogawa, M.; Niinomi, M. Isothermal aging behavior of beta titanium-manganese alloys. *Mater. Trans.* **2009**, *50*, 2737–2743.
109. Ikeda, M.; Ueda, M.; Matsunaga, R.; Ogawa, M.; Niinomi, M. Influence of Fe content of Ti-Mn-Fe alloys on phase constitution and heat treatment behavior. *Mater. Sci. Forum* **2012**, *706–709*, 1893–1898.

110. Ashida, S.; Kyogaku, H.; Hosoda, H. Fabrication of Ti-Sn-Cr shape memory alloy by PM and its properties. *Mater. Sci. Forum* **2012**, *706–709*, 1943–1947.
111. Murayama, Y.; Sasaki, S. Mechanical properties of Ti-Cr-Sn-Zr alloys. *Bull. Niigata Inst. Technol.* **2009**, *14*, 1–8.
112. Kasano, Y.; Inamura, T.; Kanetaka, H.; Miyazaki, S.; Hosoda, H. Phase constitution and mechanical properties of Ti-(Cr, Mn)-Sn biomedical alloys. *Mater. Sci. Forum* **2010**, *654–656*, 2118–2121.
113. Wang, L.Q.; Cheng, X.X.; Li, Y.; Yeung, K.W.K.; Lu, W.J.; Qin, J.; Zhang, D. Fabrication and Characterization of Porous Beta Titanium alloy. In *Titanium Alloys: Formation, Characteristics and Industrial Applications*; Zhang, L.C., Yang, C., Eds.; Nova Science Publishers: New York, NY, USA, 2013; pp. 110–127.
114. Nakai, M.; Niinomi, M.; Zhao, X.F.; Zhao, X.L. Self-adjustment of Young's modulus in biomedical titanium alloy during orthopaedic operation. *Mater. Lett.* **2011**, *65*, 688–690.
115. Hynowska, A.; Pellicer, E.; Fornell, J.; González, S.; van Steenberge, N.; Suriñach, S.; Gebert, A.; Calin, M.; Eckert, J.; Baró, M.D.; *et al.* Nanostructured β -phase Ti-31.0Fe-9.0Sn and sub- μ m structured Ti-39.3Nb-13.3Zr-10.7Ta alloys for biomedical applications: Microstructure benefits on the mechanical and corrosion performances. *Mater. Sci. Eng. C* **2012**, *32*, 2418–2425.
116. Niinomi, M.; Nakai, M.; Hieda, J. Development of new metallic alloys for biomedical applications. *Acta Biomater.* **2012**, *8*, 3888–3903.
117. Niinomi, M.; Kuroda, D.; Fukunaga, K.; Morinaga, M.; Kato, Y.; Yashiro, T.; Suzuki, A. Corrosion wear fracture of new beta type biomedical titanium alloys. *Mater. Sci. Eng. A* **1999**, *263*, 193–199.
118. Zhang, L.C.; Klemm, D.; Eckert, J.; Hao, Y.L.; Sercombe, T.B. Manufacture by selective laser melting and mechanical behavior of a biomedical Ti-24Nb-4Zr-8Sn alloy. *Scr. Mater.* **2011**, *65*, 21–24.
119. Semlitsch, M.; Willert, H.G. Properties of implant alloys for artificial hip joints. *Med. Biol. Eng. Comput.* **1980**, *18*, 511–520.
120. Niinomi, M. Mechanical properties of biomedical titanium alloys. *Mater. Sci. Eng. A* **1998**, *243*, 231–236.
121. Boyer, B.; Welsch, G.; Collings, E.W. *Materials Properties Handbook: Titanium Alloys*; ASM International: Materials Park, OH, USA, 2007; pp. 790–810.
122. Narayan, R. Materials for medical devices, fundamentals of medical implant materials. *ASM Handb.* **2012**, *23*, 6–16.
123. Niinomi, M.; Nakai, M. Titanium-based biomaterials for preventing stress shielding between implant devices and bone. *Int. J. Biomater.* **2011**, *2011*, 1–10.
124. Ari-Gur, P.; Semiatin, S.L. Evolution of microstructure, macrotexture and microtexture during hot rolling of Ti-6Al-4V. *Mater. Sci. Eng. A* **1998**, *257*, 118–127.
125. Lütjering, G. Property optimization through microstructural control in titanium and aluminum alloys. *Mater. Sci. Eng. A* **1999**, *263*, 117–126.
126. Tang, X.; Ahmed, T.; Rack, H.J. Phase transformation in Ti-Nb-Ta and Ti-Nb-Ta-Zr alloys. *J. Mater. Sci.* **2000**, *35*, 1805–1811.

127. Geetha, M.; Singh, A.K.; Gogia, A.K.; Asokamani, R. Effect of thermomechanical processing on evolution of various phases in Ti-Nb-Zr alloys. *J. Alloy. Compd.* **2004**, *384*, 131–151.
128. Qazi, J.; Marquart, B.; Allard, L.F.; Rack, H.J. Phase transformations in Ti-35Nb-7Zr-5Ta-(0.06–0.68)O alloys. *Mater. Sci. Eng. C* **2005**, *25*, 389–397.
129. Matsumoto, H.; Watanabe, S.; Hanada, S.J. Beta TiNbSn alloys with low young's modulus and high strength. *Mater. Trans.* **2005**, *46*, 1070–1078.
130. Zhao, X.L.; Niinomi, M.; Nakai, M.; Miyamoto, G.; Furuhashi, T. Microstructures and mechanical properties of metastable Ti-30Zr-(Cr, Mo) alloys with changeable Young's modulus for spinal fixation applications. *Acta Biomater.* **2011**, *7*, 3230–3236.
131. Gabriel, S.B.; Panaino, J.V.P.; Santos, I.D.; Araujo, L.S.; Mei, P.R.; de Almeida, L.H. Characterization of a new beta titanium alloy, Ti-12Mo-3Nb, for biomedical applications. *J. Alloy. Compd.* **2012**, *536*, S208–S210.
132. Zhou, Y.L.; Niinomi, M. Microstructures and mechanical properties of Ti-50 mass% Ta alloy for biomedical applications. *J. Alloy. Compd.* **2008**, *466*, 535–542.
133. Zhao, X.L.; Niinomi, M.; Nakai, M.; Ishimoto, T.; Nakano, T. Development of high Zr-containing Ti-based alloys with low Young's modulus for use in removable implants. *Mater. Sci. Eng. C* **2011**, *31*, 1436–1444.
134. Xie, K.Y.; Wang, Y.B.; Zhao, Y.H.; Chang, L.; Wang, G.C.; Chen, Z.B.; Cao, Y.; Liao, X.Z.; Lavernia, E.J.; Valiev, R.Z.; *et al.* Nanocrystalline β -Ti alloy with high hardness, low Young's modulus and excellent *in vitro* biocompatibility for biomedical applications. *Mater. Sci. Eng. C* **2013**, *33*, 3530–3536.
135. Jung, T.K.; Semboshi, S.; Masahashi, N.; Hanada, S. Mechanical properties and microstructures of β Ti-25Nb-11Sn ternary alloy for biomedical applications. *Mater. Sci. Eng. C* **2013**, *33*, 1629–1635.
136. Cao, D.P. Mechanical and electrochemical characterization of Ti-12Mo-5Zr alloy for biomedical application. *J. Alloy. Compd.* **2011**, *509*, 8235–8238.
137. Guo, S.; Meng, Q.K.; Liao, G.Y.; Hu, L.; Zhao, X.Q. Microstructural evolution and mechanical behavior of metastable β -type Ti-25Nb-2Mo-4Sn alloy with high strength and low modulus. *Prog. Nat. Sci. Mater. Int.* **2013**, *23*, 174–182.
138. Teoh, S.H. Fatigue of biomaterials: A review. *Int. J. Fatigue* **2000**, *22*, 825–837.
139. Niinomi, M.; Akahori, T. Improvement of the fatigue life of titanium alloys for biomedical devices through microstructural control. *Expert Rev. Med. Devices* **2010**, *7*, 481–488.
140. Rack, H.J.; Qazi, J.I. Titanium alloys for biomedical applications. *Mater. Sci. Eng. C* **2006**, *26*, 1269–1277.
141. Lee, D.G.; Lee, S.; Lee, C.S. Quasi-static and dynamic deformation behavior of Ti-6Al-4V alloy containing fine α_2 -Ti₃Al precipitates. *Mater. Sci. Eng. A* **2004**, *366*, 25–37.
142. Kuhlman, G.W. A Critical Appraisal of Thermomechanical Processing of Structural Titanium Alloys. *Microstructure/Property Relationships in Titanium Aluminides and Alloys*; TMS: Warrendale, PA, USA, 1991; pp. 465–532.
143. He, G.; Hagiwara, M. Bimodal structured Ti-base alloy with large elasticity and low Young's modulus. *Mater. Sci. Eng. C* **2006**, *26*, 14–19.

144. Hao, Y.L.; Niinomi, M.; Kuroda, D.; Fukunaga, K.; Zhou, Y.L.; Yang, R.; Suzuki, A. Young's modulus and mechanical properties of Ti-29Nb-13Ta-4.6Zr in relation to α' martensite. *Metall. Mater. Trans. A* **2002**, *33*, 3137–3144.
145. Valiev, R.Z.; Stolyarov, V.V.; Rack, H.J.; Lowe, T.C. SPD-Processed Ultra-Fine Grained Ti Materials for Medical Applications. *Medical Device Materials*; Shrivastava; ASM: Cleveland, OH, USA, 2004; pp. 362–367.
146. Geetha, M.; Singh, A.K.; Muraleedharan, K.; Gogia, A.K.; Asokamani, R. Effect of thermomechanical processing on microstructure of a Ti-13Nb-13Zr alloy. *J. Alloy. Compd.* **2001**, *329*, 214–223.
147. Webster, T.J.; Ejiogor, J.U. Increased osteoblast adhesion on nanophase metals: Ti, Ti6Al4V, and CoCrMo. *Biomaterials* **2004**, *25*, 4731–4739.
148. Tane, M.; Akita, S.; Nakano, T.; Hagihara, K.; Umakoshi, Y.; Niinomi, M. Peculiar elastic behavior of Ti-Nb-Ta-Zr single crystals. *Acta Mater.* **2008**, *56*, 2856–2863.
149. Cleason, T.A.; Pendleton, H.J.R. Low Modulus Biocompatible Titanium Base Alloys for Medical Devices. U.S. Patent 5,871,595 A, 16 February 1999.
150. Ouchi, C. Development and Application of New Titanium Alloy SP-700. *Metallurgy and Technology of Practical Titanium Alloys*; TMS: Warrendale, PA, USA, 1994; pp. 37–45.
151. Jablovkov, V.R.; Murray, N.G.D.; Rack, H.J.; Freese, H.L. Influence of oxygen content on the mechanical properties of Titanium-35Niobium-7Zirconium-5Tantalum beta titanium alloy. *J. ASTM Int.* **2005**, *2*, 1–12.
152. Ahmed, T.; Long, M.; Slivestri, J.; Ruiz, C.; Rack, H.J. A New Low Modulus, Biocompatible Titanium Alloy. In *Titanium '95: Science and Technology*; Blenkinsop, P.A., Evans, W.J., Eds.; Institute of Metals: London, UK, 1996; Volume 2, pp. 1760–1767.
153. Qazi, J.; Rack, H.J. The Effect of Duplex Aging on the Tensile Behavior of Ti-35Nb-7Zr-5Ta-(0.06–0.7) O Alloys. In *Titanium 2003 Science and Technology*; Lutjering, G., Albrecht, J., Eds.; Wiley-VCH Verlag, GmbH and Co. KGaA: Weinheim, Germany, 2003; Volume 1, p. 651.
154. Qazi, J.I.; Tsakiris, V.; Marquardt, B.; Rack, H.J. Effect of Aging Treatments on the Tensile Properties of Ti-35Nb-7Zr-5Ta-(0.06–0.7) O Alloys. In *Titanium 2003 Science and Technology*; Lutjering, G., Albrecht, J., Eds.; Wiley-VCH Verlag, GmbH and Co. KGaA: Weinheim, Germany, 2004; p. 1651.
155. Long, M.; Crooks, R.; Rack, H.J. High-cycle fatigue performance of solution-treated metastable- β titanium alloys. *Acta Mater.* **1999**, *47*, 661–669.
156. Ho, W.F.; Ju, C.P.; Chern Lin, J.H. Structure and properties of cast binary Ti-Mo alloys. *Biomaterials* **1999**, *20*, 2115–2122.
157. Oliveira, N.T.C.; Aleixo, G.; Caram, R.; Guastaldi, A.C. Development of Ti-Mo alloys for biomedical applications: Microstructure and electrochemical characterization. *Mater. Sci. Eng. A* **2007**, *452–453*, 727–731.
158. Oliveira, N.T.C.; Guastaldi, A.C. Electrochemical stability and corrosion resistance of Ti-Mo alloys for biomedical applications. *Acta Biomater.* **2009**, *5*, 399–405.
159. Oliveira, N.T.C.; Guastaldi, A.C. Electrochemical behavior of Ti-Mo alloys applied as biomaterial. *Corros. Sci.* **2008**, *50*, 938–945.

160. Capela, M.V.; Acciari, H.A.; Capela, J.M.V.; Carvalho, T.M.; Melin, M.C.S. Repeatability of corrosion parameters for titanium-molybdenum alloys in 0.9% NaCl solution. *J. Alloy. Compd.* **2008**, *465*, 479–483.
161. Alves, A.P.R.; Santana, F.A.; Rosa, L.A.A.; Cursino, S.A.; Codaro, E.N. A study on corrosion resistance of the Ti-10Mo experimental alloy after different processing methods. *Mater. Sci. Eng. A* **2004**, *24*, 693–696.
162. Zhang, L.C.; Lu, H.B.; Mickel, C.; Eckert, J. Ductile ultrafine-grained Ti-based alloys with high yield strength. *Appl. Phys. Lett.* **2007**, *91*, 051906:1–051906:3.
163. Kshang, D.; Lu, J.; Yao, C.; Haberstroh, K.M.; Thomas, W.J. The role of nanometer and sub-micron surface features on vascular and bone cell adhesion on titanium. *Biomaterials* **2008**, *29*, 970–983.
164. Yao, C.; Qazi, J.I.; Rack, H.J.; Slamovich, E.B.; Webster, T.J. Improved bone cell adhesion on ultrafine grained titanium and Ti-6Al-4V. In Proceedings of the 106th Annual Meeting of the American-Ceramic-Society, Indianapolis, IN, USA, 18–21 April 2004.
165. Mitchell, A. Melting, casting and forging problems in titanium alloys. *Mater. Sci. Eng. A* **1998**, *243*, 257–262.
166. Kim, H.Y.; Ikehara, Y.; Kim, J.I.; Hosoda, H.; Miyazaki, S. Martensitic transformation, shape memory effect and superelasticity of Ti-Nb binary alloys. *Acta Mater.* **2006**, *54*, 2419–2429.
167. Miyazaki, S.; Kim, H.Y.; Hosoda, H. Development and characterization of Ni-free Ti-base shape memory and superelastic alloys. *Mater. Sci. Eng. A* **2006**, *438–440*, 18–24.
168. Takahashi, E.; Sakurai, T.; Watanabe, S.; Masahashi, N.; Hanada, S. Effect of heat treatment and Sn content on superelasticity in biocompatible TiNbSn alloys. *Mater. Trans.* **2002**, *43*, 2978–2983.
169. Zhang, L.C.; Zhou, T.; Alpay, S.P.; Aindow, M.; Wu, M.H. Origin of pseudoelastic behavior in Ti-Mo-based alloys. *Appl. Phys. Lett.* **2005**, *87*, 241909:1–241909:3.
170. Li, S.J.; Cui, T.C.; Hao, Y.L.; Yang, R. Fatigue properties of a metastable β -type titanium alloy with reversible phase transformation. *Acta Biomater.* **2008**, *4*, 305–317.
171. Freyman, T.M.; Yannas, I.V.; Gibson, L.J. Cellular materials as porous scaffolds for tissue engineering. *Prog. Mater. Sci.* **2001**, *46*, 273–282.
172. Wen, C.E.; Yamada, Y.; Shimojima, K.; Chino, Y.; Hosokawa, H.; Mabuchi, M. Compressibility of porous magnesium foam: Dependency on porosity and pore size. *Mater. Lett.* **2004**, *58*, 357–360.
173. Manukyana, K.; Amirkhanyan, N.; Aydinyan, S.; Danghyan, V.; Grigoryan, R.; Sarkisyan, N.; Gasparyan, G.; Aroutiounian, R.; Kharatyan, S. Novel NiZr-based porous biomaterials: Synthesis and *in vitro* testing. *J. Chem. Eng.* **2010**, *162*, 406–414.
174. Lueck, R.A.; Galante, J.O.; Rostoker, W.; Ray, R.D. Development of an open pore metallic implant to permit attachment to bone. *Surg. Forum* **1969**, *20*, 456–457.
175. Wang, X.J.; Li, Y.C.; Xiong, J.Y.; Hodgson, P.D.; Wen, C.E. Porous TiNbZr alloy scaffolds for biomedical applications. *Acta Biomater.* **2009**, *5*, 3616–3624.
176. Zhao, X.K.; Sun, H.B.; Lan, L.; Huang, J.H.; Zhang, H.; Wang, Y. Pore structures of high-porosity NiTi alloys made from elemental powders with NaCl temporary space-holders. *Mater. Lett.* **2009**, *63*, 2402–2404.
177. Schroers, J.; Kumar, G.; Hodges, T.M.; Chan, S.; Kyriakides, T.R. Bulk metallic glasses for biomedical applications. *JOM* **2009**, *61*, 21–29.

178. Wen, C.E.; Mabuchi, M.; Yamada, Y.; Shimojima, K.; Chino, Y.; Asahina, T. Processing of biocompatible porous Ti and Mg. *Scr. Mater.* **2001**, *45*, 1147–1153.
179. Wen, C.E.; Yamada, Y.; Hodgson, P.D. Fabrication of novel TiZr alloy foams for biomedical applications. *Mater. Sci. Eng. C* **2006**, *26*, 1439–1444.
180. Pompe, W.; Worch, H.; Epple, M.; Friess, W.; Gelinsky, M.; Greil, P.; Hempel, U.; Scharnweber, D.; Schulte, K. Functionally graded materials for biomedical applications. *Mater. Sci. Eng. A* **2003**, *362*, 40–60.
181. Menini, R.; Dion, M.J.; So, S.K.V.; Gauthier, M.; Lefebvre, L.P. Surface and corrosion electrochemical characterization of titanium foams for implant applications. *J. Electrochem. Soc.* **2006**, *153*, B13–B21.
182. Gibson, L.J.; Ashby, M.F. *Cellular Solids: Structure and Properties*; Cambridge University Press: Cambridge, UK, 1997.
183. Roberts, A.P.; Garboczi, E.J. Elastic properties of model random three-dimensional open-cell solids. *J. Mech. Phys. Solids* **2002**, *50*, 33–55.
184. Bastawros, A.F.; Bart-Smith, H.; Evans, A.G. Experimental analysis of deformation mechanisms in a closed-cell aluminum alloy foam. *J. Mech. Phys. Solids* **2000**, *48*, 301–322.
185. Ford, C.M.; Gibson, L.J. Uniaxial strength asymmetry in cellular materials: An analytical model. *Int. J. Mech. Sci.* **1998**, *40*, 521–531.
186. Roberts, A.P.; Garboczi, E.J. Elastic moduli of model random three-dimensional closed-cell cellular solids. *Acta Mater.* **2001**, *49*, 189–197.
187. Prakash, O.; Sang, H.; Embury, J.D. Structure and properties of Al-SiC foam. *Mater. Sci. Eng. A* **1995**, *199*, 195–203.
188. Niu, W.; Gill, S.; Dong, H.; Bai, C. A two-scale model for predicting elastic properties of porous titanium formed with space-holders. *Comp. Mater. Sci.* **2010**, *50*, 172–178.
189. Jha Nidhi; Mondal D.P.; Majumdar Dutta J.; Badkul Anshul; Jha A.K.; Khare A.K. Highly porous open cell Ti-foam using NaCl as temporary space holder through powder metallurgy route. *Mater.Des.* **2013**, *47*, 810-819.
190. Roberts, A.P.; Garboczi, E.J. Elastic properties of model porous ceramics. *J. Am. Ceram. Soc.* **2000**, *83*, 3041–3048.
191. Malinov, S.; Guo, Z.; Sha, W.; Wilson, A. Differential scanning calorimetry study and computer modeling of phase transformation in a Ti-6Al-4V alloy. *Metall. Mater. Trans. A* **2001**, *32*, 879–887.
192. Hollister, S.J.; Maddox, R.D.; Taboas, J.M. Optimal design and fabrication of scaffolds to mimic tissue properties and satisfy biological constraints. *Biomaterials* **2002**, *23*, 4095–4103.
193. Fang, Z.; Starly, B.; Sun, W. Computer-aided characterization for effective mechanical properties of porous tissue scaffolds. *Comput. Aided Des.* **2005**, *37*, 65–72.
194. Esen, Z.; Bor, S. Characterization of Ti-6Al-4V alloy foams synthesized by space holder technique. *Mater. Sci. Eng. A* **2011**, *528*, 3200–3209.
195. Esen, Z.; Bor, S. Processing of titanium foams using magnesium spacer particles. *Scr. Mater.* **2007**, *56*, 341–344.

196. Laptev, A.; Vyal, O.; Bram, M.; Buchkremer, H.P.; Stover, D. Green strength of powder compacts provided for production of highly porous titanium parts. *Powder Metall.* **2005**, *48*, 358–364.
197. Li, C.F.; Zhu, Z.G.; Liu, T. Microhardness of pore walls in porous titanium prepared with novel powder metallurgy. *Powder Metall.* **2005**, *48*, 237–240.
198. Saha, M.C.; Mahfuz, H.; Chakravarty, U.K.; Uddin, M.; Kabir, M.; Jeelani, E. Effect of density, microstructure, and strain rate on compression behavior of polymeric foams. *Mater. Sci. Eng. A* **2005**, *406*, 328–336.
199. Raj, R.E.; Daniel, B.S.S. Structural and compressive property correlation of closed-cell aluminum foam. *J. Alloy. Compd.* **2009**, *467*, 550–556.
200. Tuncer, N.; Arslan, G.; Maire, E.; Salvo, L. Investigation of spacer size effect on architecture and mechanical properties of porous titanium. *Mater. Sci. Eng. A* **2011**, *530*, 633–642.
201. Stephani, G.; Quadbeck, P.; Andersen, O. New multifunctional lightweight materials based on cellular metals—Manufacturing, properties and applications. *J. Phys. Conf. Ser.* **2009**, *165*, 012061:1–012061:6.
202. Jiang, H.C.; Du, H.; Xie, H.M.; Rong, L.J. Investigation on the micro-deformation characteristics of porous NiTi shape memory alloy using SEM moirè method. *Acta Metall. Sin.* **2006**, *42*, 1153–1157.
203. Li, P.; Lee, P.D.; Maijer, D.M.; Lindley, T.C. Quantification of the interaction within defect populations on fatigue behavior in an aluminum alloy. *Acta Mater.* **2009**, *57*, 3539–3548.
204. Spoerke, E.D.; Murray, N.G.D.; Li, H.; Brinson, L.C.; Dunand, D.C.; Stupp, S.I. Titanium with aligned, elongated pores for orthopedic tissue engineering applications. *Mater. Res.* **2008**, *84A*, 402–412.
205. Shen, H.; Li, H.; Brinson, L.C. Effect of microstructural configurations on the mechanical responses of porous titanium: A numerical design of experiment analysis for orthopedic applications. *Mech. Mater.* **2008**, *40*, 708–720.
206. Li, H.L.; Oppenheimer, S.M.; Stupp, S.I.; Dunand, D.C.; Brinson, L.C. Effects of pore morphology and bone ingrowth on mechanical properties of microporous titanium as an orthopaedic implant material. *Jpn. Mater. Trans.* **2004**, *45*, 1124–1131.
207. Zou, C.M.; Zhang, E.L.; Li, M.W.; Zeng, S.Y. Preparation, microstructure and mechanical properties of porous titanium sintered by Ti fibres. *J. Mater. Sci. Mater. Med.* **2008**, *19*, 401–405.
208. Li, B.Q.; Yan, F.; Lu, X. Effect of microstructure on the tensile property of porous Ti produced by powder metallurgy technique. *Mater. Sci. Eng. A* **2012**, *534*, 43–52.
209. Li, B.Q.; Wang, C.Y.; Lu, X. Effect of pore structure on the compressive property of porous Ti produced by powder metallurgy technique. *Mater. Des.* **2013**, *50*, 613–619.
210. Xie, F.X.; He, X.B.; Cao, S.L.; Lu, X.; Qu, X.H. Structural characterization and electrochemical behavior of a laser-sintered porous Ti-10Mo alloy. *Corros. Sci.* **2013**, *67*, 217–224.
211. Otsuki, B.; Takemoto, M.; Fujibayashi, S.; Neo, M.; Kokubo, T.; Nakamura, T. Pore throat size and connectivity determine bone and tissue ingrowth into porous implants: Three dimensional micro-CT based structural analyses of porous bioactive titanium implants. *Biomaterials* **2006**, *27*, 5892–5900.

212. Xue, W.C.; Krishna, B.V.; Bandyopadhyay, A.; Bose, S. Processing and biocompatibility evaluation of laser processed porous titanium. *Acta Biomater.* **2007**, *3*, 1007–1018.
213. Chen, Y.J.; Feng, B.; Zhu, Y.P.; Wen, J.; Wang, J.X.; Lu, X. Fabrication of porous titanium implants with biomechanical compatibility. *Mater. Lett.* **2009**, *63*, 2659–2661.
214. Hollander, D.A.; von-Walter, M.; Wirtz, T.; Sellei, R.; Schmidt-Rohlfing, B.; Paar, O.; Erli, H.J. Structural, mechanical and *in vitro* characterization of individually structured Ti-6Al-4V produced by direct laser forming. *Biomaterials* **2006**, *27*, 955–963.
215. Jia, P.L.; Pamela, H.; Mirella, D.; Clayton, E.W.; Joost, R.W.; Clemens, A.B. Bone ingrowth in porous titanium implants produced by 3D fiber deposition. *Biomaterials* **2007**, *28*, 2810–2820.
216. Li, D.S.; Zhang, Y.P.; Ma, X.; Zhang, X.P. Space-holder engineered porous NiTi shape memory alloys with improved pore characteristics and mechanical properties. *J. Alloy. Compd.* **2009**, *474*, L1–L5.
217. Suchanek, W.; Yoshimura, M. Processing and properties of hydroxyapatite-based biomaterials for use as hard tissue replacement implants. *J. Mater. Res.* **1998**, *13*, 94–116.
218. Nakai, M.; Niinomi, M.; Akahori, T.; Tsutsumi, H.; Itsuno, S.; Haraguchi, N.; Itoh, Y.; Ogasawara, T.; Onishi, T.; Shindoh, T. Development of biomedical porous titanium filled with medical polymer by *in situ* polymerization of monomer solution infiltrated into pores. *J. Mech. Behav. Biomed. Mater.* **2010**, *3*, 41–50.
219. Niinomi, M. Mechanical biocompatibilities of titanium alloys for biomedical applications. *J. Mech. Behav. Biomed. Mater.* **2008**, *1*, 30–42.
220. Brailovski, V.; Prokoshkin, S.; Gauthier, M.; Inaekyan, K.; Dubinskiy, S. Mechanical properties of porous metastable beta Ti-Nb-Zr alloys for biomedical applications. *J. Alloy. Compd.* **2013**, *577*, S414–S417.
221. Krishna, B.V.; Bose, S.; Bandyopadhyay, A. Low stiffness porous Ti structures for load-bearing implants. *Acta Biomater.* **2007**, *3*, 997–1006.
222. Torres, Y.; Pavon, J.J.; Nieto, I.; Rodriguez, J.A. Conventional powder metallurgy process and characterization of porous titanium for biomedical applications. *Metall. Mater. Trans. B* **2011**, *42B*, 891–900.
223. Hsu, H.C.; Hsu, S.K.; Wu, S.C.; Wang, P.H.; Ho, W.F. Design and characterization of highly porous titanium foams with bioactive surface sintering in air. *J. Alloy. Compd.* **2013**, *575*, 326–332.
224. Zhang, F.M.; Otterstein, E.; Burkel, E. Spark plasma sintering, microstructures, and mechanical properties of macroporous titanium foams. *Adv. Eng. Mater.* **2010**, *12*, 863–872.
225. Aguilar Maya, A.E.; Grana, D.R.; Hazarabedian, A.; Kokubu, G.A.; Luppo, M.I.; Vigna, G. Zr-Ti-Nb porous alloys for biomedical application. *Mater. Sci. Eng. C* **2012**, *32*, 321–329.
226. Nomura, N.; Oh, I.H.; Hanada, S.; Kanehira, M.; Sasaki, K.; Chiba, A. Effect of nitrogen on mechanical properties of porous titanium compacts prepared by powder sintering. *Mater. Sci. Forum* **2005**, *2313*, 475–477.
227. Banhart, J. Manufacture, characterization and application of cellular metals and metal foams. *Prog. Mater. Sci.* **2001**, *46*, 559–632.
228. Banhart, J.; Ashby, M.F.; Fleck, N.A. Metal Foams and Foam Metal Structures. In Proceedings of the International Conference Metfoam; MIT Verlag: Bremen, Germany, 14–16 June 1999.

229. Dunand, D.C. Processing of titanium foams. *Adv. Eng. Mater.* **2004**, *6*, 369–376.
230. Angelo, P.C.; Subramanian, R. *Powder Metallurgy: Science, Technology and Applications*, Eastern Economy; PHI: Connaught Circus, New Delhi, India, 2009; pp. 41–49.
231. Arzt, E.; Ashby, M.E.; Easterling, K.E. Practical applications of hot-isostatic pressing diagrams: Four case studies. *Metall. Trans. A* **1983**, *14*, 211–221.
232. Ryan, G.; Pandit, A.; Apatsidis, P.D. Fabrication methods of porous metals for use in orthopaedic applications. *Biomaterials* **2006**, *27*, 2651–2670.
233. Taylor, N.; Dunana, D.C.; Mortensen, A. Initial stage hot pressing of monosized Ti and 90% Ti-10% TiC powders. *Acta Metall. Mater.* **1993**, *41*, 955–965.
234. Niu, W.; Bai, C.; Qiu, G.; Wang, Q. Processing and properties of porous titanium using space holder technique. *Mater. Sci. Eng. A* **2009**, *506*, 148–151.
235. Li, Y.H.; Chen, R.B.; Qi, G.; Wang, Z.T.; Deng, Z.Y. Powder sintering of porous Ti-15Mo alloy from TiH₂ and Mo powders. *J. Alloy. Compd.* **2009**, *485*, 215–218.
236. Bernard, B. Porous single-phase NiTi processed under Ca reducing vapor for use as a bone graft substitute. *Biomaterials* **2006**, *27*, 1246–1250.
237. Mansourighasri, A.; Muhamad, N.; Sulong, A.B. Processing titanium foams using tapioca starch as a space holder. *J. Mater. Process. Technol.* **2012**, *212*, 83–89.
238. Bansiddhi, A.; Dunand, D.C. Shape-memory NiTi foams produced by replication of NaCl space-holders. *Acta Biomater.* **2008**, *4*, 1996–2007.
239. Jee, C.S.Y.; Özgüven, N.; Guo, Z.X.; Evans, J.R.G. Preparation of high porosity metal foams. *Metall. Mater. Trans. B* **2000**, *31*, 1345–1352.
240. Aydogmus, T.; Bor, S. Processing of porous TiNi alloys using magnesium as space holder. *J. Alloy. Compd.* **2009**, *478*, 705–710.
241. Josephajr, G. Porous Metal Articles Having a Predetermined Pore Character. U.S. Patent 2,006,002,810 A1, 5 January 2006.
242. Patnaik, P. *Handbook of Inorganic Chemicals*; McGraw-Hill: New York, NY, USA, 2003.
243. Köhl, M.; Bram, M.; Buchkremer, H.-P.; Stöver, D.; Habijan, T.; Köller, M. *Production of Highly Porous Near-net-shape Niti Components for Biomedical Applications*; DEStech Publications Inc.: Lancaster, PA, USA, 2008; pp. 295–298.
244. Zhao, Y.Y.; Sun, D.X. A novel sintering-dissolution process for manufacturing Al foams. *Scr. Mater.* **2001**, *44*, 105–110.
245. Torres, Y.; Pavón, J.J.; Rodríguez, J.A. Processing and characterization of porous titanium for implants by using NaCl as space holder. *J. Mater. Process. Technol.* **2012**, *212*, 1061–1069.
246. Barrabés, M.; Sevilla, P.; Planell, J.A.; Gil, F.J. Mechanical properties of nickel-titanium foams for reconstructive orthopaedics. *Mater. Sci. Eng. A* **2008**, *28*, 23–27.
247. De Vasconcellos, L.M.R.; de Oliveira, M.V.; de Alencastro Graça, M.L.; de Vasconcellos, L.G.O.; Carvalho, Y.R.; Cairo, C.A.A. Porous titanium scaffolds produced by powder metallurgy for biomedical applications. *Mater. Res.* **2008**, *11*, 275–280.
248. Bram, M.; Stiller, C.; Buchkremer, H.P.; Stover, D.; Baur, H. High-porosity titanium, stainless steel and superalloy parts. *Adv. Eng. Mater.* **2000**, *2*, 196–199.
249. Gao, Z.F.; Li, Q.Y.; He, F.; Huang, Y.; Wan, Y.Z. Mechanical modulation and bioactive surface modification of porous Ti-10Mo alloy for bone implants. *Mater. Des.* **2012**, *42*, 13–20.

250. Aydogmuş, T.; Bor, Ş. Superelasticity and compression behavior of porous TiNi alloys produced using Mg spacers. *J. Mech. Behav. Biomed. Mater.* **2012**, *15*, 59–69.
251. Li, J.P.; Li, S.H.; Groot, K.; Layrolle, P. Preparation and characterization of porous titanium. *Key Eng. Mater.* **2002**, *218–220*, 51–54.
252. Asaoka, K.; Kuwayama, N.; Okuno, O.; Miura, I. Mechanical properties and biomechanical compatibility of porous titanium for dental implants. *J. Biomed. Mater. Res.* **1985**, *19*, 699–713.
253. Miyao, R.; Omori, M.; Watari, F.; Yokoyama, A.; Matsuno, H.; Hirai, T.; Kawasaki, T. Fabrication of functionally graded implants by spark plasma sintering and their properties. *J. Jpn. Soc. Powder Metall.* **2000**, *47*, 1239–1242.
254. Watari, F.; Yokoyama, A.; Omori, M.; Hirai, T.; Kondo, H.; Uo, M. Effect of spark plasma sintering pressure on the properties of functionally graded implant and its biocompatibility. *J. Jpn. Soc. Powder Metall.* **2002**, *49*, 1063–1069.
255. Zou, X.; Li, H.; Bunger, M.; Egund, N.; Lind, M.; Bunger, C. Bone ingrowth characteristics of porous tantalum and carbon fiber interbody devices: An experimental study in pigs. *Spine J.* **2004**, *4*, 99–105.
256. Ibrahim, A.; Zhang, F.; Otterstein, E.; Burkel, E. Processing of porous Ti and Ti5Mn foams by spark plasma sintering. *Mater. Des.* **2011**, *32*, 146–153.
257. Schneider, J.A.; Mishra, R.S.; Mukherjee, A.K. Plasma activated sintering of ceramic materials. *Ceram. Trans.* **1996**, *79*, 143–151.
258. Lifland, M.I.; Okazaki, K. Properties of titanium dental implants produced by electro-discharge compaction. *Clin. Mater.* **1994**, *17*, 203–209.
259. Kon, M.; Hirakata, L.M.; Asaoka, K. Porous Ti-6Al-4V alloy fabricated by spark plasma sintering for biomimetic surface modification. *J. Biomed. Mater. Res. B* **2004**, *68*, 88–93.
260. Sakamoto, Y.; Asaoka, K.; Kon, M.; Matsubara, T.; Yoshida, K. Chemical surface modification of high-strength porous Ti compacts by spark plasma sintering. *Biomed. Mater. Eng.* **2006**, *16*, 83–91.
261. Nicula, R.; Luthen, F.; Stir, M.; Nebe, B.; Burkel, E. Spark plasma sintering synthesis of porous nanocrystalline titanium alloys for biomedical applications. *Biomol. Eng.* **2007**, *24*, 564–567.
262. Oh, I.H.; Son, H.T.; Kang, C.S.; Lee, J.S.; Cho, J.I.; Bae, J.C.; Lee, B.T.; Song, H.Y. Mechanical properties and biocompatibility of porous titanium prepared by powder sintering. *Mater. Sci. Forum* **2007**, *539–543*, 635–664.
263. Zadra, M.; Casari, F.; Girardini, L.; Molinari, A. Microstructure and mechanical properties of cp-titanium produced by spark plasma sintering. *Powder Metall.* **2008**, *51*, 59–65.
264. Qiu, J.; Dominici, J.T.; Lifland, M.I.; Okazaki, K. Composite titanium dental implant fabricated by electro-discharge compaction. *Biomaterials* **1997**, *18*, 153–160.
265. Munir, Z.; Tamburini, U.A.; Ohyanagi, M. The effect of electric field and pressure on the synthesis and consolidation of materials: A review of the spark plasma sintering method. *J. Mater. Sci.* **2006**, *41*, 763–777.
266. Kutty, M.G.; Bhaduri, S.; Bhaduri, S.B. Gradient surface porosity in titanium dental implants: Relation between processing parameters and microstructure. *J. Mater. Sci. Mater. Med.* **2004**, *15*, 145–150.

267. Saitou, K. Microwave sintering of iron, cobalt, nickel, copper and stainless steel powders. *Scr. Mater.* **2006**, *54*, 875–879.
268. Upadhyaya, A.; Tiwari, S.K.; Mishra, P. Microwave sintering of W-Ni-Fe alloy. *Scr. Mater.* **2007**, *56*, 5–8.
269. Thakur, S.K.; Kong, T.S.; Gupta, M. Microwave synthesis and characterization of metastable (Al/Ti) and hybrid (Al/Ti + SiC) composites. *Mater. Sci. Eng. A* **2007**, *452–453*, 61–69.
270. Tang, C.Y.; Wong, C.T.; Zhang, L.N.; Choy, M.T.; Chow, T.W.; Chan, K.C.; Yue, T.M.; Chen, Q. *In situ* formation of Ti alloy/TiC porous composites by rapid microwave sintering of Ti6Al4V/MWCNTs powder. *J. Alloy. Compd.* **2013**, *557*, 67–72.
271. Liu, Y.; Chen, L.F.; Tang, H.P.; Liu, C.T.; Liu, B.; Huang, B.Y. Design of powder metallurgy titanium alloys and composites. *Mater. Sci. Eng. A* **2006**, *418*, 25–35.
272. Oghbaei, M.; Mirzaee, O. Microwave vs. conventional sintering: A review of fundamentals, advantages and applications. *J. Alloy. Compd.* **2010**, *494*, 175–189.
273. Zhang, X.; Ayers, R.A.; Thorne, K.; Moore, J.J.; Schowengerdt, F. Combustion synthesis of porous materials for bone replacement. *Biomed. Sci. Instrum.* **2001**, *37*, 463–468.
274. Li, B.Y.; Rong, L.J.; Li, Y.Y.; Gjunter, V.E. Synthesis of porous Ni-Ti shape-memory alloys by self-propagating high-temperature synthesis: Reaction mechanism and anisotropy in pore structure. *Acta Mater.* **2000**, *48*, 3895–3904.
275. Yea, C.L.; Sung, W.Y. Synthesis of NiTi intermetallics by selfpropagating combustion. *J. Alloy. Compd.* **2004**, *376*, 79–88.
276. Chu, C.L.; Chung, C.Y.; Lin, P.H.; Wang, S.D. Fabrication of porous NiTi shape memory alloy for hard tissue implants by combustion synthesis. *Mater. Sci. Eng. A* **2004**, *366*, 114–119.
277. Chung, C.Y.; Chu, C.L.; Wang, S.D. Porous TiNi shape memory alloy with high strength fabricated by self-propagating high-temperature synthesis. *Mater. Lett.* **2004**, *58*, 1683–1686.
278. Biswas, A. Porous NiTi by thermal explosion mode of SHS: Processing, mechanism and generation of single phase microstructure. *Acta Mater.* **2005**, *53*, 1415–1425.
279. Yuan, B.; Chung, C.Y.; Zhu, M. Microstructure and martensitic transformation behavior of porous NiTi shape memory alloy prepared by hot isostatic pressing processing. *Mater. Sci. Eng. A* **2004**, *382*, 182–187.
280. Yuan, B.; Zhang, X.P.; Chung, C.Y.; Zeng, M.Q.; Zhu, M. A comparative study of the porous TiNi shape-memory alloys fabricated by three different processes. *Metall. Mater. Trans. A* **2006**, *37*, 755–761.
281. Li, B.Y.; Rong, L.J.; Li, Y.Y. Anisotropy of dimensional change and its corresponding improvement by addition of TiH₂ during elemental powder sintering of porous NiTi alloy. *Mater. Sci. Eng. A* **1998**, *255*, 70–74.
282. Li, B.Y.; Rong, L.J.; Li, Y.Y.; Gjunter, V.E. A recent development in producing porous NiTi shape memory alloys. *Intermetallics* **2000**, *8*, 881–884.
283. Arakawa, Y.; Kobashi, M.; Kanetake, N. Effect of elemental powder size on foaming behavior of NiTi alloy made by combustion synthesis. *Materials* **2012**, *5*, 1267–1274.
284. Arakawa, Y.; Kobashi, M.; Kanetake, N. Effect of foaming agent and endothermic agent addition on foaming behavior of NiTi alloy made by combustion synthesis. *J. Jpn. Inst. Met.* **2011**, *75*, 379–385.

285. Chen, L.J.; Li, T.; Li, Y.M.; He, H.; Hu, Y.H. Porous titanium implants fabricated by metal injection molding. *Trans. Nonferr. Met. Soc. China* **2009**, *19*, 1174–1179.
286. Nihouannen, D.L.E.; Daculsi, G.; Saffarzadeh, A.; Gauthier, O.; Delplace, S.; Pilet, P.; Layrolle, P. Ectopic bone formation by microporous calcium phosphate ceramic particles in sheep muscles. *Bone* **2005**, *36*, 1086–1093.
287. Li, Y.H.; Li, R.J.; Li, Y.Y. Pore characteristics of porous NiTi alloy fabricated by combustion synthesis. *J. Alloy. Compd.* **2001**, *325*, 259–262.
288. Zhang, Y.P.; Yuan, B.; Zeng, M.Q.; Chung, C.Y.; Zhang, X.P. High porosity and large pore size shape memory alloys fabricated by using pore-forming agent (NH_4HCO_3) and capsule-free hot isostatic pressing. *J. Mater. Process. Technol.* **2007**, *192–193*, 439–442.
289. Nugroho, A.W.; Leadbeater, G.; Davies, I.J. Processing of a porous titanium alloy from elemental powders using a solid state isothermal foaming technique. *J. Mater. Sci. Mater. Med.* **2010**, *21*, 3103–3107.
290. Wegst, U.G.K.; Schecter, M.; Donius, A.E.; Hunger, P.M. Biomaterials by freeze casting. *Philos. Trans. R. Soc. A* **2010**, *368*, 2099–2121.
291. Li, J.C.; Dunand, D.C. Mechanical properties of directionally freeze-cast titanium foams. *Acta Mater.* **2011**, *59*, 146–158.
292. Yoon, B.H.; Choi, W.Y.; Kim, H.E.; Kim, J.H.; Koh, Y.H. Aligned porous alumina ceramics with high compressive strengths for bone tissue engineering. *Scr. Mater.* **2008**, *58*, 37–40.
293. Yook, S.W.; Kim, H.E.; Koh, Y.H. Fabrication of porous titanium scaffolds with high compressive strength using camphene-based freeze casting. *Mater. Lett.* **2009**, *63*, 1502–1504.
294. Jung, H.D.; Yook, S.W.; Jang, T.S.; Li, Y.; Kim, H.E.; Koh, Y.H. Dynamic freeze casting for the production of porous titanium (Ti) scaffolds. *Mater. Sci. Eng. C* **2013**, *33*, 59–63.
295. Chino, Y.; Dunand, D.C. Directionally freeze-cast titanium foam with aligned, elongated pores. *Acta Mater.* **2008**, *56*, 105–113.
296. Soon, Y.M.; Shin, K.H.; Koh, Y.H.; Choi, W.Y.; Kim, H.E. Assembling unidirectionally frozen alumina/camphene bodies for aligned porous alumina ceramics with larger dimensions. *J. Eur. Ceram. Soc.* **2011**, *31*, 415–419.
297. Cachinho, S.C.P.; Correia, R.N. Titanium porous scaffolds from precursor powders: Rheological optimization of TiH_2 slurries. *Powder Technol.* **2007**, *178*, 109–113.
298. Liu, X.; Rahaman, M.N.; Fu, Q.A. Oriented bioactive glass (13–93) scaffolds with controllable pore size by unidirectional freezing of camphene-based suspensions: Microstructure and mechanical response. *Acta Biomater.* **2011**, *7*, 406–416.
299. Yook, S.W.; Jung, H.D.; Park, C.H.; Shin, K.H.; Koh, Y.H.; Estrin, Y.; Kim, H.E. Reverse freeze casting: A new method for fabricating highly porous titanium scaffolds with aligned large pores. *Acta Biomater.* **2012**, *8*, 2401–2410.
300. Rak, Z.S.; Walter, J. Porous titanium foil by tape casting technique. *J. Mater. Process. Technol.* **2006**, *175*, 358–363.
301. Neirinck, B.; Mattheys, T.; Braem, A.; Fransaer, J.; van der Biest, O.; Vleugels, J. Preparation of titanium foams by slip casting of particle stabilized emulsions. *Adv. Eng. Mater.* **2009**, *11*, 633–636.

302. Asthana, R.; Kumar, A.; Dahotre, N.B. *Materials Processing and Manufacturing Science*; Elsevier Academic Press: Boston, MA, USA, 2006.
303. Sánchez-Herencia, A.; Millán, A.; Nieto, M.; Moreno, R. Aqueous colloidal processing of nickel powder. *Acta Mater.* **2001**, *49*, 645–651.
304. Xu, Q.; Gabbitas, B.; Matthews, S.; Zhang, D.L. Optimisation of performance of dispersants in aqueous titanium slips. *Key Eng. Mater.* **2012**, *520*, 330–334.
305. Gillissen, R.; Erauw, J.P.; Smolders, A.; Vanswijgenhoven, E.; Luyten, J. Gelcasting, a near net shape technique. *Mater. Des.* **2000**, *21*, 251–257.
306. Erk, K.A.; Dunand, D.C.; Shull, K.R. Titanium with controllable pore fractions by thermoreversible gelcasting of TiH₂. *Acta Mater.* **2008**, *56*, 5147–5157.
307. Yang, D.H.; Guo, Z.M.; Shao, H.P.; Liu, X.T.; Ji, Y. Mechanical properties of porous Ti-Mo and Ti-Nb alloys for biomedical application by gelcasting. *Procedia Eng.* **2012**, *36*, 160–167.
308. Yang, D.H.; Shao, H.P.; Guo, Z.M.; Lin, T.; Fan, L.P. Preparation and properties of biomedical porous titanium alloys by gelcasting. *Biomed. Mater.* **2011**, *6*, 045010:1–045010:8.
309. Woodfield, T.B.; Malda, J.; de Wijn, J.; Peters, F.; Riesle, J.; van Blitterswijk, C.A. Design of porous scaffolds for cartilage tissue engineering using a three-dimensional fiber-deposition technique. *Biomaterials* **2004**, *25*, 4149–4161.
310. Yang, S.; Leong, K.F.; Du, Z.; Chua, C.K. The design of scaffolds for use in tissue engineering. Part II. Rapid prototyping techniques. *Tissue Eng.* **2002**, *8*, 1–11.
311. Li, H.; Yu, Q.F.; Zhang, B.; Wang, H.; Fan, H.S.; Zhang, X.D. Fabrication and characterization of bioactive porous titanium. *Rare Met. Mater. Eng.* **2006**, *35*, 154–157.
312. Hench, L.L. Bioceramics: From concept to clinic. *J. Am. Ceram. Soc.* **1991**, *74*, 1487–1510.
313. Salito, A.; van Osten, K.U.; Breme, F. Gentle coating technique. *Sulzer Tech. Rev.* **1998**, 34–37.
314. Tan, Q.B.; Liu, P.; Du, C.L.; Wu, L.H.; He, G. Mechanical behaviors of quasi-ordered entangled aluminum alloy wire material. *Mater. Sci. Eng. A* **2009**, *527*, 38–44.
315. Liu, P.; He, G.; Wu, L.H. Uniaxial tensile stress-strain behavior of entangled steel wire material. *Mater. Sci. Eng. A* **2009**, *509*, 69–75.
316. Ducheyne, P.; Martens, M.; Aernoudt, E.; Mulier, J.; Meester, P. Skeletal fixation by metal fiber coating of the implant. *Acta Orthop. Belg.* **1974**, *40*, 799–805.
317. Lee, J.H.; Kim, H.E.; Shin, K.H.; Koh, Y.H. Improving the strength and biocompatibility of porous titanium scaffolds by creating elongated pores coated with a bioactive, nanoporous TiO₂ layer. *Mater. Lett.* **2010**, *64*, 2526–2529.
318. Li, J.P.; Li, S.H.; de Groot K, L.P. Improvement of porous titanium with thicker struts. *Key Eng. Mater.* **2003**, *240*, 547–550.
319. Balla, V.K.; Bodhak, Z.; Bose, S.; Bandyopadhaya, A. Porous tantalum structures for bone implants: Fabrication, mechanical and vitro biological properties. *Acta Biomater.* **2010**, *6*, 3349–3359.
320. Singh, R.; Lee, P.D.; Dashwood, R.J.; Lindley, T.C. Titanium foams for biomedical applications: A review. *Mater. Technol.* **2010**, *25*, 127–136.
321. Imwinkelried, T. Mechanical properties of open-pore titanium pore. *J. Biomed. Mater. Res.* **2007**, *81A*, 964–970.

322. Kato, K.; Ochiai, S.; Yamamoto, A.; Daigo, Y.; Honma, K.; Matano, S.; Omori, K. Novel multilayer Ti foam with cortical bone strength and cytocompatibility. *Acta Biomater.* **2013**, *9*, 5802–5809.
323. Yeong, W.Y.; Chua, C.K.; Leong, K.F.; Chandrasekaran, M. Rapid prototyping in tissue engineering: Challenges and potential. *Trends Biotechnol.* **2004**, *22*, 643–652.
324. Hutmacher, D.W.; Sittinger, M.; Risbud, M.V. Scaffold-based tissue engineering: Rationale for computer-aided design and solid free-form fabrication systems. *Trends Biotechnol.* **2004**, *22*, 354–362.
325. Sachlos, E.; Reis, N.; Ainsley, C.; Derby, B.; Czernuszka, J.T. Novel collagen scaffolds with predefined internal morphology made by solid freeform fabrication. *Biomaterials* **2003**, *24*, 1487–1497.
326. Sun, W.; Darling, A.; Starly, B.; Nam, J. Computer-aided tissue engineering: Overview, scope and challenges. *Biotechnol. Appl. Biochem.* **2004**, *39*, 29–47.
327. Wilson, C.E.; de Bruijn, J.D.; van Blitterswijk, C.A.; Verbout, A.J.; Dhert, W.J. Design and fabrication of standardized hydroxyapatite scaffolds with a defined macro-architecture by rapid prototyping for bone—Tissue-engineering research. *J. Biomed. Mater. Res. A* **2004**, *68*, 123–132.
328. Curodeau, A.; Sachs, E.; Caldarise, S. Design and fabrication of cast orthopedic implants with freeform surface textures from 3-D printed ceramic shell. *J. Biomed. Mater. Res.* **2000**, *53*, 525–535.
329. Sachlos, E.; Czernuszka, J.T. Making tissue engineering scaffolds work. Review: The application of solid freeform fabrication technology to the production of tissue engineering scaffolds. *Eur. Cell Mater.* **2003**, *5*, 29–39.
330. Mazumder, J.; Qi, H. Fabrication of 3D components by laser-aided direct metal deposition. *Proc. SPIE* **2005**, *5706*, 38–59.
331. Traini, T.; Mangano, C.; Sammons, R.L.; Mangano, F.; Macchi, A.; Piattelli, A. Direct laser metal sintering as a new approach to fabrication of an isoelastic functionally graded material for manufacture of porous titanium dental implants. *Dent. Mater.* **2008**, *24*, 1525–1533.
332. Garrett, E.R.; Abhay, S.P.; Dimitrios, P.A. Porous titanium scaffolds fabricated using a rapid prototyping and powder metallurgy technique. *Biomaterials* **2008**, *29*, 3625–3635.
333. Kumar, S. Selective laser sintering: A qualitative and objective approach. *JOM* **2003**, *55*, 43–47.
334. Eosoly, S.; Brabazon, D.; Lohfeld, S.; Looney, L. Selective laser sintering of hydroxyapatite/poly-e-caprolactone scaffolds. *Acta Biomater.* **2010**, *6*, 2511–2517.
335. Savalani, M.M.; Hao, L.; Dickens, P.M.; Zhang, Y.; Tanner, K.E.; Harris, R.A. The effects and interactions of fabrication parameters on the properties of selective laser sintered hydroxyapatite polyamide composite biomaterials. *Rapid Prototyp. J.* **2012**, *18*, 16–27.
336. Shishkovsky, I.V.; Kuznetsov, M.V.; Morozov, Y.G. Porous titanium and nitinol implants synthesized by SHS/SLS: Microstructural and histomorphological analyses of tissue reactions. *Int. J. Selfpropag. High Temp. Synth.* **2010**, *19*, 157–167.
337. Wu, X.; Mei, J. Near net shape manufacturing of components using direct laser fabrication technology. *J. Mater. Proc. Technol.* **2003**, *135*, 266–270.
338. Schwendner, K.I.; Banerjee, R.; Collins, P.C.; Brice, C.A.; Fraser, H.L. Direct laser deposition of alloys from elemental powder blends. *Scr. Mater.* **2001**, *45*, 1123–1129.

339. Liu, W.; DuPont, J.N. Fabrication of functionally graded TiC/Ti composites by laser engineered net shaping. *Scr. Mater.* **2003**, *48*, 1337–1342.
340. Banerjee, R.; Collins, P.C.; Bhattacharyya, D.; Banerjee, S.; Fraser, H.L. Microstructural evolution in laser deposited compositionally graded α/β titanium-vanadium alloys. *Acta Mater.* **2003**, *51*, 3277–3292.
341. Dutta, M.J.; Pinkerton, A.; Liu, Z.; Manna, I.; Li, L. Microstructure characterisation and process optimization of laser assisted rapid fabrication of 316L stainless steel. *Appl. Surf. Sci.* **2005**, *247*, 320–327.
342. Bandyopadhyay, A.; Espana, F.; Krishna, B.V.; Bose, S.; Ohgami, Y.; Davies, N.M. Influence of porosity on mechanical properties and *in vivo* response of Ti6Al4V implants. *Acta Biomater.* **2010**, *6*, 1640–1648.
343. Zhao, J.; Lu, X.; Weng, J. Macroporous Ti-based composite scaffold prepared by polymer impregnating method with calcium phosphate coatings. *Mater. Lett.* **2008**, *62*, 2921–2924.
344. Mullen, L.; Stamp, R.C.; Brooks, W.K.; Jones, E.; Sutcliffe, C.J. Selective laser melting: A regular unit cell approach for the manufacture of porous, titanium, bone ingrowth constructs, suitable for orthopedic applications. *J. Biomed. Mater. Res. B Appl. Biomater.* **2008**, *89B*, 325–334.
345. Brånemark, R.; Rydevik, B.; Myers, R.; Brånemark, P.I. Osseointegration in skeletal reconstruction and rehabilitation: A review. *J. Rehabil. Res. Dev.* **2001**, *38*, 175–181.
346. Otani, T.; Whiteside, L.A. Failure of cementless fixation of the femoral component in total hip arthroplasty. *Orthop. Clin. North Am.* **1992**, *23*, 335–346.

© 2014 by the authors; licensee MDPI, Basel, Switzerland. This article is an open access article distributed under the terms and conditions of the Creative Commons Attribution license (<http://creativecommons.org/licenses/by/3.0/>).